Daily Three-dimensional Ultrasound Imaging for Monte Carlo Based Adaptive Radiotherapy of Prostate Cancer

By

Yong Chen

Master of Science

Medical Physics Unit, Faculty of Medicine

McGill University
Montreal, Quebec, Canada

Jun. 06, 2009

A thesis submitted to the Faculty of Graduate and Postdoctoral Studies in partial fulfillment of the requirements of the degree of Master of Science

Abstract

This thesis retrospectively analyzes prostate's daily motion provided by three-dimensional US localization and investigates its dosimetric impacts based on XVMC calculation which takes into account patient geometry, heterogeneity and prostate motion correction.

The retrospective analysis on 32 prostate patients shows that the mean ± SD displacements of prostate in the AP, SI, and RL directions are -3.3 ± 7.9 mm, -1.1 ± 6.4 mm, -0.2 ±5.6 mm, respectively. The largest rotation occurs about lateral axis with mean ± SD of -0.9° ± 4.6°, ranging between -6.7° and 8.0° from a preliminary study including three patients.

To assess the dosimetric impacts of prostate motion, five motion scenarios including with and without prostate translation and correction, with translation and rotation but no correction or only having translation correction are simulated. Analysis based on dose-volume histograms and isodose curves shows that prostate motion (translation and rotation) will deteriorate the dose delivered to patient target and OARs. With translation correction method, the degraded patient dose could be recovered nearly completely. For the scenarios with both translation and rotation, translation correction method could dramatically improve the degraded patient dose, but could not completely eliminate the dosimetric impact of prostate motion.

Besides, the dosimetric impact of metal prosthesis in three patients has been analysed as well. Up to 5% discrepancies in their $D_{90\%}$, $D_{95\%}$, $V_{90\%}$, and $D_{95\%}$ for PTV have been observed.

Abrégé

Le mouvement de la prostate est un problème critique dans le traitement conforme du cancer de la prostate, le plus commun cancer parmi les hommes au Canada. La radiothérapie guidée par l'image (IGRT) utilisant les images ultrasons (US) quotidiennes est une technique largement utilisée pour régler ce problème. Une nouvelle technique de localisation ultrasons en trois dimensions, basée sur une méthode de vérification intra modalités, a été testée à l'Hôpital General de Montreal en 2005. L'objectif principal de cette thèse a été de mieux quantifier l'amplitude du mouvement de la prostate à travers une analyse rétrospective de 32 patients et d'évaluer son impacte dans la dosimétrie des traitements de la prostate avec et sans localisation US. L'analyse rétrospective a montré que la moyenne ± écart-type des mouvements de la prostate dans les directions AP, SI et DG est de -3.3 ± 7.9 mm, -1.1 ± 6.4 mm et -0.2 ± 5.6 mm, respectivement. La plus grande rotation survient autour de l'axe latérale, avec une moyenne ± écart-type de -0.9° ± 4.6°, s'échelonnant entre -6.7° et 8.0°. Pour estimer l'impacte dosimétrique du mouvement rigide de la prostate, la dose a été calculée en utilisant la méthode XVMC, qui prend en considération la géométrie du patient, les hétérogénéités et les corrections pour le mouvement. Une déviation moyenne de la $D_{95\%}$ de jusqu'à -11.9% a été observe pour le PTV, -5.1% pour le CTV et -4.2% pour le GTV. Le $V_{95\%}$ du PTV a été réduit par un facteur de -22.2% lorsque la translation quotidienne de la prostate était présente mais aucune correction n'a été appliquée. La dégradation de la dose à la cible a pu être corrige presque complètement en appliquant une correction du mouvement de translation, cependant lorsque la rotation a été prise en compte, le recouvrement de la dose a été moins adéquat. L'effet des prothèses métalliques présentes dans trois patients dans le calcul de la dose a aussi été analysé. L'impacte dosimétrique significatif des mouvements non négligeable de la prostate a révélé l'importance et la valeur clinique du IGRT dans le traitement par radiation du cancer de la prostate.

ACKNOWLEDGMENTS

First of all, I would like to express my sincere thanks to my supervisor, Dr. Frank Verhaegen, for guiding me into the exciting fields of clinical Monte Carlo based treatment planning, for his support during my thesis work, and for his kindness and help throughout my two years of graduate study. The similar thanks go to my co-supervisor, William Parker, for his guidance in US imaging and lots of advices on my thesis work

Special thanks go to Dr. Ervin Podgorsak for his devoted teaching, advice and for giving me the opportunity to study and develop my knowledge and skills in the notable medical physics department.

Much of my thesis relies on clinical treatment planning system, CT and US images, clinical patient data and Monte Carlo calculations. A warm-heart thank goes to Gabriela Stroian for her translation my abstract into French version The same thank goes to Dr. Brigitte Reniers for her help on patient treatment planning and image processing. Much thanks also goes to Dr. Wamied Abdel-Rahman for his advice and help with my Monte Carlo calculations. I benefited a lot from them during my thesis work.

I would also like express my sincere thanks to Danielle Fraser for her long-term guidance, valuable advice, and discussions on Monte Carlo methods, 3D ultrasound imaging, and adaptive conformal radiation therapy techniques. My gratitude also goes to Emily Poon for providing to me her well-coded BrachyGUI program and many modifications specific for my research.

Special thanks go to Magdalena Bazalova for her help on de-artefact CT images of patients with metal prosthesis. The same thanks go to Andrew Alexander for his kind permission to use his MMCTP program and help in modeling Linac components.

I would like thank all other staff and graduate students in the medical physics department at McGill University for their kind help and invaluable comments with regards to my English, especially Derek Liu and Arman Sarfehnia.

Finally, I would like to express my special gratitude to my wife, Yan Li, and my beloved son, Xiyuan Chen, for their love and support. My life and study at McGill would not have been so enjoyable without all the people mentioned above and from whose association I have benefited.

CONTENTS

CONTENTS.....V
LIST OF TABLES.....VIII
LIST OF FIGURES.....IX

Chapter 1 Introduction.....1
1.1 Radiotherapy Treatment for Prostate Cancer.....1
1.2 Prostate motion in Radiotherapy Treatment.....2
1.3 Challenges imposed by prostate motion.....2
1.4 Potential solutions for prostate motion.....3
1.5 US localization in Conformal Radiotherapy.....4
1.6 Potential use provided by Restitu™ System.....5
1.7 Purpose of this thesis.....5
1.7.1 A Statistical analysis of prostate daily displacement.....5
1.7.2 Patient dose recalculation using a BEAMnrc-XVMC method.....6
1.7.3 Prostate rotation measurements.....7
1.7.4 Dosimetric impact of prostate motion and metal hip prosthesis.....7
1.8 Structure of this thesis.....7

Chapter 2 Methods and Materials (1).....9
A Retrospective Analysis and Rotation Measurement.....9
2.1 Method for retrospective analysis on prostate daily displacement.....9
2.1.1 Data acquisition.....10
US Localization System.....10
Simulation CT and US scan.....11
US scan before treatment.....11
Measurements.....12
Criteria for selecting patient data.....13
2.1.2 Data analysis.....14
2.2 Rotation measurement.....15
2.2.1 Extracting 3D prostate contours.....16
2.2.2 MI registration method based on 3D contour.....16
2.2.3 Implementation of detecting prostate rotation.....18

Chapter 3 Methods and Materials (2).....19
Patient Dose Calculation and Evaluation.....19
3.1 Introduction.....19
3.2 XVMC – a fast MC Method.....20
3.2.1 Linac simulation.....21
3.2.1.1 Physics models for a Varian 2300C linac.....21
3.2.1.2 Strategy for the acquisition of ph-sp file.....23
3.2.2 Patient dose simulation with XVMC code.....24
3.2.2.1 Patient treatment planning parameters.....25

3.2.2.2 Transferring between CADPlan™ and XVMC coordinate systems 25
3.2.2.3 Introducing the daily shift of prostate 26
3.2.2.4 Fraction dose calculation procedure 26
3.3 Patient total dose calculation 27
3.3.1 Calibration of XVMC simulation 27
3.3.2 Dose calculation considering daily prostate motion 28
3.4 Evaluation methods 32
3.4.1 DVH analysis and comparison of isodose curves 32
3.4.2 Statistical Analysis 34

Chapter 4 Results and Discussion (1) 35
Retrospective analysis of prostate daily displacements 35
4.1 Fraction-based statistical results for individual patient 35
4.2 Statistical Analysis on all patients 38
4.2.1 Statistical results based on all fractions 39
4.2.2 Statistical results based on individual patient 42
4.3 Primary assessment of the PTV margin 44
4.4 Daily Rotation Measurement 44
4.5 Discussion 46

Chapter 5 Results and Discussion (2) 49
Dosimetric Impacts of daily motion on prostate EBRT 49
5.1 Dose distributions of original plans 49
5.1.1 Isodose curves 50
5.1.3 DVH evaluation 50
5.2 Dosimetric comparison: scenario 2 vs. scenario 1 51
5.2.1 Comparison of Isodose curves for patient No. 1 51
5.2.2 Comparison of DVH curves for patient No. 1 52
5.2.3 Statistics on percent variations of DVH indices 53
5.3 Dosimetric comparison: scenario 3 vs. scenario 1 55
5.3.1 Comparison of Isodose curves 55
5.3.2 Comparison of DVH curves 56
5.3.3 Statistics on DVH variations 57
5.4 Dosimetric comparison: scenario 4 vs. scenario 1 59
5.4.1 Comparison of Isodose curves for patient No. 1 59
5.4.2 Comparison of DVH curves with scenario 1 60
5.4.3 Statistics on DVH variations 61
5.5 Dosimetric comparison: scenario 5 vs. scenario 1 62
5.5.1 Comparison of Isodose curves for patient No. 1 62
5.5.2 Comparison of DVH curves 63
5.5.3 Statistics on DVH variations 63
5.6 Discussion 64

Chapter 6 Results and Discussion (3).....67
Dosimetric Impacts of Metal Prostheses on Prostate EBRT 67
6.1 Introduction.....67
6.2 Comparison of PTVs from artifact-degraded, artifact-corrected and US-aided CT images 67
6.3 DVH comparison: artifact-degraded vs. artifact-corrected scenarios.....70
6.4 DVH comparison: artifact-degraded PTV vs. US-aided PTV 73
6.5 Discussion.....74

Chapter 7 Conclusion 76
7.1 Summary of Retrospective analysis on daily displacements.....76
7.2 Summary of Dosimetric impact of prostate motion.....76
7.3 Summary of Dosimetric impact of metal prosthesis.....77

Bibliography 79

LIST OF TABLES

Scheme 1: Algorithm for maximum MI registration method 17
Table 1: Five hypothesized scenarios with considering translation and rotation . 20
Table 2: Simulation parameters for the CL2300 linac components 23
Table 3: Formulae for calculating patient total dose 31
Table 4: Statistical results from a typical patient with 39 ultrasound localizations. All shifts are relative to target isocenter..... 35
Table 5: Statistical results on 890 ultrasound localizations from 32 patients..... 39
Table 6: Statistical results on mean values of displacements and percent volume changes for 32 patients 43
Table 7: Population statistics and margins calculated using equation 2.2. 44
Table 8: Statistical results of prostate daily rotations for 3 patients 45
Table 9: Mean displacements with respected to three main directions from several author's studies. 47
Table 10: Average prostate volume ratios computed for different imaging modalities 48
Table 11: Statistical results of percent variations of DVH indices for PTV, CTV and GTV between scenario 2 and scenario 1 for 32 patients 53
Table 12: Statistical results of percent variations of DVH indices for bladder and rectum between scenario 2 and scenario 1 for 32 patients 54
Table 13: Statistical result of percent variations of DVH indices for PTV, CTV, and GTV between scenario 3 and scenario 1 for 32 patients 57
Table 14: Statistical results of percent variations of DVH indices for bladder and rectum between scenario 3 and scenario 1 for 32 patients 59
Table 15: $\Delta D_{95\%}/D_{95\%\_ori}$ and $\Delta V_{95\%}/V_{95\%\_ori}$ for PTV, CTV and GTV between scenario 4 and scenario 1 for 3 patients 61
Table 16: $\Delta D_{95}/D_{95\_ori}$ and $\Delta V_{95}/V_{95\_ori}$ for PTV, CTV and GTV compared scenario 5 to scenario 1 for 3 patients 64
Table 17: Volume and percent volume change of PTV relative to artifact-degraded PTV for three patients..... 70
Table 18: Percent change of DVH indices on PTV between artifact-degraded and artifact-corrected scenarios for three patients 73
Table 19: Percent change of DVH indices on bladder and rectum between artifact-degraded and artifact-corrected scenarios for three patients 73
Table 20: Percent changes of DVH indices for US-aided PTV relative to artifact-corrected PTV under four scenarios: artifact-degraded, artifact-degraded with displacements, artifact-degraded with displacement correction, and artifact-corrected scenarios..... 74

LIST OF FIGURES

Figure 1: The scheme of 3D Restitu™ US localization system 10
Figure 2: A display of couch movement parameters from Restitu™ system 12
Figure 3: (a) Probe calibration and (b) Room calibration by aligning laser to the reference point on surface of the calibration phantom..... 13
Figure 4: Ant/Post directional histogram of displacement for one patient with 37 fractions..... 15
Figure 5: Coordinate systems for three rotations 17
Figure 6: PRV surface (in blue) and PGV surface (in red) after MI-registration . 18
Figure 7: Physic Models of Varian CL 2300 Linac [74] 22
Figure 8: (a) CADPlan™ coordinate system and (b) XVMC coordinate system 25
Figure 9: Scenarios of daily prostate motion and corrections..... 30
Figure 10: Frequency histograms of daily prostate displacement calculated for each direction (a) anterior-posterior, (b) superior-inferior, (c) right-left, and (d) volume changes for a typical patient 36
Figure 11: Scatter plots illustrating the daily displacements of 39 fractions for a patient in the axial, coronal, and sagittal planes. 37
Figure 12: Plots of daily displacements for the three major axes and volume change vs. fraction (trends with time)..... 38
Figure 13: Frequency histograms of prostate displacements calculated for each direction (a) anterior-posterior, (b) superior-inferior, (c) right-left) and (d) volume changes from 890 US localizations of 32 patients 40
Figure 14: Scatter plots illustrating the daily displacements in the axial, coronal, and sagittal planes for 890 US localizations of 32 patients. 41
Figure 15: Plots of 890 daily displacements for the three major axes and percent volume change vs. fraction number. 42
Figure 16: Frequency histograms of prostate displacements based on the mean shifts in three major directions: (a) AP, (b) SI, (c) LAT, and (d) percent volume changes for 32 patients. 43
Figure 17: Frequency histograms of daily rotation along three main axes: (a) along lateral axis, (b) along AP axis, (c) along SI axis for three patients (78 fractions in total)..... 45
Figure 18: Plots of daily rotation angles vs. patient number for three patients studied: (a) rotation along lateral axis, (b) rotation along AP axis, (c) rotation along SI axis 46
Figure 19: 2D axial isodose curves calculated by XVMC based on the original treatment plan for patient No.1. 50
Figure 20: DVH curves of MC-calculated total dose from original plan for patient No. 1. Bladder and Rectum are the selected OARs 51
Figure 21: $D_{95\%}$ and $V_{95\%}$ of PTV, CTV and GTV (in % of prescribed dose) for 32 patients based on their original plans, calculated by the BEAMnrc/XVMC method..... 51

Figure 22: Comparison of isodose curves between scenario 2 (daily translation without correction) and scenario 1 (original plan, no motion) at the isocentric axial plane 52
Figure 23: Comparison of DVH curves for PTV, CTV, bladder and rectum between scenario 2 (daily translation without correction) and scenario 1 (original plan, no motion). 53
Figure 24: Diagrams plotting (a) $\Delta D_{95\%}/D_{95\%\_ori}$ and (b) $\Delta V_{95\%}/V_{95\%\_ori}$ for PTV, CTV and GTV between scenario 2 and scenario 1 vs. plan numbers for 32 patients 54
Figure 25: Diagrams plotting $\Delta D_{50\%}/D_{50\%\_ori}$ and $\Delta V_{50\%}/V_{50\%\_ori}$ of bladder and rectum between scenario 2 and scenario 1 vs. plan numbers for 32 patients 55
Figure 26: Comparison of isodose curves between scenario 3 (daily translation with correction) and scenario 1 at the isocentric axial plane 56
Figure 27: Comparison of DVH curves for PTV, CTV, bladder and rectum between scenario 3 (daily translation with correction) and scenario 157
Figure 28: Diagrams plotting (a) $\Delta D_{95\%}/D_{95\%\_ori}$ and (b) $\Delta V_{95\%}/V_{95\%\_ori}$ for PTV, CTV and GTV between scenario 3 and scenario 1 vs. plan numbers for 32 patients 58
Figure 29: Diagrams plotting $\Delta D_{50\%}/D_{50\%\_ori}$ and $\Delta V_{50\%}/V_{50\%\_ori}$ for bladder and rectum between scenario 3 and scenario 1 vs. plan numbers for 32 patients 59
Figure 30: Comparison of isodose curves between scenario 4 (daily translation plus rotation without correction) and scenario 1 at the isocentric axial plane for patient No. 1. 60
Figure 31: Comparison of DVH curves for PTV, CTV, bladder and rectum between scenario 4 (daily translation plus rotation without correction) and scenario 1 for patient No. 1 61
Figure 32: Comparison of isodose curves between scenario 5 (daily translation-plus-rotation with translation correction) and scenario 1 (original plan) at the isocentric axial plane for patient No. 1. 62
Figure 33: Comparison of DVH curves for PTV, CTV, bladder and rectum between scenario 5 (daily translation plus rotation with translation correction and no rotation correction) and scenario 1 for patient No. 1. 63
Figure 34: Axial CT images of a patient © with one hip prosthesis: a) original CT image with metal streaking artifacts; b) artifact-corrected CT image; c) original CT image fused with US image; d) prostate contoured on US-aided CT images. 69
Figure 35: PTV contours from artifact-degraded, artifact-corrected and US-aided CT images for patient C at isocenter axial slice. 70
Figure 36: Isodose curve comparison at isocenter axial slice for (a) patient A, (b) patient B, and (c) patient C: artifact-degraded vs. artifact-corrected scenarios..... 71
Figure 37: DVH curves for PTV, bladder, and rectum derived from artifact-degraded and artifact-corrected scenarios for patient B. 72

Chapter 1 Introduction

1.1 Radiotherapy Treatment for Prostate Cancer

Prostate cancer is the most common cancer among Canadian men. It is estimated that 24,700 men will be diagnosed with prostate cancer and 4,300 will die of it in 2008. In general, 1 in 7 men will develop prostate cancer during his lifetime and 1 in 27 will die of it [1].

Several treatment options can be used alone or in combination to treat malignant prostate cancer, based on the stage of the cancer and other case-specific considerations. These options include radiation therapy, brachytherapy, radical prostatectomy, hormonal therapy, and chemotherapy. Among them, radiation therapy has been used to treat the majority of prostate cases [2].

In general, a radiation therapy prescription calls for delivering as large a dose as possible to the tumour in order to kill all tumour cells while limiting the dose to the surrounding normal sensitive tissues as much as possible [3].

External (photon) beam radiotherapy (EBRT) is the common choice, accounting for approximately 90% of all radiotherapy treatments while the remainder are treated with other approaches including brachytherapy [4]. In recent years, EBRT has advanced greatly, especially in clinical applications of emerging techniques such as 3D Conformal Radiation Therapy (CRT), Intensity-Modulated Radiation Therapy (IMRT) and Image-Guided Radiation Therapy (IGRT) like TomoTherapy® [5-7]. IGRT adopts imaging technology to guide the localization of radiation target during RT treatment. Computed Tomography (CT), KV or MV portal imaging, and ultrasound imaging (US) have been employed as image guidance. With the help of guidance imaging, modern RT techniques have the potential advantages of further reducing the treatment margin by more accurately positioning the target. A more highly conformal dose can be delivered to the target tissue while lower dose is delivered to the surrounding normal tissue and Organs-At-Risk (OARs). Conforming is the main advantage of the emerging techniques over conventional radiotherapy and helps to deliver a higher fraction dose to lesions with fewer complications and relatively low morbidity [8, 9].

1.2 Prostate motion in Radiotherapy Treatment

The prostate usually translates, rotates, and alters its shape and volume during the course of radiotherapy. Generally, these changes are defined as "motion" which can be divided into interfraction motion (between fractions) and intrafraction motion (during one fraction). Intrafraction motion is mainly due to filling of bladder and rectum, rectum gas, and respiratory. At the MGH, the entire prostate is set as the treatment target in EBRT. Since the target is located far from the lungs and surrounded by pelvic bone, its deformation and intrafraction motion are negligible [10]. However in some cases, especially those treated in combination with hormone therapy, up to 20% reduction in prostate volume had been reported [11].

The prostate's interfraction motion, including rigid translation and rotation, mainly comes from variation in the filling of the rectum and bladder as well as leg rotation between fractions. Previous studies [11-13] show that prostate interfraction translation is most significant in the anterior-posterior (A/P) direction with a maximum magnitude of 1 - 2 cm, followed by the superior-inferior (S/I) and right-left (R/L) directions. The majority of rotation occurs along the R/L axis. Small rotation may occur along the S/I and A/P axes, respectively [14, 15].

1.3 Challenges imposed by prostate motion

The existence of interfraction motion imposes a challenge for conformal EBRT of prostate cancer [16-19]. To achieve the maximum radiobiological effects, high radiation dose should be delivered to the target volume in accordance with the treatment plan and fractionation [20]. Because a treatment plan is developed before the first fraction, based on pre-treatment images, fractionation unavoidably produces intrafraction geometric discrepancies between the planning stage and the treatment stage due to the uncontrolled motion of the position, orientation, shape, and size of the patient body, target and internal organs. At the same time, conformal delivery techniques shape the beam to fit the target with very sharp dose gradients in the transition region between the target and normal tissue. Therefore, the conformal dose plan would easily lose its advantages if a large intrafraction or interfraction geometric discrepancy exists, because the relation between the patient target and the beams will differ considerably from what was planned [19, 21].

EBRT planning utilizes large margins to account for the motion of the target, as addressed by ICRU Reports 50 and 62 (34, ICRU 1993, 1999). These reports define the relevant terminology. First, the gross tumour volume (GTV) is defined as the volume containing demonstrated tumour. Second, the clinical target volume (CTV) is defined to enclose the GTV plus a margin to account for possible sub-clinical disease. The planning target volume (PTV) is defined by the CTV plus an "appropriate" margin to allow for geometrical variations such as patient movement, setup uncertainty and organ motion. Typically, up to 1.5 - 2 cm margins would be added to the CTV to define the PTV for prostate cancer treatment. Although adding large margins increases the likelihood of target coverage, it also exposes larger volumes of surrounding tissue to a higher radiation dose thus increasing the risk of complication. Conformal EBRT has the potential to produce sharper dose gradients at the edge of the PTV, enabling an escalation of the tumour dose without increasing the risk of complications. However, a highly conformal EBRT plan is inherently more sensitive to (prostate) target motion which could lead to delivering a dose to the tumour significantly lower than the prescribed dose thus resulting in failure of tumour control. Therefore, considering the potential risk of patient and organ motion, the benefit of conformal radiotherapy for prostate cancer could become negligible or even negative if we do not correct for motion of the target.

1.4 Potential solutions for prostate motion

IGRT has been investigated in the last decade and is widely considered as the best solution to correct for interfraction motion of the prostate. Various imaging modalities have been used in IGRT for prostate cancer. Portal Imaging was originally used for daily prostate target localization by implanting radio-opaque/gold markers into the prostate [22, 23]. By realigning the patient prior to each fraction, prostate motion could be compensated, allowing for the use of tighter margins around the CTV. Computed Tomography-guided EBRT has also been implemented in some institutions in which integrated CT/linac systems were used [7, 13, 24-27]. For example, the recently developed TomoTherapy device which incorporates an on-board imager (MV and kV CT) is a potentially ideal candidate for IGRT to treat prostate cancer. However, some pitfalls of these CT-guided techniques include their low soft-tissue contrast and additional radiation dose to the patient. An alternative with high intrinsic soft tissue

contrast without any ionizing radiation is found to be the ultrasound (US) imaging. US imaging has been used for interfraction guidance for motion correction during prostate cancer treatment as early as 1999 [28], and is anticipated to play an important role in future IGRT of prostate cancer.

To address the intra-fraction prostate motion, which is significant in the cases of radio-surgery and escalation of dose, real-time tracking and correcting techniques such as an infra-red (IR) optical camera system combined with a stereoscopic kV x-ray imaging system in ExacTrac X-ray 6D (BrainLab AG, Heimstetten, Germany), continual on-line fluoroscopy x-ray imaging in Cyberknife (Accuray Inc., Sunnyvale CA), and 4D US localization system utilizing implanted electromagnetic transponders in Calypso System (Calypso Medical, Seattle, WA) have been developed and studied recently [24, 86, 87].

1.5 US localization in Conformal Radiotherapy

With the advantages of high soft-tissue contrast, a non-invasive technique, high resolution and no radiation hazards, US imaging is not only widely used for the diagnosis of various diseases, but also used to visually and quantitatively localize tumour targets for IGRT, surgery, and brachytherapy seed-implantation. B-mode Acquisition and Targeting (BAT) ultrasound localization system was developed and introduced into radiotherapy in the late 1990s. The BAT system (NOMOS, Sewickley, PA) commercialized in 1999 is now widely used in more than 300 treatment centers in the United States and Canada [29]. Since then, several advanced 3D US imaging localization systems have been developed and applied in clinical practice. All these US localization techniques have the capability of further improving EBRT of prostate cancer [30-32].

The Restitu™ 3D US localization system (Resonant Medical, Montreal, Canada) takes 3D US images at both the planning and treatment stages, and utilizes intra-modality image comparison methods for prostate target localization. Its accuracy, reproducibility, and inter-observer variability have been investigated and verified by many published studies by comparing it with a BAT system, CT, and implanted seed marker localization methods (SM method) [4, 33-38]. The displacement effect due to probe compression was investigated by Ding *et al* 2007 [39]. His group found the displacement of the prostate due to probe pressure was non-negligible when the depression exceeded 20 mm on the patient's abdomen. Conversely, Johnston *et al* 2008 [40] had claimed that the Restitu™

system can not produce localization as well as those obtained with the SM method, thus providing no significant clinical advantages in prostate IGRT.

1.6 Potential use provided by Restitu™ System

Besides its designated function, the Restitu™ system provides physicians with a potential opportunity to measure daily rotation of the prostate. Currently, Restitu™ system only provides the translation parameters for clinicians to correct daily prostate motion. However, the prostate can rotate a large amount if the patient rotates their body or changes their posture [15]. Intra- and inter-fraction rotations change the orientation of the prostate, thus affecting the distribution of the dose actually deposited even if the displacement effects have been fully corrected. This effect is most significant when the prostate has an irregular shape. Consequently, providing rotation parameters for prostate cancer treatments may be therapeutically useful, at least when it comes to accurately assessing the actual dose delivered to the prostate tumour [41, 42].

Fortunately, the positioning reference volume (PRV) which is obtained by US scan at the CT-scan stage and the daily Positioning Guidance Volume (PGV) which is obtained pre-treatment can be extracted from the Restitu™ system. Rigid body co-registration between the PRV and the PGV provides six transformation parameters: 3 for translation and 3 for rotation. Therefore, daily rotation of the prostate can be derived by these transformation parameters.

1.7 Purpose of this thesis

Restitu™ is a newly-developed 3D US localization system and has been utilized in the clinic since 2005. Its clinical outcomes and dosimetric effects have been investigated and published by several authors [43-46]. The purpose of this thesis is to further evaluate the clinical value of this innovative system. Based on patient data collected at the Department of Radiation Oncology in the Montreal General Hospital (Montreal, Quebec, Canada) since 2006, five distinct, but related, topics will be addressed in this thesis.

1.7.1 A Statistical analysis of prostate daily displacement

2D US localization of the prostate has long been suspected of being problematic due to misidentification target structures, probe pressure, and inter-observer variability. Further investigation on these factors is crucial to understanding the limits of its clinical application. This is also true for the Restitu™ 3D system. Making a retrospective

statistical analysis on the data set of prostate daily displacements can provide a measure of the mean displacement along with the systematic and random uncertainties of an average prostate position. The statistical results of prostate displacement provided by Restitu™ can be used to compare with those obtained from other localization systems such as the BAT system, implanted seed marker and CT imaging. Comparisons of these results would provide a measure of typical prostate motion. The statistical results could be also used to establish an optimal CTV-to-PTV margin for prostate CRT when a prostate motion correction method has not been adopted.

1.7.2 Patient dose recalculation using a BEAMnrc-XVMC method

The key to assessing the dosimetric impact of daily displacement corrections in EBRT is to calculate the total dose from the sum of the dose delivered at each fraction, which should include the actual measured motion and the corresponding beam parameters from individual sessions. Commercial treatment planning systems (TPS) can be used to recalculate the fraction dose and then to evaluate the dose in terms of the dose volume histogram (DVH), the tumour control probability (TCP), and the normal tissue complication probability (NTCP) [43, 44]. However, their results are somewhat controversial since current commercial TPSs normally use pencil beam convolution/superimposition algorithms to calculate the patient dose distribution. These algorithms are based on the assumption of a homogenous patient phantom and neglect the complex details of organ and tissue variations. Prior studies reported that these assumptions may produce a difference of up 10% between the calculated and measured doses at interfaces between soft tissue and high density organs [45, 46]. Even after applying heterogeneity corrections, the dose distributions calculated by different methods such as analytical algorithm and Monte Carlo (MC) method, show a significant difference in patient DVH analysis [45, 47-49].

MC methods are currently recognized to be the most accurate dose calculation method in accounting for complex geometries and patient heterogeneities. Mark *et al* 2005 adopted the McGill Monte Carlo Treatment Planning system (MMCTP) to recalculate the dose delivered at each treatment fraction, taking into account the changes of prostate position and volume [4]. The DVH analysis in her study was based on the

fraction dose distribution instead of the total dose distributions which would account for all the patient's sessions.

In this thesis, a fast MC method called XVMC (VMC method for X-ray beam) will be employed to calculate the patient's fraction dose [50]. In order to obtain total dose distributions of prostate patients, the fraction doses are summed by adding doses in the matrices with taking into account their daily shifts.

1.7.3 Prostate rotation measurements

As mentioned above, prostate rotation may be very important in clinical applications. When the prostate rotates too much, the dose actually delivered may be affected. In these cases, changing the posture of the patient's body may be necessary to reduce their rotation. Theoretically, by the PGV-to-PRV registration process, the daily prostate rotation can be determined.

In this thesis, an algorithm based on Mutual Information (MI) registration has been developed to detect the prostate rotation along three axes. The rotation parameters will be used to assess its dosimetric effect on the patient treatment.

1.7.4 Dosimetric impact of prostate motion and metal hip prosthesis

The dosimetric effect of prostate motion has long been recognized although its significance remains uncertain. With the help of the XVMC method, patient's fraction and total dose distributions can be more accurately calculated for the cases with and without prostate motions, with and without metal artifact, as well as the case with prostate motion correction. This thesis will compare their differences with regard to DVH analysis and statistical measures. Their results are expected to display the extent of influence by prostate daily motion and metal hip prosthesis to appreciate the value of US localization system.

1.8 Structure of this thesis

The structure of this thesis is as follows:

Chapter 2 describes the retrospective statistical method and MI registration on daily prostate volume.

Chapter 3 describes the XVMC dose calculation and DVH analysis method including linac modeling, calibration and verification.

Chapter 4 presents the retrospective analysis on daily displacements of prostate patients.

Chapter 5 gives the DVH analysis results of 32 simulated patients with and without motion correction under five hypothesized scenarios.

Chapter 6 presents the dosimetric impact of metal artefacts in three prostate patients.

Chapter 7 makes an overall conclusion and discusses some future works.

Chapter 2 Methods and Materials (1)
A Retrospective Analysis and Rotation Measurement

Prostate cancer is the second most common cancer among males, only outnumbered by lung cancer. At the Montreal General Hospital (MGH) we treat approximately 100 prostate cancer patients every year of which more than 60% chose conformal EBRT, 10% chose brachytherapy, and the rest chose non-radiation treatment like chemotherapy and prostatectomy.

US localization for prostate radiotherapy has been incorporated into clinical routine at the MGH since 2001 when a 2D US BAT (B-mode Acquisition and Targeting, North American Scientific, Chatsworth, CA) system was introduced. In 2006, the MGH began using Restitu™ US system which utilizes an intra-modality verification method (IMVM) to monitor the prostate displacement based on 3D images [4]. Interfraction daily displacement (translation) data for 890 fractions between July 1st, 2006 and January 28th, 2008 has been collected and analyzed from 32 patients. In addition to displacement, organ rotation is also considered for 3 specifically-chosen patients as a preliminary study.

2.1 Method for retrospective analysis on prostate daily displacement

A descriptive statistics (see section 2.1.1) were used for the retrospective analysis on clinically treated patients. Its results can be used to determine the amount of prostate motion, which is essential for oncologist to determine the internal CTV-to-PTV margin. Our analysis will examine 3D US localized prostate motion in terms of the three major axes (anterior-posterior, lateral, and superior-inferior), including the mean displacement (systematic error) and standard deviation (random error), in addition to deriving corresponding PTV margin in each axis direction. These results will be compared to 2D US system, CT and portal imaging. By utilizing the same statistical measures as employed in prior studies, the statistical results from 3D US system can be comparable to published data. This comparison will add useful information about prostate displacement into the existing data set while, simultaneously, verifying the accuracy and effectiveness of the 3D Restitu™ system.

2.1.1 Data acquisition

Data from 32 patients with a total of 890 treatment fractions of conformal EBRT with Restitu™ localization have been acquired. All patients involved in this study gave their written consent to participate. In a typical treatment cycle a patient has a simulation CT scan and a reference US scan before treatment planning. A localization US scan immediately before treatment normally indicates a need for repositioning the patient before treatment delivery takes place. The prostate volume and 3D daily displacements measured via the US localization procedure were then extracted from the US workstation.

US Localization System

The 3D Restitu™ US localization system which includes the tracking camera, US probe, calibration phantom, workstation and their functional interconnections is shown in Figure 1.

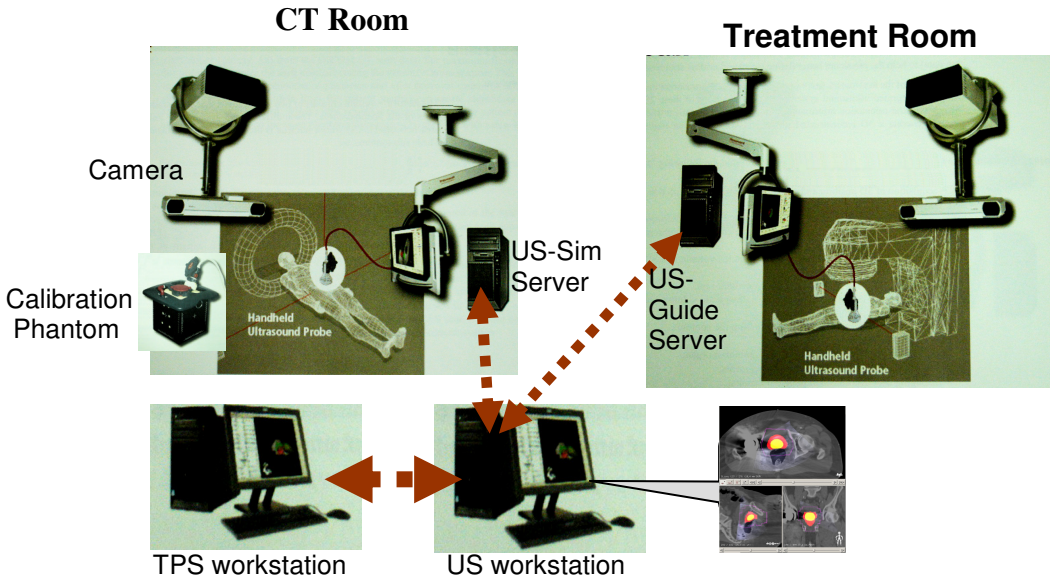

Figure 1: The scheme of 3D Restitu™ US localization system [Courtesy of Resonant Medical Inc]

Restitu™ uses B-mode 2D US probes and optical tracking to arrange images into a 3D US volume as shown in Figure 1. Usually high frequency probe C5-2 probe is chosen to scan the patient prostate. The working frequency of US probe ranges between 3.5 MHz to 13 MHz, determined by the chosen image depth. The image depth can be set as 13 cm, 15 cm, or 18 cm, based on patient's size (small, medium, or large). The US probe is placed on the patient's abdomen with an infrared light emitting diode array (IRLED) to send infra-red signals that get detected in space by two tracking cameras. As the probe is

swept through an arc, approximately 200 2D US images are acquired and sent to the US workstation. Each 2D US image has a typical size of 640 x 405 or 640 x 473 pixels. The US scan for one patient can be completed within 5 minutes by therapists with help of oncologists, radiologists and medical physicists.

Simulation CT and US scan

Patients were positioned in a supine position without any special immobilization devices and tattooed at their skin for laser aligning in the simulation CT room. Three bead balls (BBs) were attached on the anterior and lateral tattoos to define the isocenter of the original CT images. These tattoos were not changed throughout treatment courses, providing a fixed reference system. Once the patients were positioned, the therapists performed a 3D US scan over patient pelvis with Restitu™ prior to its CT scan. US images then are transmitted into the US workstation and are reconstructed to produce 3D image. Prostate contouring is manually or automatically made on US images by an oncologist. Based on the outlined contours, a prostate volume known as positioning reference volume (PRV) is calculated.

After US scanning, a Philips AcQSim CT scanner (Philips Medical Systems, Andover, MA) is used to obtain CT images for treatment planning. A technique of 120 kV, 300 mA was adopted to obtain 2.5 mm thick slices through the pelvis for all 32 patients. Patients were contoured based on CT images on the AcQSim Software (Phillips Medical Systems, MA). The CADPlan treatment planning system (Varian Oncology System, CA) was used to make conformal treatment planning for these patients. Conventional prescribed doses of around 72 Gy in total were given to the prostate in 20-40 fractions. Before each fraction treatment, the isocenter position of patient target and treatment parameters were uploaded to the treatment machine while prostate contours based on CT images were uploaded to the Restitu™ US workstation for US-CT registration. After daily US localization, treatments were delivered with 18 MV X-ray beams on a Varian 2300 C/D linear accelerator using a conformal prostate technique of five beams.

US scan before treatment

Patients in this study took supine position on the treatment couch. To immobilize the patient, first step is to move patient and couch so that their tattoos would align with treatment room lasers. Second, patient is shifted according its treatment plan to locate the

treatment target at the machine isocenter, then new reference marks indicating target position are tattooed onto patient skin or immobilization devices. These new tattoos are used to align the target with the machine isocenter for all successive treatment fractions.

After patient has been immobilized, a 3D US scan for localizing the prostate is performed using the same Restitu™ system. Similar to obtaining PRV in CT room, a daily prostate volume called positioning guidance volume (PGV) can be produced and calculated based on the US scan just before each fraction treatment. The PGV is in the same coordinate space of the PRV. Mutual Referencing™ technology which automatically compares the PRV acquired at planning simulation to the PGV acquired prior to each treatment delivery is then employed by Restitu™ to derive three orthogonal axial displacements between the PGV and PRV, based on rigid body model.

To correct these displacements, repositioning patient is used at the MGH. This is realized by inversely moving the patient couch according to the daily displacement. The movement directions and distance of couch will be provided by Restitu™ system and displayed on its monitor, as shown in Figure 2. The couch movement is then monitored and fed back to the Restitu™ system to ensure that the proper shift had been made. After repositioning the patient, the treatment was delivered and the displacement data was recorded.

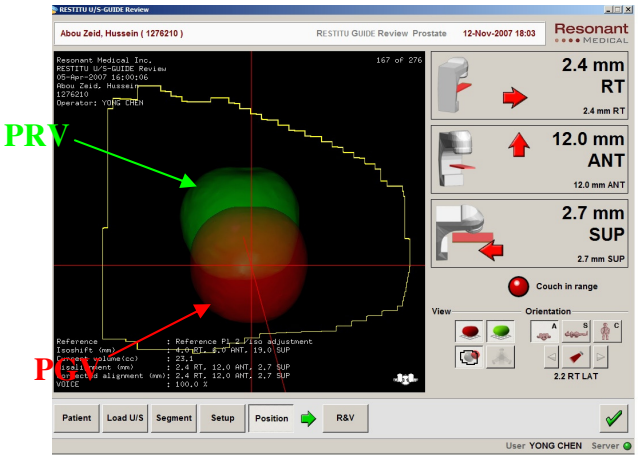

Figure 2: A display of couch movement parameters from Restitu™ system

Measurements

Daily displacement is obtained by using Mutual Referencing™ technology provided by the Restitu™ system. To do so, it is necessary to ensure that both PRV and PGV have a

same coordinate space. This is realized by a procedure called as room calibration, as shown in Figure 3.

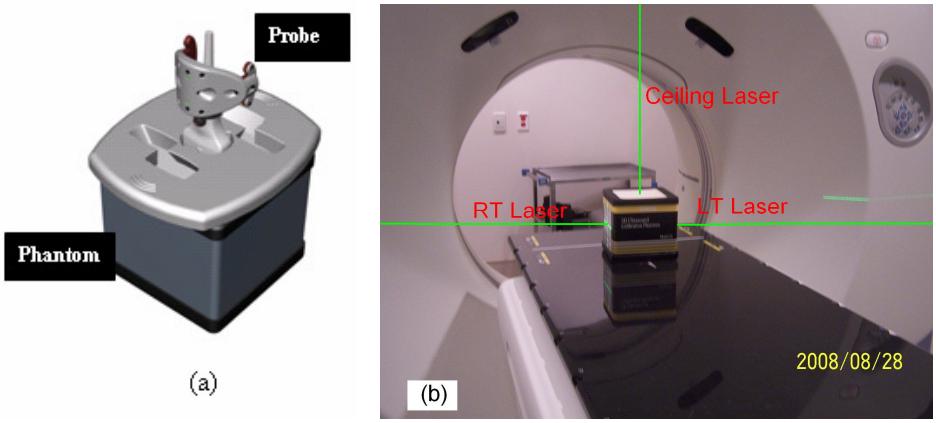

Figure 3: (a) Probe calibration and (b) Room calibration by aligning laser to the reference point on surface of the calibration phantom

The spatial relationship between the images and the isocenter in the CT room or treatment room is derived using a calibration phantom with known external reflectors and known internal structures. With the phantom aligned to the CT or treatment room lasers, the infrared camera determines the room coordinate system by measuring the distance to the external reflectors.

Restitu™ derives the actual couch movement based on the daily prostate displacement. The direction and distance of couch movements for all patients have been saved in the US workstation. The displacement data for 32 patients were obtained by retrieving these couch movements and then reversing their directions.

Criteria for selecting patient data

From July of 2006 to January of 2008, 43 patients were treated with prostate localization using the Restitu™ system at the MGH, however only data of 32 patients among them are included in this study. The reasons for excluding eleven patients were: incomplete images, partial fraction using US localization technique, setup errors existed thereby invalidating the collected data, or a lack of consent given by the patient for the purpose of this study. Therefore, the selection criteria for including a patient are set as follows:

1. The patient was treated with conformal external beam radiotherapy;
2. The Restitu™ system was used to localize the prostate for more than 4 fractions;

3. No known setup errors existed in the CT simulation and treatment procedure;
4. A signed written consent was obtained from the patient to allow their information to be used for this research.

2.1.2 Data analysis

A descriptive statistics (including the mean and the standard deviation) is used in the analysis of daily prostate displacements. 32 prostate patients in this study have a total sample size of 890 localizations. Daily prostate displacement is presented in three spatial directions: Ant/Post, lateral, and Sup/Inf. Majority of collected data also includes daily volume changes for their prostates.

Statistical analysis is performed on data from each patient. The data is used to compute the individual mean displacements ($\overline{\Delta x_i}, \overline{\Delta y_i}, \overline{\Delta z_i}$) and standard deviations ($\sigma_{x_i}, \sigma_{y_i}, \sigma_{z_i}$). Note that the mean displacement and standard deviation include both systematic and random interfraction uncertainties in the treatment planning and patient setup procedures [51]. The sample population systematic and random uncertainties were computed for the entire data set from the individual patient means and uncertainties as equation (2.1) [52] for lateral, Ant/Pos, and Sup/Inf directions:

RT/LT direction:

$$\Sigma_x = \frac{1}{N-1}\sqrt{\sum_{i=1}^{N}\left(\overline{\Delta x_i} - \overline{\Delta x}\right)^2}, \qquad \sigma_x = \sqrt{\frac{1}{N}\sum_{i=1}^{N}\sigma_{xi}^{\ 2}} \qquad (2.1)$$

Where, Σ_x represents the standard deviation of systematic uncertainties of all samples; σ_x represents the standard deviation of random uncertainties; *N* is the total number of sampled patients.

Another statistical analysis is performed on the entire data set, which does not distinguish patients individually, to investigate the statistical distribution of daily prostate displacement. A typical frequency histogram based on fractions of a chosen patient was shown in Figure 4.

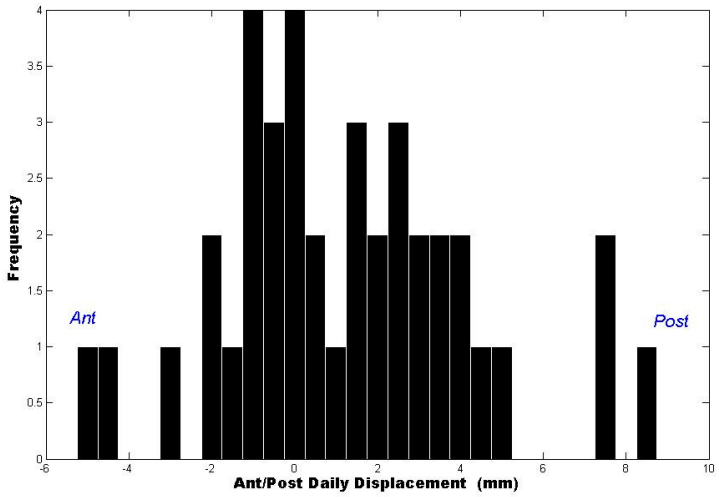

Figure 4: Ant/Post directional histogram of displacement for one patient with 37 fractions

Based on coverage probability, the contributions to the PTV margin attributable to systematic effects are assessed to be about three times as large as the contributions due to purely random deviations [53]. Therefore, systematic and random uncertainties for the entire sample could be used as a measure of realistic PTV margins along each axis [54, 55] to quantitatively evaluate the internal PTV. A margin recipe proposed by Stroom *et al* [54] is adopted in this study, shown as equation 2.2:

$$D_x = 2\Sigma_x + 0.7\sigma \tag{2.2}$$

The main reason to choose Stroom's margin recipe is that it combines the systematic and random uncertainties of prostate daily motion to work out a PTV margin, thus helpful to make a quantitative comparison between different proposed methods. The authors used clinically shaped CTVs and clinical distributions in its derivation to ensure more than 99% of the CTV could get at least 95% of the prescribed dose.

2.2 Rotation measurement

The Restitu™ system only provides a measure of the daily displacement of the prostate for therapists to realign the patient. An in-house code was developed in this study to derive the daily rotation of prostate based on the PRV and PGV which structures were exported from Restitu™ in terms of DICOM files. The code can recalculate the translation and rotation of the prostate by registering PGV to PRV with the maximum mutual information (MI) registration algorithm.

2.2.1 Extracting 3D prostate contours

The PRV and PGV are defined by contours at the CT and treatment stages using pre-treatment US images. In-house software, *BrachyGUI* [56], was used to extract prostate contours from their US DICOM images. These extracted contours are expressed in absolute coordinates and saved as separate 3-by-*N* matrices whose columns are the $\boldsymbol{x}$, $\boldsymbol{y}$, $\boldsymbol{z}$ coordinates of the points at the surface of the volume. The 3D PRV and PGV images can be reconstructed by setting a weight of 1 for all points on the contour surface and a weight of 0 for all other points.

2.2.2 MI registration method based on 3D contour

The purpose of applying the MI registration method in the study is to derive the daily translation and rotation of the prostate. The conventional MI registration algorithm originally based on image contrast was modified to base on prostate contour surface. Assuming that the prostate is a rigid body over the entire course of treatment, the maximum MI will exist between the daily PGV and PRV (from the CT simulation stage). Therefore, the object of registration is to find a rigid transformation matrix, $\boldsymbol{A} = [\boldsymbol{R}, \boldsymbol{t}]$, *that* transforms the PGV data set and ensures that maximum MI will exist between the PRV and the transformed PGV. Where, $\boldsymbol{A}$ is a 4 by 4 translation matrix, $\boldsymbol{R}$ is a 3 by 3 rotation matrix with the constraint of $\boldsymbol{R}\boldsymbol{R}^{T} = \boldsymbol{I}$ = identity matrix, and $\boldsymbol{t}$ is a 3 by 1 translation vector.

The translation vector is obtained directly from the Restitu™ translation parameters: $\boldsymbol{t} = (\Delta x\ \Delta y\ \Delta z)^{-1}$. $\boldsymbol{R}$ was decomposed into three orthogonal rotations $\boldsymbol{Rx}$, $\boldsymbol{Ry}$, $\boldsymbol{Rz}$, so that

$$\boldsymbol{R} = \boldsymbol{Rx}(\alpha)\,\boldsymbol{Ry}(\beta)\,\boldsymbol{Rz}(\gamma) \qquad (2.3)$$

Equation 2.3 represents a rotation about the z axis through an angle of γ, followed by a rotation about the y axis through an angle of β, and followed by a rotation about the x axis through an angle of α. The definitions of α, β, γ are illustrated in Figure 5.

The normalized MI used in our method is defined as [57]:

$$MI = -\sum P_{AB}(i,j)\log\frac{P_{AB}(i,j)}{P_A(i)P_B(j)}\Bigg/\sum P_{AB}(i,j)\log P_{AB}(i,j) \qquad (2.4)$$

Where $\boldsymbol{i}, \boldsymbol{j}$ are the intensity levels (0 or 1 for our cases) of images A and B; A is the PRV image and B is the PGV image; $P_{..}(..)$ is the probability distribution of the corresponding intensity levels.

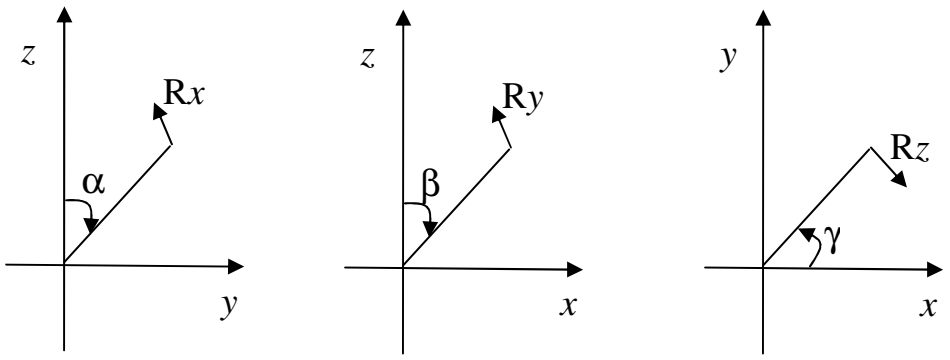

Figure 5: Coordinate systems for three rotations

The larger the value of MI, the better is the registration. Finding the rotation $\boldsymbol{R}$ is then simply a problem of maximizing the MI subject to the constraint that $\boldsymbol{RR}^{\mathrm{T}} = \boldsymbol{I}$. A global search method has been used to solve the problem which benefited from the limited range of prostate rotation. The algorithm developed for maximum MI registration method is listed in Scheme 1.

Let $\boldsymbol{A}$ denote the rigid transformation matrix, $\boldsymbol{R}$ denote rotation matrix, and $\boldsymbol{t}$ denote the translation matrix.

1. Initialization: $\boldsymbol{R(0,0,0)}$, $\boldsymbol{t} = (\Delta x \ \Delta y \ \Delta z)^{\mathrm{T}}$;
2. Construct $\boldsymbol{A}$ from $\boldsymbol{R}$ and $\boldsymbol{t}$: $\boldsymbol{A} = [\boldsymbol{R}, \boldsymbol{t}]$.
3. Transform the PGV image using the transformation matrix $\boldsymbol{A}$;
4. Calculate the normalized MI between the transformed PGV and PRV;
5. Use iteration step size of 0.1° for all angular variables, and 0.1 mm for all translation variables;
6. Ranges of variables are limited to: -10.0°- - 10.0° for $\boldsymbol{Rx}$; -5.0° - 5.0° for $\boldsymbol{Ry}$ and $\boldsymbol{Rz}$; -1 mm -1 mm for translation;
7. Loop from step 1 to 5, use all possible values for the above variable ranges to search one set of $\boldsymbol{R}$ and $\boldsymbol{t}$ which corresponds to the maximum value of the MI, and then record the set.

Scheme 1: Algorithm for maximum MI registration method

2.2.3 Implementation of detecting prostate rotation

A software program, MI-Registration, based on MATALAB 7.0 has been developed by the author to implement the maximum MI registration algorithm outlined in Scheme 1. It takes PRV contours, PGV contours, and the daily displacement data as its inputs. The registration process is completely automated; however, the results could be evaluated manually. Registering a PRV with a PGV by using a Pentium 1.73 GHz processor requires approximately twenty minutes. Figure 6 shows that there is a good match between the PGV and PRV after registration. The rigid body transformation matrix $\boldsymbol{A}$ is uniquely determined by finding the Maximum MI value. The required translation and rotation parameters then could be directly derived from $\boldsymbol{A}$.

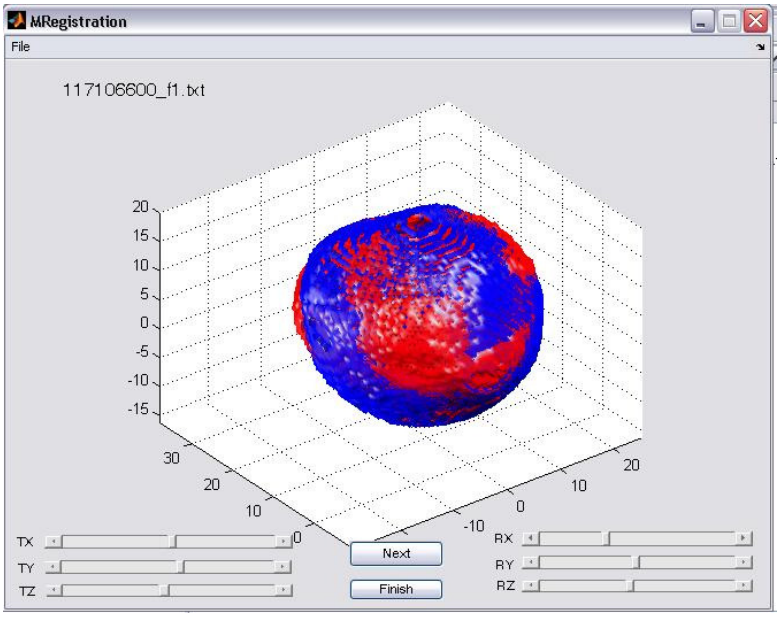

Fraction	Tx mm	Ty mm	Tz mm	Rx degree	Ry degree	Rz degree
1	-1.03	-2.44	0.96	-3.42	-0.07	-0.24

Figure 6: PRV surface (in blue) and PGV surface (in red) after MI-registration

Chapter 3 Methods and Materials (2)
Patient Dose Calculation and Evaluation

3.1 Introduction

Prostate motion produces a different dose distribution delivered compared to the initial treatment plan, resulting in a loss of TCP and a high NTCP. Interfraction prostate motion which is up to 2 cm in many statistical studies [41, 58] represents a target localization problem in prostate EBRT. 3D US localization system could be employed to localize and realign the target at the beam isocenter by repositioning patient on the treatment couch [59, 60].

Another crucial issue then arises: what is the dosimetric consequence of repositioning the patient based on daily US localization? Wertz *et al* 2007 [60] reported that translational corrections based on image guidance methods can improve the dose distribution and target coverage in most cases. But his analyses are just based on single treatment fraction dose distribution re-calculated by using Eclipse TPS and MC methods with taking into account the daily displacement of prostate. In addition, the prostate may have a non-negligible deformation and rotation (when the prostate base and apex do not move rigidly) impact on the dose distribution [61, 62]. However, up to now, it is not clear whether a 3D translation correction really improves target coverage, or whether it is also necessary to correct for rotation by accordingly rotating the treatment couch or changing patient posture [63-65].

To answer these questions, the key is to recalculate the patient total dose based on actual treatment setups and delivery parameters, and to make a dosimetric analysis based on the real target volume which may move or alter during treatment. In this chapter, the BEAMnrcmp/EGSnrcmp and XVMC Monte Carlo codes (NRC, Ottawa, Canada) [66] are used to recalculate the fraction dose to the patient. After patient fraction doses were calculated, they are summed to suggest a total dose distribution. A program was developed to sum the fraction dose by taking all daily shits into account. Finally, the dose distribution to target and OARs are evaluated in terms of isodose curves and DVH analysis. This experimental process is shown in diagram 1 as following:

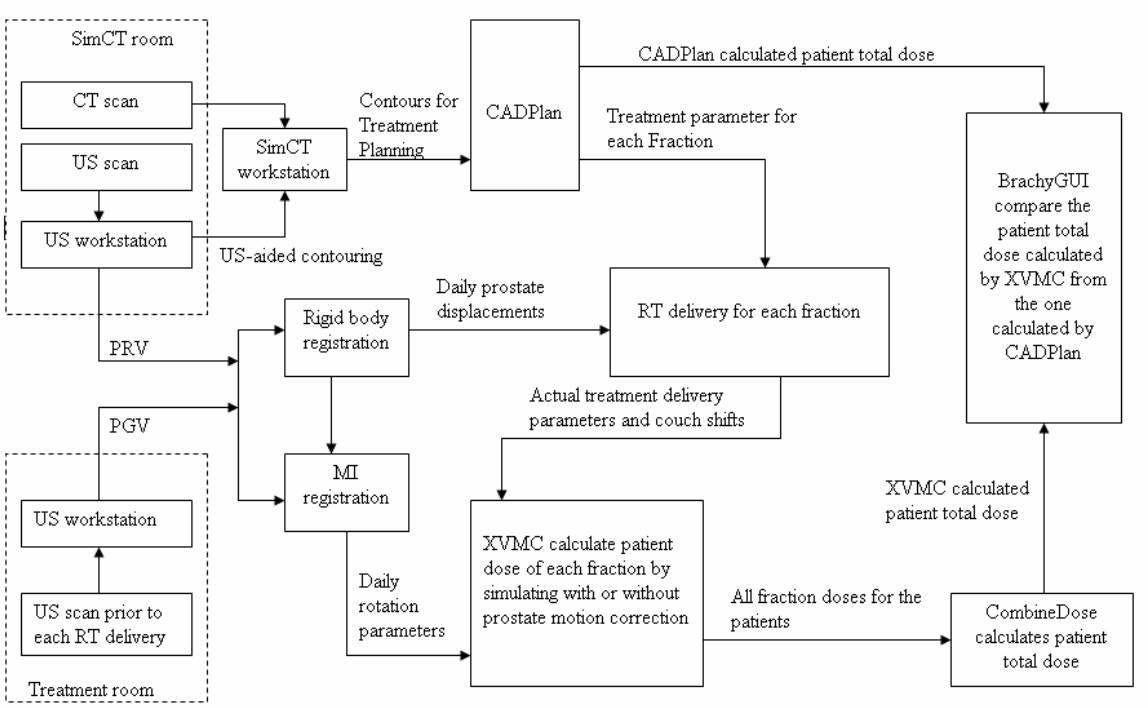

Diagram 1: Experimental process for assessing the dosimetric impacts of prostate motion

In this analysis, five hypothetical scenarios have been simulated, as shown in Table 1.

Scenario No.	Prostate Motion	Correction Methods
1	No translation	No correction
2	Translation	No correction
3	Translation	Translation-correction
4	Translation and rotation	No correction
5	Translation and rotation	Translation-correction only

Table 1: Five hypothesized scenarios with considering translation and rotation

3.2 XVMC – a fast MC Method

By compromising between computation speed and accuracy, the EGSnrcmp/BEAMnrc [67] was used to model the 18MV Varian 2300C linac. Its components are simulated separately to obtain a patient-specific phase space (ph-sp) file at the lower surface of the exit window. The XVMC code [68] is then used to calculate the fraction dose distribution to the patient CT matrix. Compared to the BEAMnrc/DOSXYZnrc approach (NRC, Ottawa, Canada) which generally takes eight hours to complete a simulation for one fraction dose, the BEAMnrc/XVMC simulation speed can be improved dramatically. The time for one simulation could be reduced to less than one hour on the McGill Blade cluster with a clinically acceptable statistical

uncertainty (±2%). The McGill Blade cluster is consists of 20 dual CPU, a PIII 500 GHz master server, and two slave computers (a PIII 900 GHz, P4 3.4GHz and an AMD 1800 processors).

3.2.1 Linac simulation

The BEAMnrc code (NRC, Ottawa, Canada) has been proven to be an accurate method for linac simulation in many prior studies [66-71]. The MC group in McGill has established a set of component modules for the Varian 2300C linac which was used to treat the prostate patients in this study [72]. To speed up the simulation for linac head components, the established modules have been simplified. The simplification of these modules is verified by comparing simulated dose distributions with those measured in a water phantom.

3.2.1.1 Physics models for a Varian 2300C linac

All prostate patients involved in this study were treated with 18 MV photon beams from a Varian linac 2300 C/D at the MGH. Two main factors have been considered to simplify the linac modules for this study: (1) to focus on the dose to the prostate target and OARs, and neglect the patient's surface dose and whole-body dose; (2) to neglect Compton scattered electron, photo-electron, pair production products incident on the linac multi-leaf collimator (MLC) leaves for they contribute less than 0.05% to the open field dose for all field sizes by comparing to the dose with fully simulation those particle transportations [73] This means that we can reduce the outer boundaries of the linac components, and neglect the tongue-groove effect of MLC. With considering the above-mentioned factors, we established the linac model in BEAMnrc code as shown in Figure 7. In Figure 7, CL2300 Linac is modeled as ten components, encompassed by vacuum. Their parameters for BEAMnrc simulation are listed in Table 2.

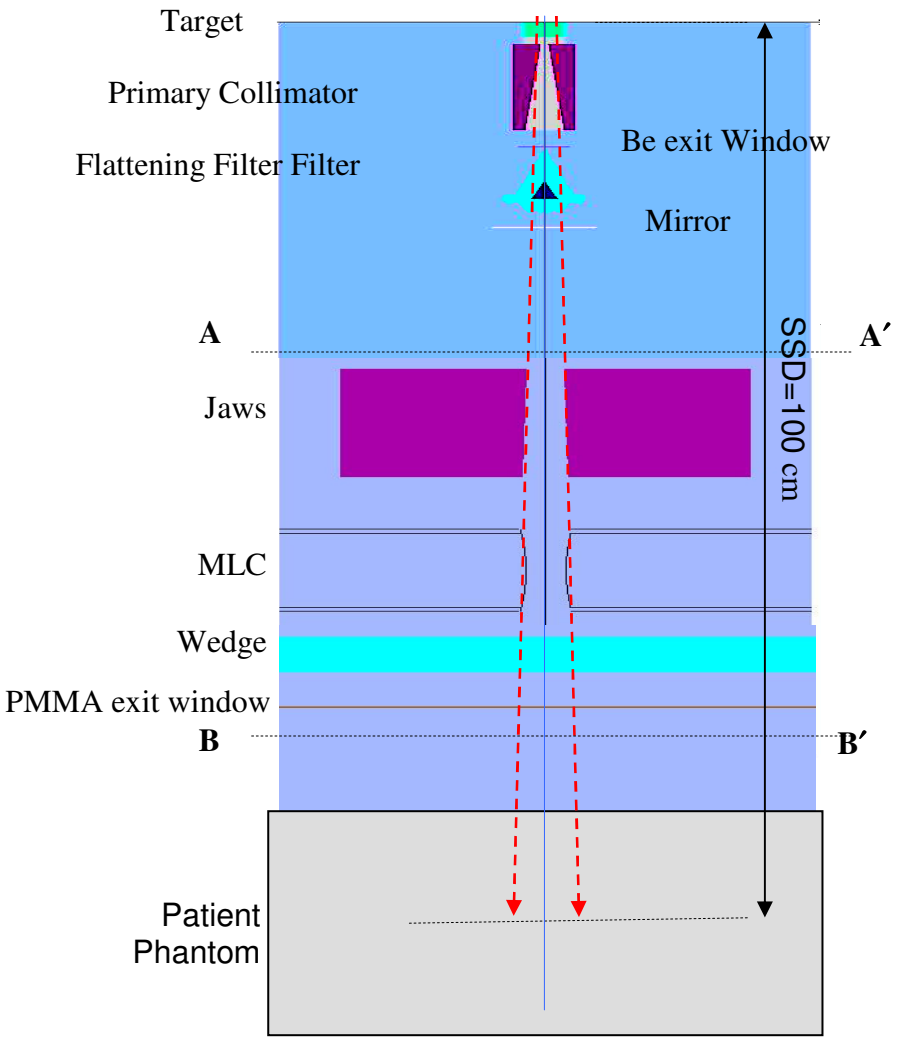

Figure 7: Physic Models of Varian CL 2300 Linac [74]

Target modules (TMs) are defined as those modules labelled 1-6 in Table 2 including the target, primary collimator, flattening filter. The rest modules including jaws, MLC, wedges and PMMA window are defined as the beam modification modules (BMMs). TMs are fixed and specific for CL2300C linac while BMMs are patient-specific for their opening and outside boundaries change with each patient treatment plan. To reduce the simulation time on BMMs, their outer boundaries are set only 3 cm larger than the planned primary beam. The PMMA window is specifically set to eliminate low energy electrons. The ph-sp file is collected immediately after the PMMA window. The materials around TMs and BMMS are set to vacuum and air, respectively.

No.	Components	Materials	Thickness (cm)	Distance to Target (cm)
1	Target	W	0.0635	0
		Cu	0.51	1.016
2	Primary Collimator	W	6.2	1.6
3	Exit window	Be	0.0254	9
4	Flattening filter*	Cu, Fe	5.0	9.27
5	Monitor chamber	Kapton	2.018	14.2
6	Mylar Mirror	MICA	0.00508	17
7	Upper Jaw	W	7.8	28
	Lower Jaw	W	7.8	36.7
8	MLC (McGill)	W	5.94	48.25
9	Static Wedge	Steel	8	57
10	PMMA window	PMMA	0.03	65

Note: * The flattening filter is comprised of 13 layers [74]

Table 2: Simulation parameters for the CL2300 linac components

Among the BMMs, the MLC is modeled as VARMLC provided by the BEAMnrc code, and the static wedge is modeled as SWDG proposed by van der Zee and Welleweerd (2002) [75]. Both were modified in our group to fit an 18 MV beam from the CL2300C [76, 77]. The kinetic electron and photon cut off energies (ECUT and PCUT) are set as 0.521 MeV and 0.01 MeV for all components except MLC where Ecut was set to 18.3 MeV to ensure that all electrons were stopped if they incident on the MLC. The total number of histories was set to 50 million to reach a statistical uncertainty of less than 2% at the beam center. Using the above simplified model, the simulation time for one setup can be significantly reduced from 3 hours to 20 minutes.

3.2.1.2 Strategy for the acquisition of ph-sp file

The ph-sp file collected at the lower PMMA window surface is used as the virtual linac for patient dose calculations. The ph-sp file is a binary file that contains the energy, charge, position, direction, and previous history of millions of particles (including photon, electron and positron). It can be scored at any plane, and can be used as the input (virtual source) for further particle transport in the rest of linac geometry. This method has been used in our study to increase the simulation speed for patient specific beam geometry, because the TMs need only be simulated once. As shown in Figure 7, two ph-sp files are collected at the plane of AA′ and BB′ in the BEAMnrc simulation. The level AA′ is situated at the upper surface of the jaw module. Beyond this level, a complete simulation is carried out to acquire the first ph-sp file. The ph-sp file scored at plane AA' is called as the target ph-sp file. One target ph-sp file is collected for the 18 MV beam of the CL2300C linac by projecting one billion primary histories on the target, producing approximately 50 million particles with a statistical accuracy less than 1%.

The plane BB′ is situated at the lower surface of the PMMA exit window which is 70 cm from the target. Then the ph-sp file collected at the plane BB'is called as the virtual beam ph-sp file. The virtual beam ph-sp file is patient specified and is used as virtual linac by XVMC or DOSXYZnrc to calculate the dose distribution to the patent phantom or water phantom. The total number of particle histories for XVMC simulation is set to 50 million, reaching a statistical accuracy less than 2% in the dose matrix calculated. In our study, five virtual beam ph-sp files are independently simulated for one patient, because a five field isocentric beam technique was used at the MGH for 3D conformal EBRT. Each field may have a different field size, gantry angle, collimator angle, MLC shape, and wedge angle in order to conform the beam to each patient's target.

3.2.2 Patient dose simulation with XVMC code

The XVMC code is a fast MC algorithm for 3D photon dose calculation in radiation therapy. It is based on the Voxel Monte Carlo (VMC) code for electron beams developed by Kawrakow *et al* [69, 70]. XVMC was developed by Fippel *et al* [71]. It was verified by comparing the dose distributions calculated with XVMC to those with the EGS code. The main difference between the two codes is that a fast electron transport algorithm and an initial ray tracing technique have been used in XVMC code in order to reduce the electron transportation time. Fippel *et al* presented that XVMC is more efficient than

EGS4/PRESTA photon dose calculations by a factor of more than 15 [71]. XVMC can complete a simulation of photon beam for one field in about 20 minutes on a typical personal computer.

3.2.2.1 Patient treatment planning parameters

The CADPlan TPS (Varian Oncology System, CA) was used to make five- field 3D-CRT prostate treatment plans for all studied patients. The fields were manually optimized based on the contours of target and organs-at-risk (OARs) drawn on the 5 mm slice thickness CT image sets. The total prescribed dose was given as about 72 Gy, delivered in 2 Gy per fraction, varied with patient individual situation.

Patient treatment parameters were extracted from the database in the CADPlan™ system and transferred into our research network for the MC calculation. The extracted parameters for one patient include: (1) the patient planning CT images, (2) the contours of body surface, PTV, CTV, GTV and OARs (bladder, rectum, and femoral heads), (3) the coordinates of the isocenter, (4) the field sizes, (5) the beam weights, (6) the couch, collimator and gantry angles, (7) the wedge angles and positions, (8) the MLC leaf positions, and (9) the prescribed total and fraction dose values.

3.2.2.2 Transferring between CADPlan™ and XVMC coordinate systems

To do the patient dose calculation, it is important to keep the constancy in transferring patient data from the CADPlan™ system to XVMC system. Figure 8 illustrates the coordinate systems of CADPlan™ and XVMC.

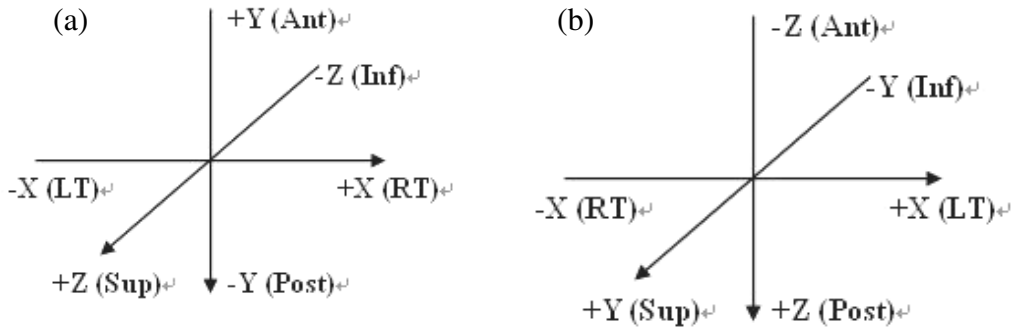

Figure 8: (a) CADPlan™ coordinate system and (b) XVMC coordinate system

The origin in a CADPlan™ system is defined by patient skin markers, at the center of marker slice, while the original points for XVMC locates at the left-up corner of first CT slice. The coordinate transformation equations are given as follow:

$$x(VMC) = \left(\frac{dimension(CT)}{2} \right) \times pixel\_size + x(CADPlan) \quad (3.1)$$

$$y(VMC) = z(CADPlan) - z(first\_CT\_slice) \quad (3.2)$$

$$z(VMC) = \left(\frac{dimension(CT)}{2} \right) \times pixel\_size - y(CADPlan) \quad (3.3)$$

3.2.2.3 Introducing the daily shift of prostate

Restitu™ US system gives the couch movements which are opposite to the prostate shifts in order to realign the target at the isocenter during patient treatment. To simulate this, these daily shifts of prostate have been introduced into the dose calculation for the corrected cases in two manners: a) in the input vmc file for XVMC simulation, the beam isocenter was shifted according to the prostate daily shifts to produce corresponding fraction dose distributions or matrices, and then b) all fraction dose matrices of one patient are pinned back to a reference matrix (the original patient matrix from CT images) to obtain the patient's total dose distribution.

The coordinates of new isocenter in .vmc file can be calculated with following equations:

$$x_{shiftedISO}(XVMC) = x_{ISO}(XVMC) - \Delta x(US) \quad (3.4)$$

$$y_{shiftedISO}(XVMC) = y_{ISO}(XVMC) + \Delta z(US) \quad (3.5)$$

$$z_{shiftedISO}(XVMC) = z_{ISO}(XVMC) - \Delta y(US) \quad (3.6)$$

Where, $x_{..}(XVMC)$, $y_{..}(XVMC)$ and $z_{..}(XVMC)$ are the coordinates in XVMC coordinate system; $\Delta x(US)$, $\Delta y(US)$ and $\Delta z(US)$ are the daily shifts of prostate provided by Restitu™ 3D US localization.

3.2.2.4 Fraction dose calculation procedure

The fraction dose is calculated by including the prostate displacement or not. It is simulated by using BEAMnrc/XVMC approach. The first step is to obtain the beam ph-sp file which is collected at the lower surface of the PMMA exit window. The treatment parameters extracted from CADPlan™ are used to set up the jaws and wedge. The VARMLC component module, which describes the position coordinates of 25 leaf-pairs,

was derived from the CADPlan MLC sequence file [76]. The SWDG and VARMLC component modules were used in the BEAMnrc input file. Then, the patient-specific beam ph-sp file can be created using BEAMnrc, which takes the CL2300 target ph-sp file as its input source. Each beam has one independent beam ph-sp file which contains approximately 20 million particles.

The second step is to create a patient phantom from the planning CT images. Unlike DOSXYZ using the electronic density, XVMC directly use the material properties including collision and radiation stopping power and scattering power, as well as attenuation coefficients to simulate photon-electron effect and Compton scattering in particle transportation [71]. An in-house routine is used to convert the Hounsfield numbers of patient CT images into a 3D data matrix of physical properties including the geometry and tissue properties of the patient [76, 77].

The third step is to create the .vmc file for XVMC. Prostate daily displacement data has been included to obtain the repositioned target isocenter for corrected cases. The original plan (without prostate motion) is calculated as well. Other simulation parameters such as beam ph-sp file, angle, energy, and total particle number are also edited in the .vmc file.

The fourth step is to run the XVMC code to calculate the dose deposited in the patient phantom. The simulation task was submitted to a Blade cluster computer. One simulation takes less than 20 minutes. The dose distribution and its statistical uncertainties are stored in .d3d file for further analysis.

3.3 Patient total dose calculation

Patient dose distributions are computed by summing up all fraction doses. A patient may have up to 40 fractions, and hence 40 fraction dose calculations. A dose calculation obtained from XVMC is expressed in terms of dose per incident particle (Gy/particle). It is necessary to convert this unit to dose per monitor unit (MU). This procedure is called as the calibration of the XVMC simulation.

3.3.1 Calibration of XVMC simulation

Similar to the calibration of the linac machine, we create a 30 cm cubic water phantom with voxel dimensions of 0.5 cm x 0.5 cm x 0.5 cm. The water phantom is set up at a source-to-surface distance (SSD) of 100 cm. A 10 cm × 10 cm open field was

used. To realize a statistical uncertainty of less than 0.5%, one billion histories were simulated using particle recycling of the target ph-sp file, with a factor of twenty, which contained approximately 50 million particles. This simulation could give the dose at the reference point which is located at a depth of 3 cm (dmax for an 18 MV photon beam) in water phantom.

The dose at reference point for 18 MV photon beam was obtained as 0.398996 through our XVMC simulation by giving 100 MU with Varian CL2300 linac, based on a 30 cm^3 water phantom under the above-mentioned standard calibration conditions. The value of 0.398996 a.u. should be calibrated to 100 cGy at the reference point. Therefore, calculate the calibration factor (CF) as following:

$$CF = \frac{100cGy}{0.398996\ a.u. \times 100\ MU} = 2.5063cGy/(a.u.\cdot MU) \tag{3.7}$$

The patient absolute dose can be calculated with Equation 3.8:

$$D^{absolute}(x,y,z) = CF \times D^{XVMC}(x,y,z) \times MU(beam) \tag{3.8}$$

Where, $D^{absolute}(x,y,z)$ represents the calibrated dose in a pixel with x, y and z coordinates; $D^{XVMC}(x,y,z)$ represents the dose calculated by XVMC in the same pixel; and $MU(beam)$ is the monitor units given to that beam according to the patient treatment plan.

After calibration, the patient dose for fraction *m* can be calculated by summing each field *i* as follows:

$$\begin{aligned} D_m(x,y,z) &= \sum_{i=1}^{5} D_{m,i}(x,y,z) \\ &= \sum_{i=1}^{5} CF \times D_{m,i}^{XVMC}(x,y,z) \times MU(beam_i) \end{aligned} \tag{3.9}$$

3.3.2 Dose calculation considering daily prostate motion

Daily prostate motion induces changes in its position, shape, and volume. By repositioning the patient, the treatment geometry of the delivery beams is changed. These factors make it difficult and complicated to accurately sum the fraction dose distributions.

In order to obtain some results of clinical value, the following hypothesis has been made to simplify the real situation in the calculation of patient total doses:

a) Prostate motion includes only translation and rotation as a rigid body.
b) The shape and volume of the prostate do not change during treatment.
c) OARs including the bladder and rectum translate with the prostate, but do not rotate, or change their shape or volume.

Under the above hypothesis, five scenarios listed in Table 1 and illustrated in Figure 9 have been simulated. Since prostate motion exists in scenarios 2 through 5, we set the CT-derived patient phantom in scenario 1 as the reference phantom (3D matrix). The dose matrix in the other 4 scenarios will be referred back to the reference one.

According to Figure 9, two beam geometries (one with shifted target isocenter and beams geometry, another without shift) have been simulated to obtain two sets of patient fraction dose distribution, called the original dose distribution ($\mathbf{D}_m^{Ori}$) and correction dose distribution ($\mathbf{D}_m^{Corrt}$), respectively. Based on the two sets of fraction dose, the patient total doses for the five scenarios are calculated by using equations shown in Table 3, in which $\mathbf{D}_{total}^{target}(x,y,z)$ presents the total dose distribution for prostate target, and $\mathbf{D}_{total}^{OARs}(x,y,z)$ for OARs including bladder and rectum. (x_T, y_T, z_T) and (x_{TR}, y_{TR}, z_{TR}) are the translated coordinates and translated-plus-rotated coordinates for a certain point (x,y,z) in the reference phantom, respectively.

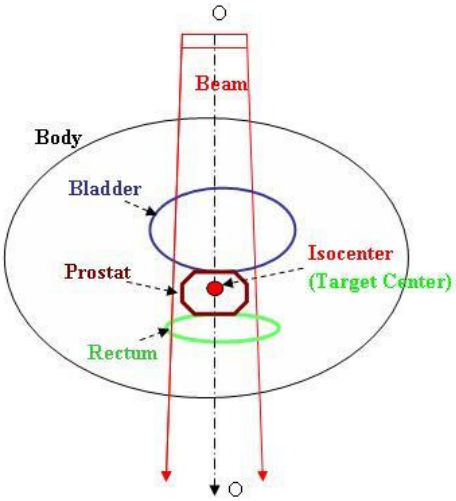

Scenario 1: no motion, no correction

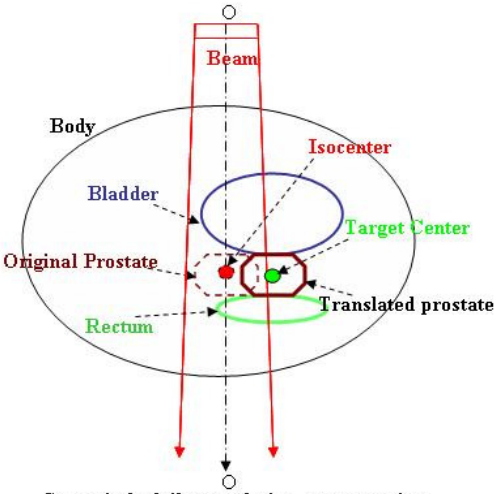

Scenario 2: daily translation, no correction

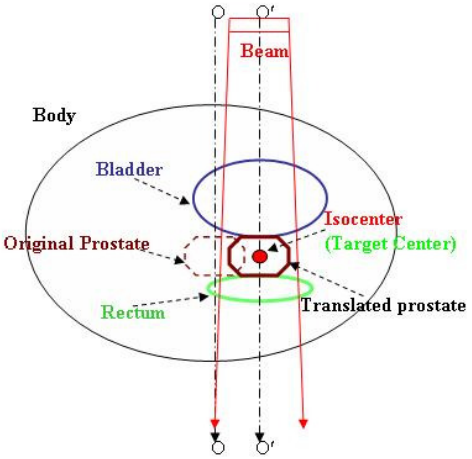

Scenario 3: daily translation with correction

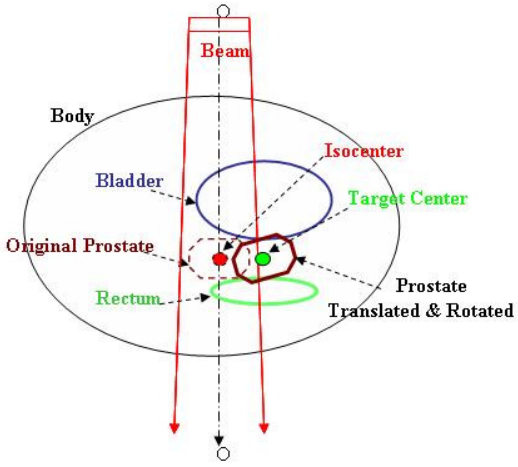

Scenario 4: daily translation and rotation, no correction

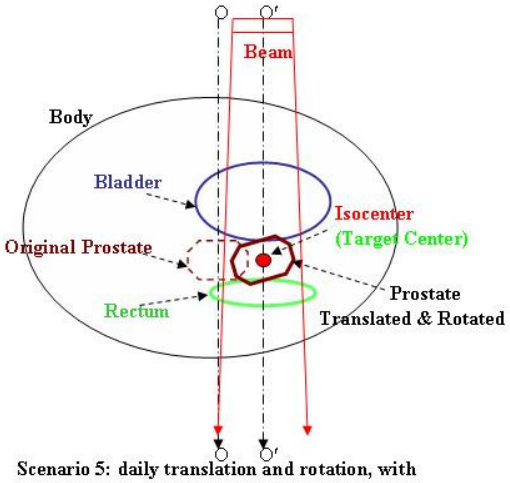

Scenario 5: daily translation and rotation, with translation correction

Figure 9: Scenarios of daily prostate motion and corrections. Line OO is the central axis of the original beam given by patient treatment plan; Line $O'O'$ is the central axis of the actual delivery beam. Beam translates in three dimensions. Patient body contour does not translate. Bladder and rectum translate with prostate, but not rotate.

Scenario	Fraction dose	$\mathbf{D}_{total}^{target}(x,y,z)$	$\mathbf{D}_{total}^{OARs}(x,y,z)$
1	$\mathbf{D}_m^{Ori}$	$\sum_{m=1}^{M}\mathbf{D}_m^{Ori}(x,y,z)$	$\sum_{m=1}^{M}\mathbf{D}_m^{Ori}(x,y,z)$
2	$\mathbf{D}_m^{Ori}$	$\sum_{m=1}^{M}\mathbf{D}_m^{Ori}(x_T,y_T,z_T)$	$\sum_{m=1}^{M}\mathbf{D}_m^{Ori}(x_T,y_T,z_T)$
3	$\mathbf{D}_m^{Corrt}$	$\sum_{m=1}^{M}\mathbf{D}_m^{Corrt}(x_T,y_T,z_T)$	$\sum_{m=1}^{M}\mathbf{D}_m^{Corrt}(x_T,y_T,z_T)$
4	$\mathbf{D}_m^{Ori}$	$\sum_{m=1}^{M}\mathbf{D}_m^{Ori}(x_{TR},y_{TR},z_{TR})$	$\sum_{m=1}^{M}\mathbf{D}_m^{Ori}(x_T,y_T,z_T)$
5	$\mathbf{D}_m^{Corrt}$	$\sum_{m=1}^{M}\mathbf{D}_m^{Corrt}(x_{TR},y_{TR},z_{TR})$	$\sum_{m=1}^{M}\mathbf{D}_m^{Corrt}(x_T,y_T,z_T)$

Table 3: Formulae for calculating patient total dose

Assuming that $\Delta x_m(US)$, $\Delta y_m(US)$ and $\Delta z_m(US)$ represent the prostate translations for m-th treatment fraction, α_m, β_m, γ_m are the rotation angles about the ***x, y, z*** axis, respectively, the (x_T, y_T, z_T) can be calculated as Equation 3.10:

$$\begin{pmatrix} x_T \\ y_T \\ z_T \end{pmatrix} = \begin{pmatrix} x \\ y \\ z \end{pmatrix} - \begin{pmatrix} \Delta x_m(US) \\ \Delta y_m(US) \\ \Delta z_m(US) \end{pmatrix} \tag{3.10}$$

The (x_{TR}, y_{TR}, z_{TR}) can be calculated as Equation 3.11:

$$\begin{pmatrix} x_{TR} \\ y_{TR} \\ z_{TR} \end{pmatrix} = \mathbf{R}_m \begin{pmatrix} x \\ y \\ z \end{pmatrix} - \begin{pmatrix} \Delta x_m(US) \\ \Delta y_m(US) \\ \Delta z_m(US) \end{pmatrix} \tag{3.11}$$

Where, $\boldsymbol{R}_m$ is a rigid body rotation matrix, which can be expressed as Equation 3.12.

$$\mathbf{R}_m = \mathbf{R}_x(\alpha_m)\,\mathbf{R}_y(\beta_m)\,\mathbf{R}_z(\gamma_m) \tag{3.12}$$

And $\mathbf{R}_x(\alpha_m)$, $\mathbf{R}_y(\beta_m)$, $\mathbf{R}_z(\gamma_m)$ can be expressed as follows:

$$\mathbf{R}_x(\alpha_m)=\begin{bmatrix}1 & 0 & 0\\ 0 & \cos\alpha_m & \sin\alpha_m\\ 0 & -\sin\alpha_m & \cos\alpha_m\end{bmatrix},\quad \mathbf{R}_y(\beta_m)=\begin{bmatrix}\cos\beta_m & 0 & \sin\beta_m\\ 0 & 1 & 0\\ -\sin\beta_m & 0 & \cos\beta_m\end{bmatrix},$$

$$\mathbf{R}_z(\gamma_m)=\begin{bmatrix}\cos\gamma_m & -\sin\gamma_m & 0\\ \sin\gamma_m & \cos\gamma_m & 0\\ 0 & 0 & 1\end{bmatrix}$$

After a translation or a translation-plus-rotation transformation, the new data point (x_T, y_T, z_T) or (x_{TR}, y_{TR}, z_{TR}) usually do not locate exactly at the sampling points of the fraction dose matrix. For this situation, a double spline interpolation function has been employed to get a good guess of the dose to that point.

The total dose distributions of 32 patients for first 3 scenarios were calculated using in-house Matlab program called CombineDose. Only three patients were available for scenarios 4 and 5 since the absence of actual daily prostate volume for the rest of patients disallow deriving the daily rotation of prostate.

3.4 Evaluation methods

A DVH analysis on dose distributions and a comparison of isodose curves has been employed to evaluate the dosimetric impact of prostate motion. Based on the results of individual DVHs, a descriptive statistical method has been employed to analyze dosimetric values in terms of $D_{95\%}$, $D_{90\%}$, and $V_{90\%}$ for the studied group.

3.4.1 DVH analysis and comparison of isodose curves

DVH analysis is a well accepted method to evaluate patient treatment plan by calculating the cumulative or differential volumetric information on a 3D dose distribution. By quantitatively comparing the cumulative DVH between correction and un-correction scenarios, we evaluate the dosimetric consequence of motion correction with US localization system. Since the DVH analysis loses spatial information of the dose distribution, it may lose some dose information of clinical importance, such as “hot” and “cold” spots inside the volumes of interest. To compensate this drawback, comparisons of isodose curves are made based on an axial slice.

An in-house program called BrachyGUI [56] was used to make the DVH analysis and comparison of isodose curves. Our DVH calculation is based on the XVMC patient

phantom derived from patient planning CT images. The voxel size was determined by the planning CT images. Two voxel sizes: (1) 2.15 mm x 2.15 mm x 3 mm; (2) 1.83 mm x 1.83 mm x 3 mm are used in the studied group. The contours of ROIs are input into BrachyGUI and imposed on the phantom images slice by slice. In the contour edge region, the voxel is considered belonging to a ROI if the contour covers two-thirds of the voxel volume. To calculate the percentage of volume covered by the percent dose such as V_{90} and V_{50}, the dose at the target isocenter in scenario 1 has been chosen as the normalization dose (corresponding to the prescribed dose in CADPLAN™).

According to motion characteristics, five scenarios can be divided into three groups: ideal group, translation group and translation-plus-rotation group. The scenario 1 is the ideal case with exactly the same treatment setup and geometry as designed by the original treatment plan. We take its dose distribution, isodose curve and DVH analysis as the reference (baselines for comparison). Scenario 2 and 3 belong to translation group, and scenario 4 and 5 the translation-plus-rotation group. For each group, two comparisons have been made: (1) between uncorrected scenario and scenario 1 (original plan); (2) between corrected scenario and scenario 1. The first comparison could illustrate how the daily prostate motion degrades the dosimetric consequence of the treatment plan. The second comparison could reveal how much the motion-correction by US localization system could improve the degraded treatment.

To make the dosimetric analysis, first step is to input BrachyGUI the patient phantom and contours of ROIs including PTV, CTV, bladder and Rectum, then the dose matrixes for scenario 1 and the compared scenario (one of scenario 2 to 5). The second step is to normalize both dose matrixes to the dose at isocenter from the original plan. After normalization, a comparison of isodose curves for selected phantom slice is displayed. The next step is to calculate the DVH indices such as $D_{95\%}$, $D_{90\%}$, $D_{50\%}$, $D_{10\%}$, V_{955}, $V_{90\%}$ and $V_{50\%}$, and output them to a *.txt* file. The last step is to calculate the percent change of the DVH indices relative to their reference values which are computed from reference dose matrix, using the following equations:

$$\Delta D_{\#\#\%***}(\%) = \left[\frac{\left(D_{\#\#\%***}\right)_{Compared\_scenario} - \left(D_{\#\#\%***}\right)_{Scenario\_1}}{\left(D_{ref}\right)_{Scenario\_1}} \right] \times 100 \qquad (3.13)$$

$$\Delta V_{\#\#\%\_***}(\%) = \left(\frac{\left(V_{\#\#\%\_***}\right)_{Compared\_scenario} - \left(V_{\#\#\%\_***}\right)_{Scenario\_1}}{\left(V_{\#\#\%\_***}\right)_{Scenario\_1}} \right) \times 100 \quad (3.14)$$

Where, ##% represents one of specific percentages: 95%, 90%, 50%, and 10%; *** represents one of ROIs: PTV, CTV, GTV, bladder, or rectum; compared scenario is one of scenario 2 to scenario 5.

3.4.2 Statistical Analysis

The standard statistical method described in section 2.5 has been employed here to analyse the percent change of DVH indices for scenario 2 to scenario 3, based on data sets of 32 patients. The mean value and standard deviation are drawn and compared, so that the clinical values of motion correction method could be evaluated.

Frequency histogram, scatter plot, and bar diagram are also used to display the statistical results and enhance the conclusions drawn from quantitative analysis.

For the translation-plus-rotation group, the available data sets are only from 3 patients due to the absence of actual daily prostate volumes for the rest of studied patients. For these patients, copying PRV contours to PGV, instead of drawing the PGV contours based on daily US images, was used to perform the daily localization.

An analysis is also made on the translation-plus-rotation group. From the statistical results, a primary conclusion about whether the translation-correction approach is adequate to address the translation-plus-rotation problem for prostate EBRT can be drawn. Due to the limited sample number, further study is required to give a sound conclusion.

Chapter 4 Results and Discussion (1)

Retrospective analysis of prostate daily displacements

A total of 32 patients were included in this study. All patients received daily Restitu™ 3D US localization for their treatment courses, producing 890 localizations and 2670 shifts (AP, SI, and RL). On average, each patient underwent 28 localizations, ranging from 9 to 40.

4.1 Fraction-based statistical results for individual patient

A patient who underwent 39 fractions of treatment with US localization has been chosen as a typical patient for the presentation of its statistical results. The statistical analysis is based on all the daily displacement data obtained in the treatment course.

Table 4 displays the statistical shift results with respect to the PRV position, and percent volume changes relative to the volume of the PRV obtained during the CT scan stage. The largest mean shift is in the AP direction, 4.2 mm posterior, with a SD of 5.4 mm. A mean shift of 3.9 mm superior with a SD of 3.1 mm is found in the SI direction, and a mean shift of 0.1 mm to the left with a SD of 2.9 mm on the lateral axis. The mean prostate percent volume change based on US contours is found to be -0.8% with a SD of 2.8 and a maximum value of -7.6%.

Axis of Motion	Ant(+) /Post(-) Displacement	Sup(+)/Inf(-) Displacement	RT(+)/LT(-) Displacement	Percent Volume Change (%)
Mean (mm)	-4.2	3.9	-0.1	-0.8
Median (mm)	-4.9	3.8	-0.5	-0.2
SD (σ) (mm)	5.4	3.1	2.9	2.7
Range (mm)	-14.2 - 6.3	-1.8 - 11.1	-5.1 - 6.4	-7.6 - 4.1

Table 4: Statistical results from a typical patient with 39 ultrasound localizations. All shifts are relative to target isocenter. Ant = anterior; Post = posterior; Sup = superior; Inf = inferior; RT =right; LT= left

Figure 10 presents the histograms of shifts for each fraction along the AP, SI, and RL axes, and the prostate volume change. For volume changes, the distribution fits well to a normal distribution with a very narrow standard deviation of 2.75%.

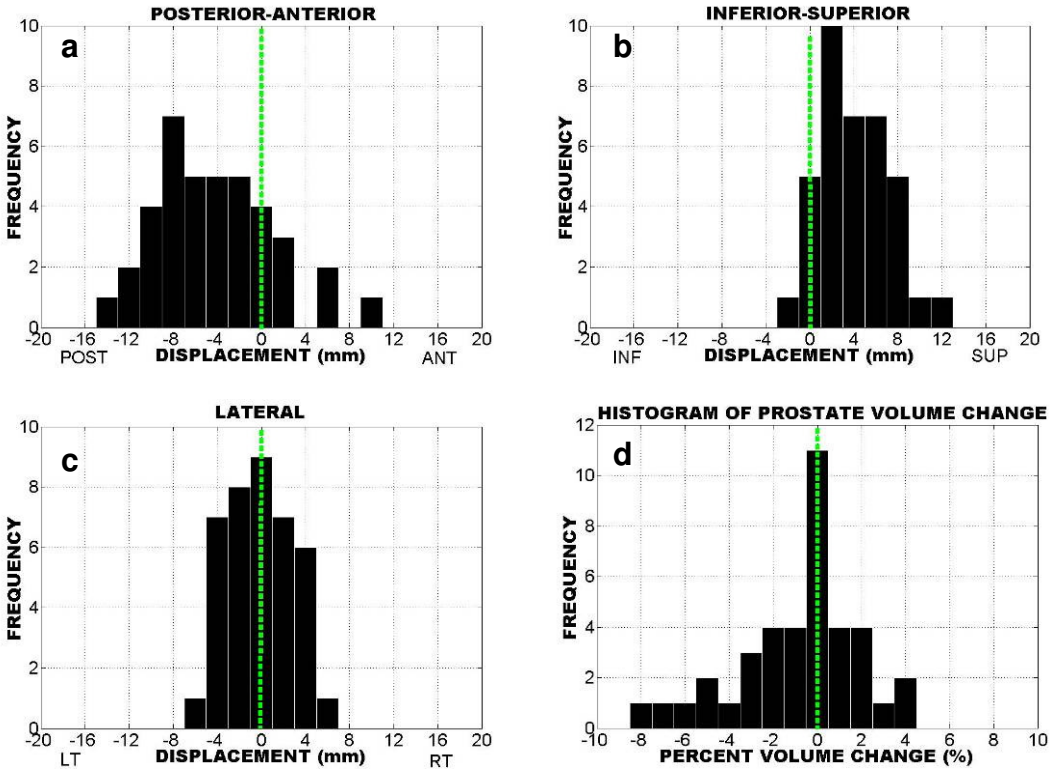

Figure 10: Frequency histograms of daily prostate displacement calculated for each direction (a) anterior-posterior, (b) superior-inferior, (c) right-left, and (d) volume changes for a typical patient

Figure 11 shows the scatter plots of prostate daily displacements for the patient for the axial, coronal, and sagittal planes. In the axial plane, the data points distribute approximately around the isocenter (0, 0). In the coronal and sagittal planes, the data points locate in one or two quadrants of the coordinate system, showing a systematic deviation from the isocenter.

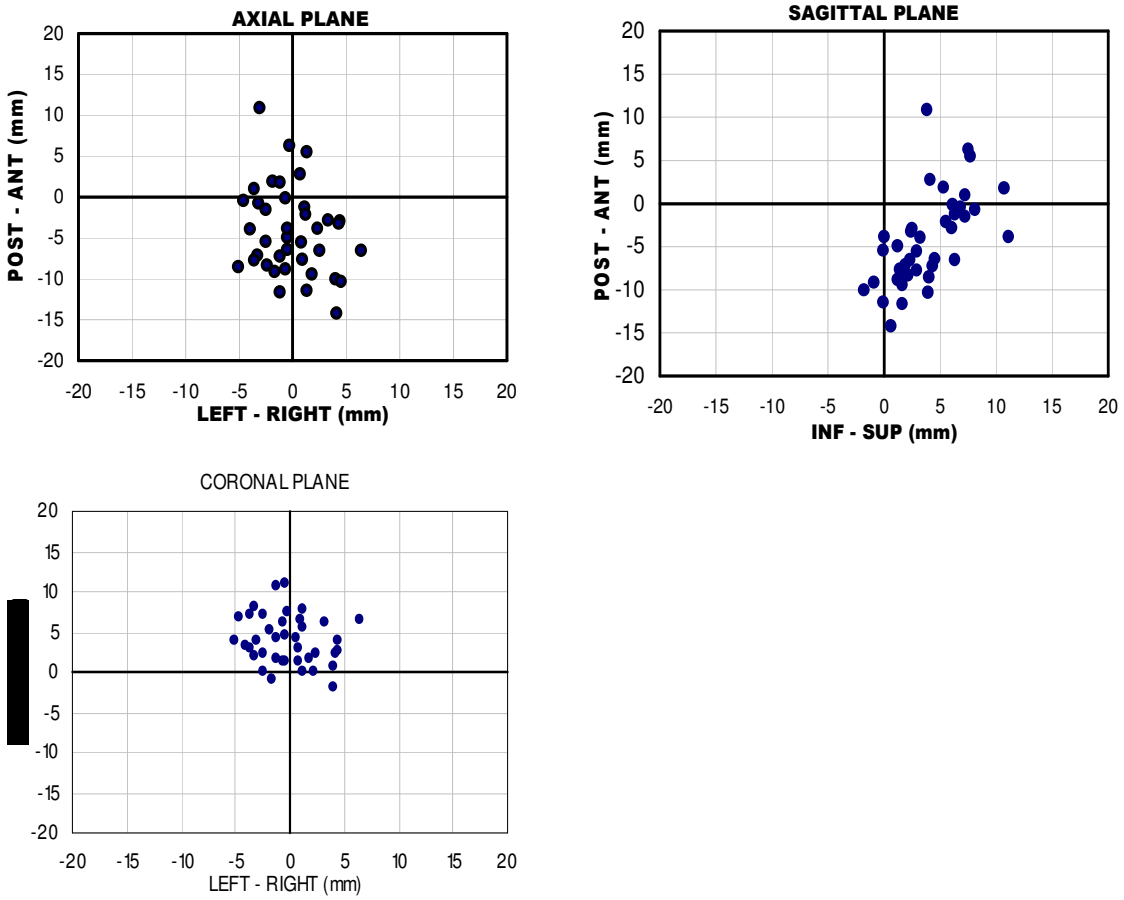

Figure 11: Scatter plots illustrating the daily displacements of 39 fractions for a patient in the axial, coronal, and sagittal planes.

Figure 12 plots the daily displacement in three directions as a function of time (represented by fraction number) for evaluating the trend of change during the course of treatment. For this patient, the prostate tends to increase the motion to posterior and right directions, and keep almost the same displacement in inferior direction. The prostate volume tends to shrink during treatment.

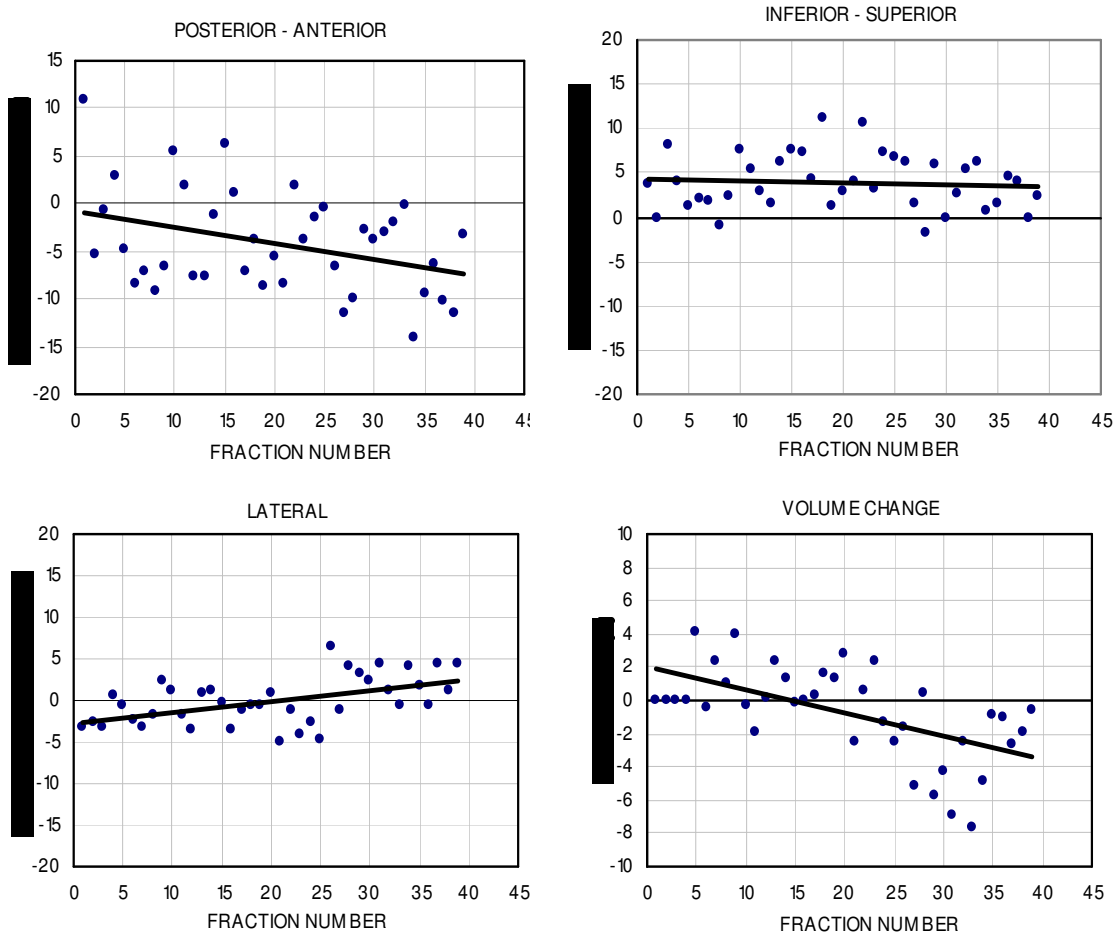

Figure 12: Plots of daily displacements for the three major axes and volume change vs. fraction (trends with time)

4.2 Statistical Analysis on all patients

Two methods are used for population statistics. The first method is to take all fractions from 32 patients as one sampling group and make a descriptive statistical analysis. The second is to calculate the mean displacement and standard deviation for each patient, and then make a statistical analysis based on patient mean values and SDs.

4.2.1 Statistical results based on all fractions

32 patients treated with EBRT at the MGH between July 1st, 2006 and January 28th, 2008 have been included in this analysis. To make sense of the statistical analysis, fraction volume changes are normalized to the PRV volume of the corresponding patient to obtain the percent volume changes. The results are shown in Table 5.

Axis of Motion Measurement	Ant(+) /Post(-) Displacement	Sup(+)/Inf(-) Displacement	RT(+)/LT(-) Displacement	Percent Volume Change (%)
Mean (mm)	-3.3	-1.1	-0.2	-1.4
Median (mm)	-2.8	-0.9	-0.6	-0.8
SD (σ) (mm)	7.9	6.4	5.6	3.0
Range (mm)	-33.5 - 19.1	-39 - 21.5	-16.6 - 22.3	-10.4 - 8.8

Table 5: Statistical results on 890 ultrasound localizations from 32 patients

These displacements are computed with respect to the target isocenter. The mean value and SDs of the prostate motion in the AP, SI, and lateral directions are -3.3 mm (SD 7.9 mm), -1.1 mm (SD 6.4mm), and -0.2 mm (SD 5.6 mm), respectively, while maximum displacements observed in the AP, SI, and lateral directions are 33.5 mm posterior, 39 mm inferior, and 22.3 mm right. The mean value and SDs of the percent volume change of prostate are -1.4% (SD 3.0%) with a maximum change of -10.4% for the sample population.

Figure 13 presents the frequency histograms of prostate displacement calculated for each axis of translation. The displacement data were tested for normal distribution with a 95% CI using the Lilliefors Test for Normality [78]. Figure 13(d) shows there are a large number of data points having zero prostate volume change. These data are not corrected because therapist had copied the PRV as daily PGV to make the daily localization of prostate. Therefore, these data points should be excluded for statistical analysis. With excluding these incorrect data points, a mean percent volume change of prostate is derived as -2.5 %.

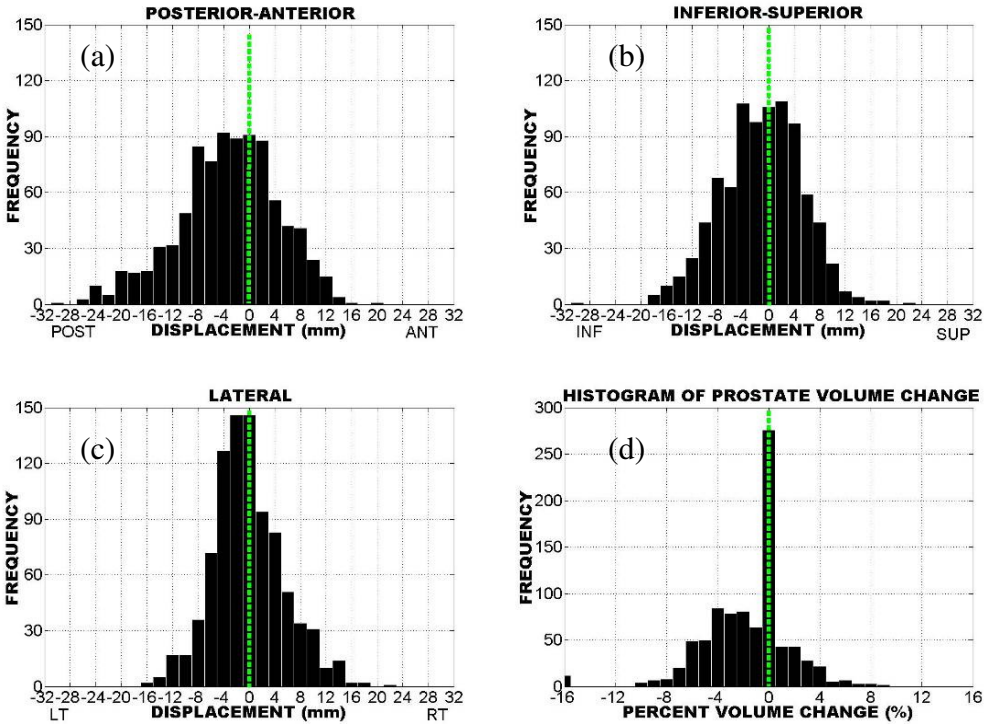

Figure 13: Frequency histograms of prostate displacements calculated for each direction (a) anterior-posterior, (b) superior-inferior, (c) right-left) and (d) volume changes from 890 US localizations of 32 patients

Scatter plots of the daily displacements for the axial, coronal, and sagittal planes are shown in Figure 14. Figure 15 plots the displacement data in three orthogonal directions and percent volume changes versus fraction number.

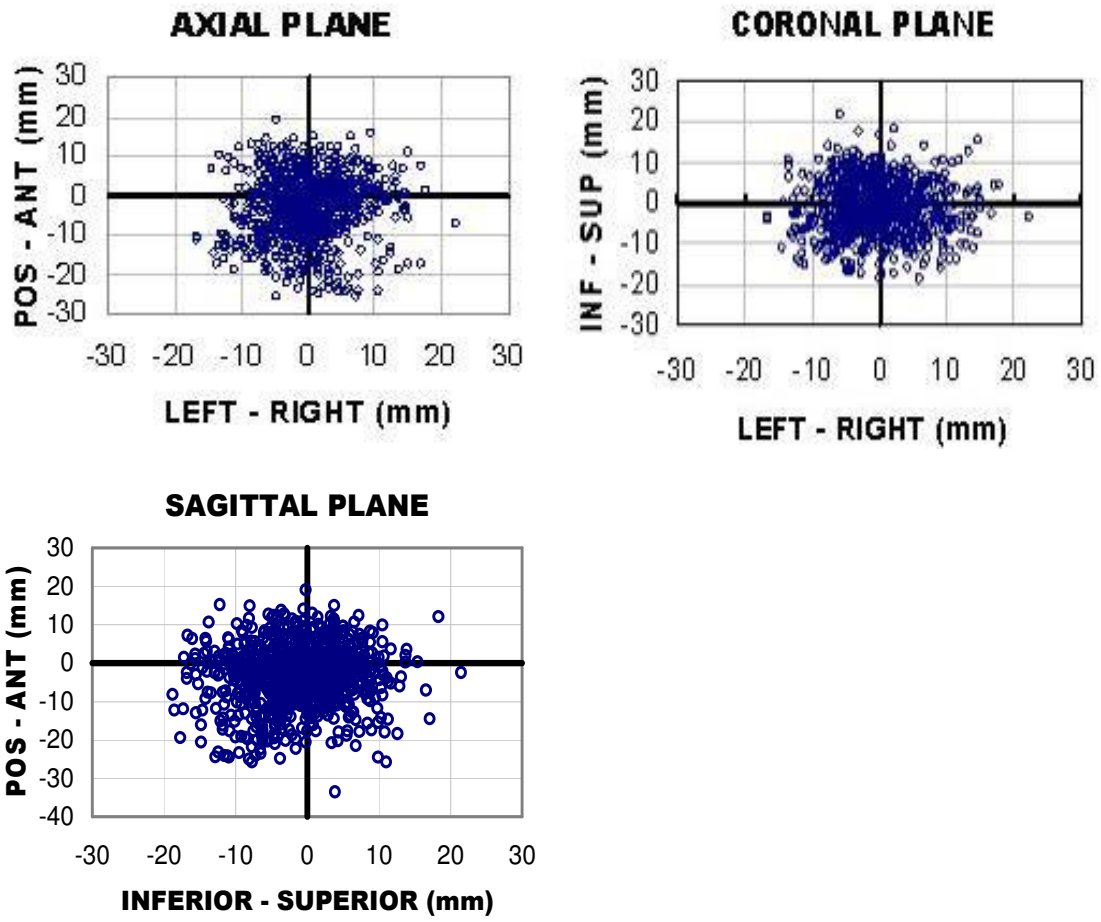

Figure 14: Scatter plots illustrating the daily displacements in the axial, coronal, and sagittal planes for 890 US localizations of 32 patients.

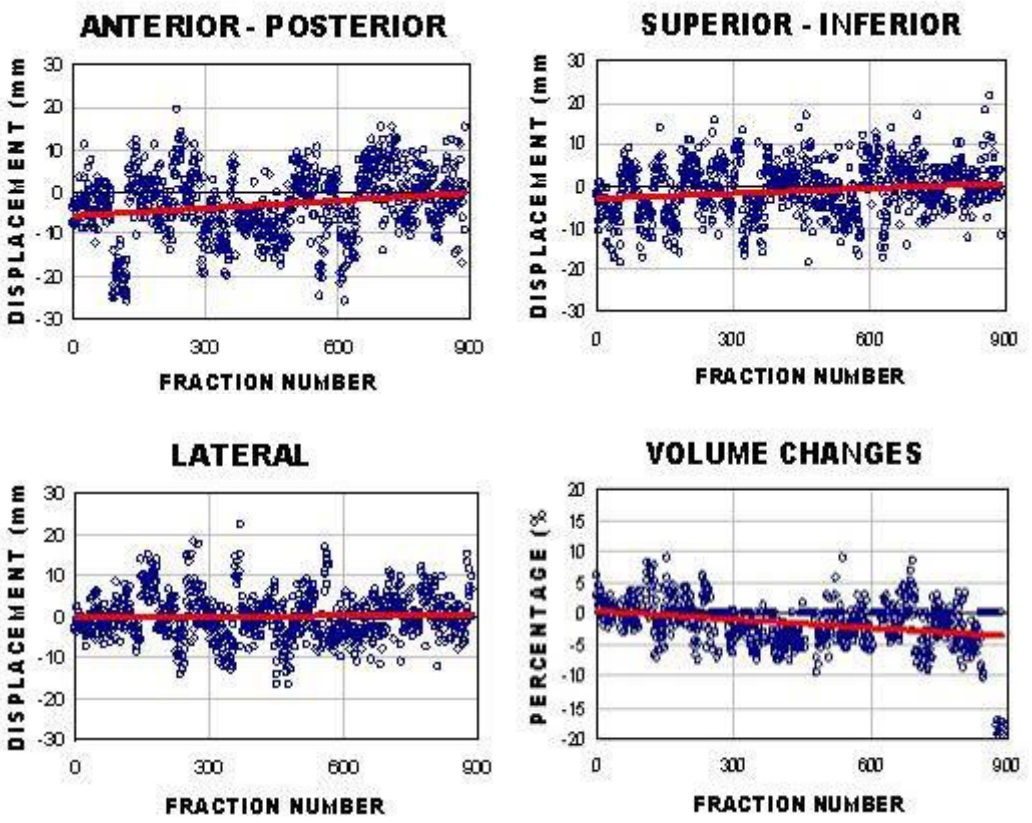

Figure 15: Plots of 890 daily displacements for the three major axes and percent volume change vs. fraction number.

4.2.2 Statistical results based on individual patient

Table 6 presents the statistical analysis on the mean displacement of each patient with respect to direction, and mean volume changes for 32 patients. The largest mean shift is observed in the AP direction, 3.6 mm posterior with an SD of 6.4 mm, ranging between 20.4 mm posterior and 7.5 mm anterior. The following is mean shift of 1.4 mm inferior with an SD of 4.8mm in the SI direction. The mean shift in lateral direction is close to zero with a SD of 4.8mm. The mean percent volume change is -1.4% with an SD of 3.0%. The frequency histograms of the mean displacements in AP, SI and LAT direction and a histogram of percent volume changes are shown in Figure 16.

Axis of Motion Measurement	Ant(+) /Post(-) Displacement	Sup(+)/Inf(-) Displacement	RT(+)/LT(-) Displacement	Percent Volume Change (%)
Mean (mm)	-3.6	-1.4	-0.0	-1.4
Median (mm)	-2.6	-0.7	-0.9	-0.8
SD (σ)(mm)	6.7	4.8	4.8	3.0
Range (mm)	-20.4 - 7.5	-10.3 - 7.6	-7.0 - 12.4	-10.4 - 8.8

Table 6: Statistical results on mean values of displacements and percent volume changes for 32 patients

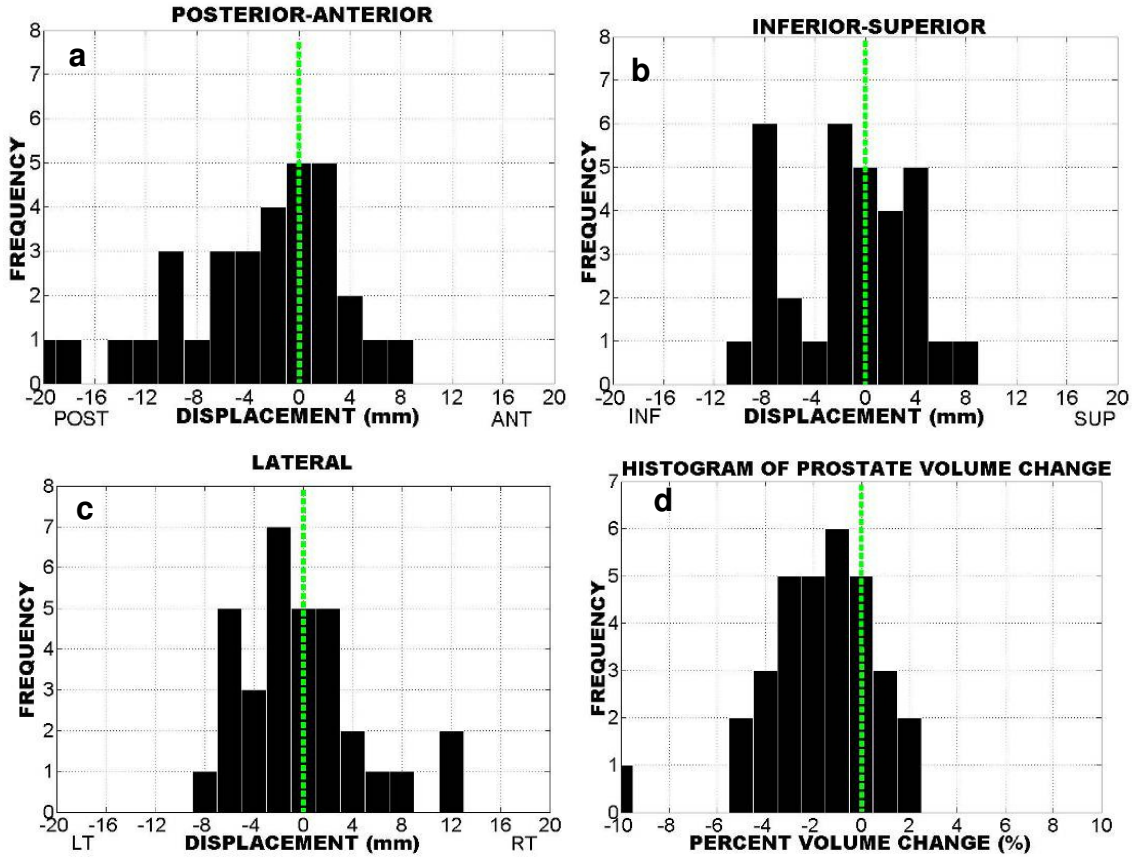

Figure 16: Frequency histograms of prostate displacements based on the mean shifts in three major directions: (a) AP, (b) SI, (c) LAT, and (d) percent volume changes for 32 patients.

4.3 Primary assessment of the PTV margin

Equation 2.2 is used to assess the PTV margin which requires encompassing the prostate for 95% of all displacements (if US localization was not available). The population systematic and random errors are computed based on the mean displacement and standard deviation using Equation 2.1.

Table 7 shows the results of population statistics and directional margins based on daily US localization for 32 patients. Without considering the patient systematic deviation, a PTV margin of 16.8 mm is required to cover 95% of the CTV volume. When the population mean displacement is considered, margins of 13.2 mm anterior and 20.4 mm posterior, 11.4 mm superior and 14.2 mm inferior, and 12.1 mm lateral are required.

Directions	Mean* (mm)	Σ (mm)	σ (mm)	Margin (mm)
AP	-3.6	6.7	4.8	16.8
SI	-1.4	4.8	4.5	12.8
RL	-0.0	4.8	3.6	12.1

Table 7: Population statistics and margins calculated using equation 2.2. Mean* represents the mean value from mean displacements for each patient, Σ represents the population systematic uncertainty, and σ is the population random uncertainty.

4.4 Daily Rotation Measurement

Daily rotation measurement is a primary study for 3D US localization by using an in-house program based on a modified maximum MI registration method. Three patients who have 36, 20, and 22 treatment fractions with US images, respectively, are included. Their prostate contours were extracted from the Restitu^{TM} workstation and used to derive daily rotations about the lateral, AP, and SI axes. Table 8 shows the statistical results for daily rotations in terms of the mean rotation, standard deviation, and range. The largest rotation occurred along the lateral axis with a mean rotation of -0.9° with a SD of 4.6°, ranging from -6.7° to 8.0°.

Patient No.	Rotation Axis	Mean Rotation (°)	SD (°)	Range (°)
1	Lateral	-0.3	1.9	-3.4 - 4.9
	AP	0.1	0.3	-0.2 - 0.8
	SI	0.0	0.2	-0.4 - 0.4
2	Lateral	-0.3	3.6	-5.4 - 4.7
	AP	0.2	1.1	-1.8 - 1.9
	SI	0.4	1.1	-1.7 - 1.8
3	Lateral	-0.9	4.6	-6.7 - 8.0
	AP	0.2	1.6	-3.1 - 2.5
	SI	0.5	1.2	-1.7 - 2.3

Table 8: Statistical results of prostate daily rotations for 3 patients

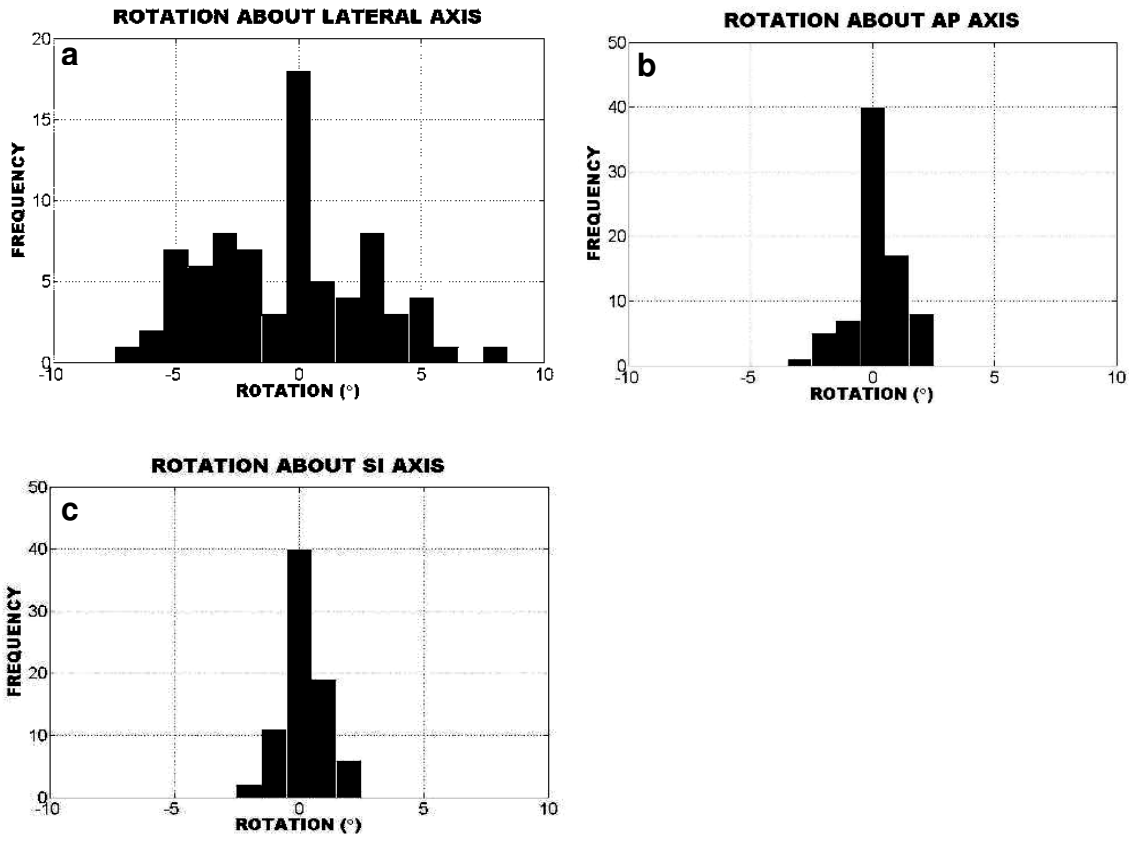

Figure 17: Frequency histograms of daily rotation along three main axes: (a) along lateral axis, (b) along AP axis, (c) along SI axis for three patients (78 fractions in total)

Since only 3 patients were studied (78 fractions in total) for prostate rotation study, the data is not suitable for population statistics. Figure 17 gives frequency histograms of daily rotation for all studied fractions. Figure 18 plots diagrams of daily rotation angles vs. patient number along three axes for the three patients studied. The mean rotation of

around zero degree is observed in Figures 17 and 18; however, the rotation along the lateral axis has a much larger variation range than the other two directions.

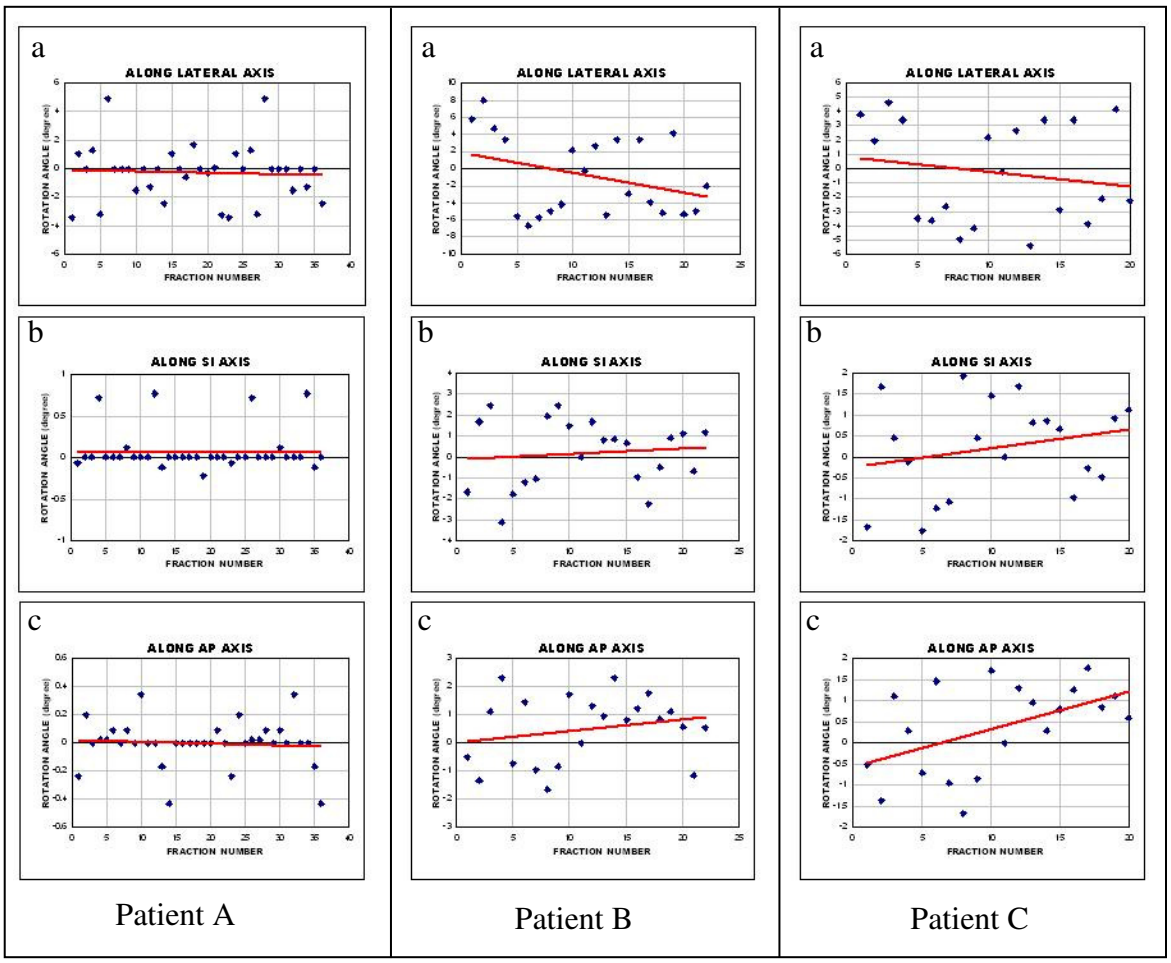

Figure 18: Plots of daily rotation angles vs. patient number for three patients studied: (a) rotation along lateral axis, (b) rotation along AP axis, (c) rotation along SI axis

4.5 Discussion

Two statistical methods (on all population fractions and on individual fractions) are used for the retrospective analysis on 3D US daily localizations of prostate, obtaining similar results shown in Tables 4 and 5. An examination on them shows that the largest mean displacement occurs in the anterior-posterior direction with the largest SD (-3.3 ± 7.9 mm vs. -3.6 ± 6.7 mm), followed by the superior-inferior direction (-1.1 ± 6.4 mm vs. -1.4 ±4.8 mm) and the lateral direction (-0.2 ± 5.6 mm vs. -0.0 ± 4.8 mm).

The overall results of our study are comparable with those found in the literature by using various localization systems and study sample size as shown in Table 9. The means of this study are within the range observed by other authors. Our results for interfraction SD (7.9 mm AP, 6.4mm SI, 5.6 mm RL) agree well with the results of Cury et al (2003) [33] (7.7 mm AP, 5.6 mm SI, 3.7 mm RL), and a little larger than the results from Poli et al (2007) [79] (4.4 mm AP, 4.5 mm SI, 3.60mm RL) which was derived from a data set of 387 patients with 10327 2D localizations. The difference may come from different imaging modalities used for localization and different study sample sizes.

	Mean Displacement (mm)			Imaging Modality
	RT(+)/LT(-)	ANT(+)/POST(-)	SUP(+)/INF(-)	
Present work	-0.2	-3.3	-1.1	3D US
Cury et al [33]	0.9	-3.8	1.4	3D US
Nigel et al [31]	-0.2	1.1	-1.0	3D US
Scarbrough et al [30]	1.9	0.8	-3.5	3D US
Poli et al [79]	0.5	-6.1	2.1	2D US
Little et al [82]	0.8	1.4	1.7	2D US
Little et al [82]	0.0	-0.2	0.0	Portal Film
Djemil et al [14]	0.9	-2.7	1.7	EM
Scarbrough et al [30]	0.8	-1.1	0	Seed Marker
John et al [40]	0.8	-2.7	-1.3	Fiducial Marker

Table 9: Mean displacements with respected to three main directions from several author's studies. EM= Electromagnetic Transponders.

Frequency histograms shown in Figure 13 illustrate that the daily prostate displacements in the AP, SI and lateral directions are normally distributed. This agrees with the results from Poli et al 2007 [79].

The prostate volume changes are computed by comparing US-based PGV volume to the PRV volume which is contoured at the CT stage. As shown in Table 10, the prostate volume varies with different imaging modalities. Due to this reason, the results of prostate volume changes shown in Tables 5 and 6 would be only used as a reference for prostate daily variation.

	CT/MRI	US/MRI	CT/US	CT/Pathologic
Average volume ratio	1.16	0.9	1.3 - 2.0	1.46

Table 10: Average prostate volume ratios computed for different imaging modalities [80]. MRI= Magnetic Resonance Imaging

As for individual prostate patients, the mean displacement and SD may vary, as shown in Tables 4 and 5. Although the population mean displacement is less than 5 mm, the daily displacements of the prostate from its intended treatment position is detected to be up to 33.5 mm posterior, 39 mm inferior, and 22.3 mm right. This difference among individual patients may come from the filling of the bladder and rectum, treatment setup uncertainty, and inter-user variability for US localization. A decreasing trend has been observed in the prostate volume change with one patient's treatment proceeding as shown in Figure 12.

Table 8 shows the mean rotation, SD, and range for three patients. The largest rotation from the intended position is observed along the lateral axis by as much as 8.0°, though its mean rotation is less than 1° for the whole treatment courses. Even if statistical analysis based on population has not been done due to a small patient sample size, the data from three patients also show that the preliminary study on rotation agrees with the results reported by Padhani et al [81] who concluded that the mean rotations over a population were close to zero but large outliers existed. Frequency histograms shown in Figure 17 clearly illustrate that rotation about the lateral axis has a much larger standard deviation than rotation about the other two axes. No trend with time is found in Figure 18 for daily prostate rotation.

Margin recipe proposed by Stroom et al [54] is used to derive PTV margins by taking the systematic and random errors into account. This recipe can ensure ≥ 95% prescription dose coverage ≥ 99% of the clinical target volume (CTV) or gross tumour. Population systematic and random uncertainties for prostate displacement are assessed from the mean values and SDs of each patient, as shown in Table 7. A non-uniform PTV margin across the major axes (16.8 mm AP, 12.8 mm SI, and 12.1 mm RL) has been derived in our retrospective study. These results are similar to those found by Poli et al (2007) [79] who suggested a PTV margin of 9-15 mm.

Chapter 5 Results and Discussion (2)
Dosimetric Impacts of daily motion on prostate EBRT

This chapter presents the MC calculated dose distribution and DVH analysis for 5 scenarios defined in chapter 3.5. Dosimetric comparisons between original plan (scenarios 1) and one of 4 clinical actual scenarios has been made in terms of DVH analysis. Statistics on percent variations of DVH indices has been done in order to investigate the dosimetric impacts of daily motion on prostate EBRT.

Patient total dose distributions are computed by summing all fraction doses which are simulated by BEAMnrc/XVMC approach under 5 hypothesized scenarios. They are presented in this thesis in terms of isodose curves and DVH curves. Comparisons of isodose curves and DVH curves have been made relative to the XVMC-calculated dose of original plan, not the dose originally calculated by CADPlan™.

Fraser *et al* (2008) [45] pointed out that there exists a significant difference between CADPlan™ and MC calculated patient dose distribution. Comparison of investigated dose relative to MC-calculated total dose from initial plan can effectively eliminate the influence from dose calculation algorithm, and protrude the impacts of daily prostate motion.

A typical patient (called patient No. 1) who was treated with 36 fractions using conformal EBRT is selected for in-detail investigation because his case is involved in both translation and translation-plus-rotation studies.

5.1 Dose distributions of original plans

Patient original treatment plan was made by dosimetrists using CADPlan™ TPS and approved by medical physicists at the MGH. A 7mm margin was added to patient CTV to obtain PTV. The isocentric 5-beam technique had been employed to give a conformal dose distribution to PTV target. The total dose was given by fractions, 1.8 Gy, 2 Gy, or 3 Gy per fraction, 5 fractions per week, based on individual situation and clinical considerations. The prescription dose is given to target isocenter or 95% isodose curve to derive the MU numbers required for each beam.

5.1.1 Isodose curves

The patient dose distribution is normalized to the XVMC-calculated isocenter dose to work out the percent isodose curves.

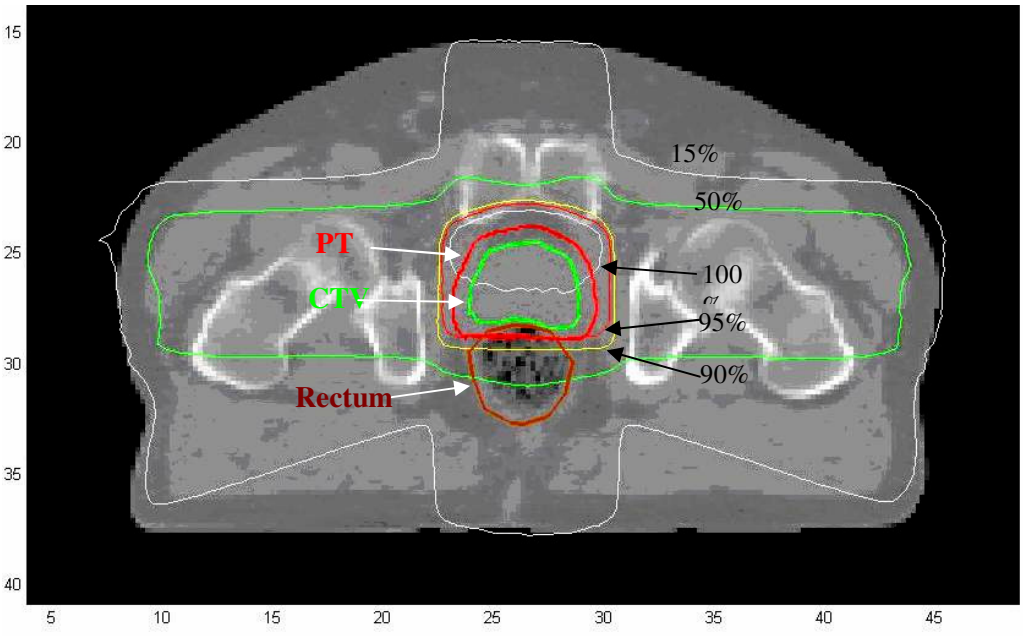

Figure 19: 2D axial isodose curves calculated by XVMC based on the original treatment plan for patient No.1.

Figure 19 displays five isodose curves for patient No.1 in an axial plane which passes through the PTV isocenter. The normalization dose is set as the XVMC-calculated isocenter dose. The figure shows that the 95% isodose curve covers the whole PTV, and matches well the shape of PTV. Only about one quarter of the nearby rectum volume is covered by the 90% isocurve.

5.1.3 DVH evaluation

Figure 20 displays the DVH curves of patient No. 1 derived from MC calculated total dose for its original plan. The 95% line (in blue) illustrates that approximately 100% of the CTV received 95% of the isocenter dose, and the 90% line (in red) shows that approximately 100% of the PTV received 90% of the isocenter dose.

Figure 21 displays the $D_{95\%}$ and $V_{95\%}$ of PTV, CTV and GTV for 32 patients based on their original plans. Their total doses are calculated by BEAMnrc-XVMC method and normalized to their isocenter doses. Although three $V_{95\%}$ of as low as 80% for PTV are observed in Figure 21, all $V_{95\%}$ and $D_{95\%}$ for CTV and GTV exceeds 90%.

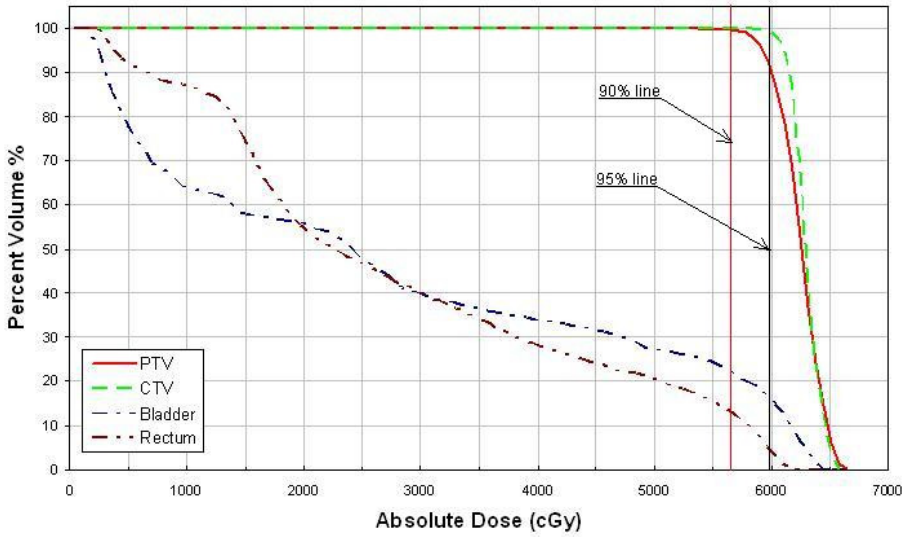

Figure 20: DVH curves of MC-calculated total dose from original plan for patient No. 1. Bladder and Rectum are the selected OARs

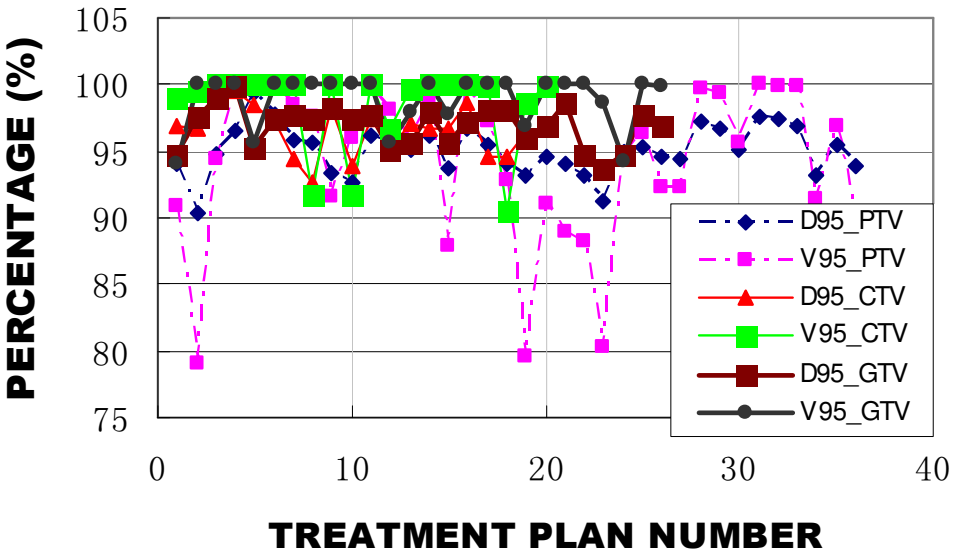

Figure 21: $D_{95\%}$ and $V_{95\%}$ of PTV, CTV and GTV (in % of prescribed dose) for 32 patients based on their original plans, calculated by the BEAMnrc/XVMC method

5.2 Dosimetric comparison: scenario 2 vs. scenario 1

5.2.1 Comparison of Isodose curves for patient No. 1

Figure 22 compares the isodose curves derived from scenario 2 (daily translation without correction) to scenario 1 (original plan, no motion). Scenario 2 simulates the actual patient treatment situation when daily localization is not used to account for

prostate daily motion. Obvious differences in all isodose curves were observed in Figure 22, especially the 90% isodose curve.

Investigation on isodose-curve comparisons for the rest of the patients observes a similar difference. Among them, the difference of patient No. 1 shown in Figure 22 is the smallest, implying the smallest dosimetric impact of prostate motion.

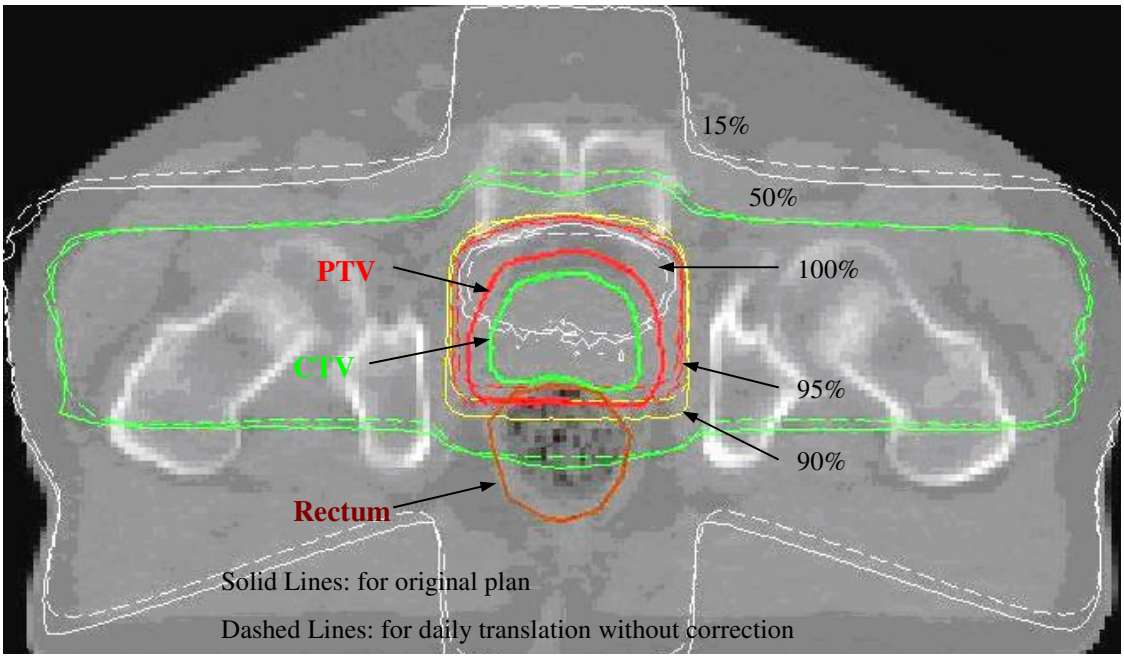

Figure 22: Comparison of isodose curves between scenario 2 (daily translation without correction) and scenario 1 (original plan, no motion) at the isocentric axial plane

5.2.2 Comparison of DVH curves for patient No. 1

Figure 23 displays the comparison of DVH curves for PTV, CTV, bladder as well as rectum between scenario 2 and scenario 1. “UnCrt” here means the scenario 2 in which prostate has daily translation but is treated without adopting the translation correction technique. The 90% and 95% lines are relative to the XVMC-calculated isocenter dose from the original plan (this definition is fixed in this thesis). An obvious change of DVH curves for PTV, CTV, bladder and rectum are observed. $D_{95\%}$ for PTV decreases from 59.1 Gy in scenario 1 to 57.0 Gy in scenario 2 while $D_{95\%}$ for CTV decreases from 60.8 Gy to 60.2 Gy. For the OARs, the $D_{50\%}$ for bladder slightly increases from 23.8 Gy to 26.8 Gy while the $D_{50\%}$ for rectum slightly decreases from 22.4 Gy to 21.4 Gy. This shows that daily prostate translations of patient No. 1 bring up a non-negligible dosimetric impact on the PTV, CTV， bladder and rectum.

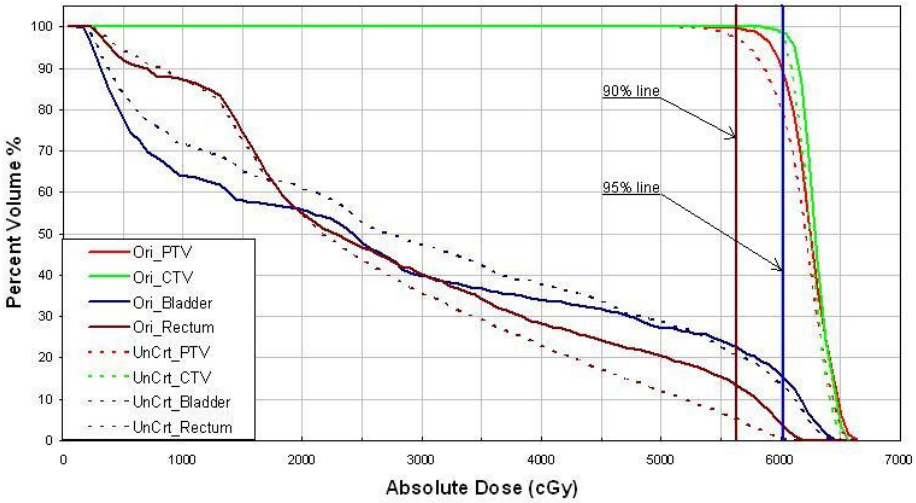

Figure 23: Comparison of DVH curves for PTV, CTV, bladder and rectum between scenario 2 (daily translation without correction) and scenario 1 (original plan, no motion).

5.2.3 Statistics on percent variations of DVH indices

To assess the dosimetric impact of prostate translation, percent variations of DVH indices have been computed for all 32 patients using equations 3.13 and 3.14. These DVH indices include D_{mean}, $D_{90\%}$, $D_{95\%}$, $V_{90\%}$, and $V_{95\%}$ for PTV, CTV and GTV. Their results are shown in Table 11 which shows that, without daily translation correction, up to -11.9% mean variation of $D_{95\%}$ and -22.2% of $V_{95\%}$ may happen for the PTV. For CTV and GTV, the variations of $D_{95\%}$ (-5.1 for CTV and -4.2% for GTV) due to daily translation are also significant.

	PTV	CTV	GTV
	Mean ± SD	Mean ± SD	Mean ± SD
$\Delta D_{mean}/D_{mean\_ori}$ (%)	-3.5 ± 4.3	-2.3 ± 4.7	-1.5 ± 2.1
$\Delta D_{90\%}/D_{90\%\_ori}$ (%)	-9.1 ± 11.3	-4.8 ± 9.6	-3.2 ± 5.2
$\Delta D_{95\%}/D_{95\%\_ori}$ (%)	-11.9 ± 13.7	-5.1 ± 10.0	-4.2 ± 7.3
$\Delta V_{90\%}/V_{90\%\_ori}$ (%)	-14.1 ± 20.1	-6.7 ± 16.1	-7.4 ± 20.4
$\Delta V_{95\%}/V_{95\%\_ori}$ (%)	-22.2 ± 21.2	-11.7 ± 21.6	-9.5 ± 15.7

Table 11: Statistical results of percent variations of DVH indices for PTV, CTV and GTV between scenario 2 and scenario 1 for 32 patients

Figure 24 plots $\Delta D_{95\%}/D_{95\%\_ori}$ and $\Delta V_{95\%}/V_{95\%\_ori}$ of PTV, CTV and GTV for 32 patients. 39 treatment plans (some patients have more than one treatment plan) in total have been included. Several data points with more than -40% of $\Delta D_{95\%}/D_{95\%\_ori}$ and more than 70% of $\Delta V_{95\%}/V_{95\%\_ori}$ for PTV have been observed. These results show that, for an

individual prostate patient, the dosimetric change due to daily translation could be quite large.

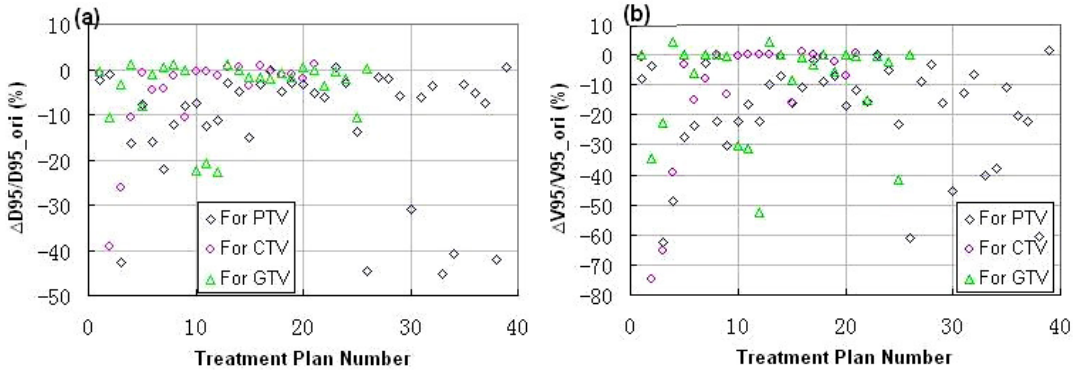

Figure 24: Diagrams plotting (a) $\Delta D_{95\%}/D_{95\%\_ori}$ and (b) $\Delta V_{95\%}/V_{95\%\_ori}$ for PTV, CTV and GTV between scenario 2 and scenario 1 vs. plan numbers for 32 patients

Statistics on bladder and rectum between scenario 2 and scenario 1 has been presented in Table 12 and Figure 25. Table 12 displays the mean and SD of percent variation of D_{mean}, $D_{50\%}$ and $V_{50\%}$ for bladder and rectum. An increase in mean $\Delta V_{50\%}/V_{50\%\_ori}$ for bladder (9.0%) and a decrease for rectum (-15.8%) are observed. Figure 25 plots $\Delta D_{50\%}/D_{50\%\_ori}$ and $\Delta V_{50\%}/V_{50\%\_ori}$ of bladder and rectum as a function of plan numbers.

	Bladder	Rectum
	Mean ± SD	Mean ± SD
$\Delta D_{mean}/D_{mean\_ori}$ (%)	3.7 ± 17.5	-9.7 ± 19.3
$\Delta D_{50\%}/D_{50\%\_ori}$ (%)	6.5 ± 41.7	-3.9 ± 26.9
$\Delta V_{50\%}/V_{50\%\_ori}$ (%)	9.0 ± 25.3	-15.8 ± 35.8

Table 12: Statistical results of percent variations of DVH indices for bladder and rectum between scenario 2 and scenario 1 for 32 patients

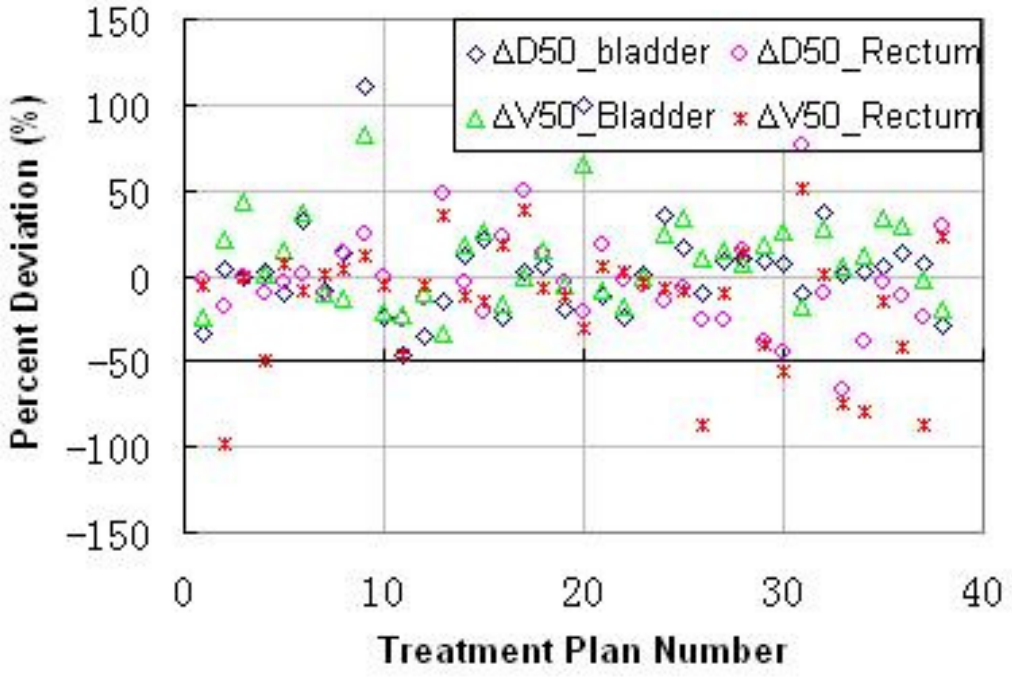

Figure 25: Diagrams plotting $\Delta D_{50\%}/D_{50\%\_ori}$ and $\Delta V_{50\%}/V_{50\%\_ori}$ of bladder and rectum between scenario 2 and scenario 1 vs. plan numbers for 32 patients

5.3 Dosimetric comparison: scenario 3 vs. scenario 1

5.3.1 Comparison of Isodose curves

Figure 26 compares the isodose curves derived from scenario 3 to scenario 1 for the selected patient No. 1. Scenario 3 simulates the actual patient treatment situation when US localization is used to address daily translations of prostate. With translation correction, a very good agreement in isodose curves of 15%, 50%, 90%, 95%, and 100% between scenario 3 and scenario 1 has been observed in Figure 26 when compared to the corresponding one in Figure 22.

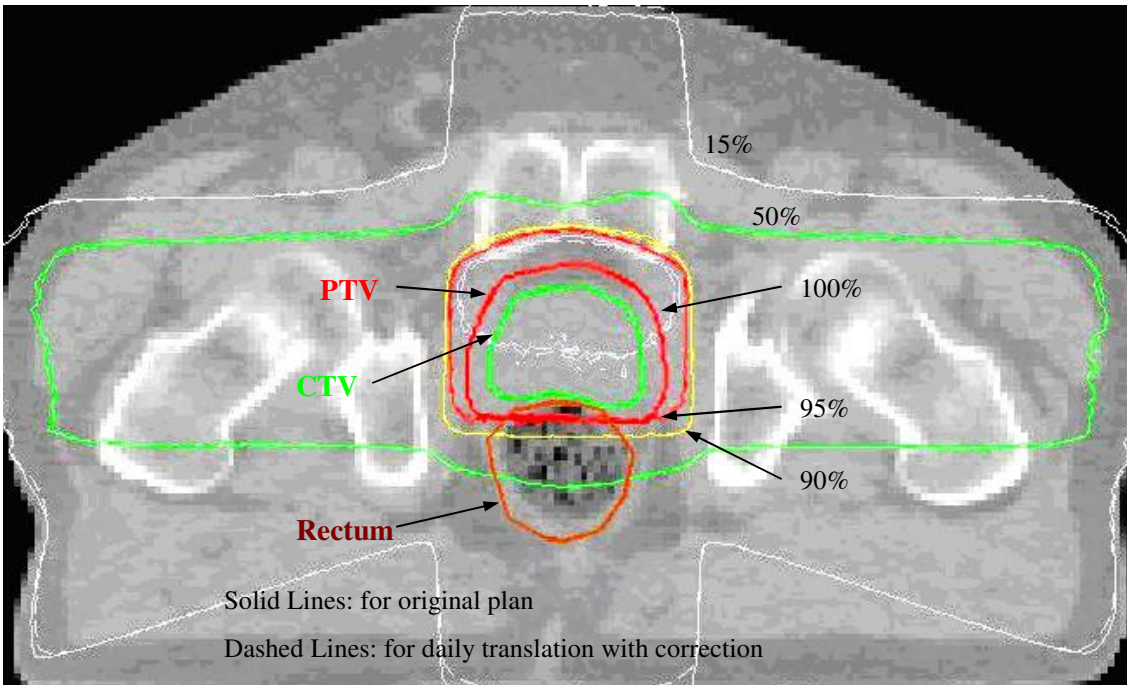

Figure 26: Comparison of isodose curves between scenario 3 (daily translation with correction) and scenario 1 at the isocentric axial plane

5.3.2 Comparison of DVH curves

Figure 27 compares the DVH curves for PTV, CTV, bladder and rectum between scenario 3 and scenario 1. "Crt" here is the abbreviation of correction, representing the scenario 3 in which prostate daily translations are localized by 3D US system and corrected by repositioning patient before each treatment. Figure 27 shows a very good agreement between the DVH curves derived from scenario 3 and scenario 1 for PTV, CTV, bladder and rectum. Percent variation of $D_{95\%}$ for PTV and CTV are 0.2% (-3.5 % for translation-uncorrected) and 0.5% (- 1.0% for translation-uncorrected), respectively. Percent variation of $D_{50\%}$ is about -0.8% (12.5% for translation-uncorrected) for bladder, and 0.6% (-4.4% for translation-uncorrected) for rectum. This shows that with translation correction the total dose distribution delivered to patient No. 1 has been effectively corrected for the organ motion impact.

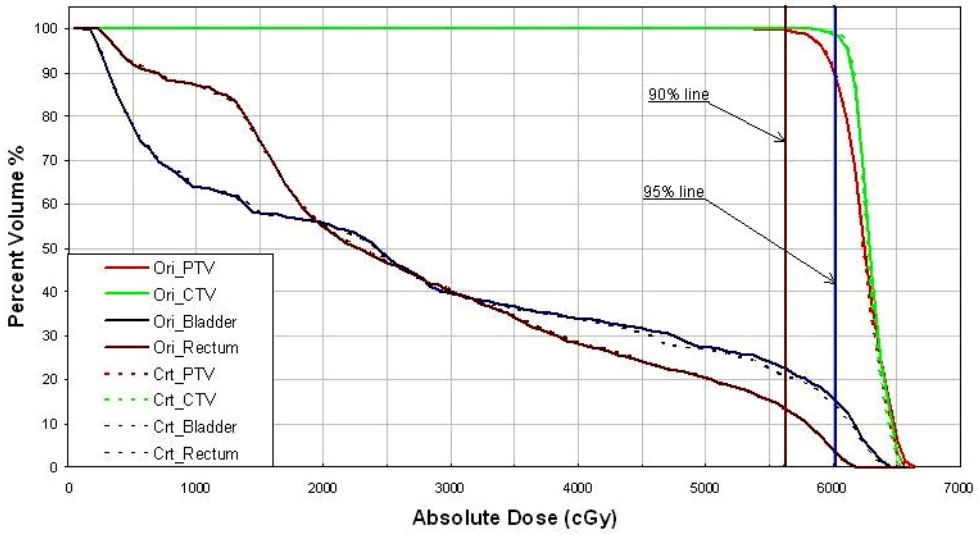

Figure 27: Comparison of DVH curves for PTV, CTV, bladder and rectum between scenario 3 (daily translation with correction) and scenario 1

5.3.3 Statistics on DVH variations

Similar to section 5.2.3, a statistical analysis on percent variations of DVH indices is made for all 32 patients. Table 13 displays the results of percent variations of DVH indices for PTV, CTV and GTV between scenario 3 and scenario 1. Except $\Delta V_{95\%}/V_{95\%\_ori}$, mean values for percent variation of DVH indices are close to zero with relative small SDs. This shows translation correction method has effectively improved or eliminated the dosimetric impact of daily prostate motion (assuming only translation is happened and is accurately detected by the US localization system).

	PTV	CTV	GTV
	Mean ± SD	Mean ± SD	Mean ± SD
$\Delta D_{mean}/D_{mean\_ori}$ (%)	-0.5 ± 1.8	-0.2 ± 0.6	-0.4 ± 2.2
$\Delta D_{90\%}/D_{90\%\_ori}$ (%)	-0.5 ± 2.1	-0.1 ± 0.8	-0.2 ± 2.3
$\Delta D_{95\%}/D_{95\%\_ori}$ (%)	-0.6 ± 2.5	-0.1 ± 1.0	-0.2 ± 2.4
$\Delta V_{90\%}/V_{90\%\_ori}$ (%)	-1.8 ± 6.0	-0.2 ± 0.5	-0.1 ± 0.7
$\Delta V_{95\%}/V_{95\%\_ori}$ (%)	-5.5 ± 17.0	-1.5 ± 3.9	-4.9 ± 19.8

Table 13: Statistical result of percent variations of DVH indices for PTV, CTV, and GTV between scenario 3 and scenario 1 for 32 patients

for PTV, CTV and GTV, their $\Delta V_{95\%}/V_{95\%\_ori}$ are -5.5 ± 17.0 (Mean ± SD), -1.5 ± 3.9, and -4.9 ± 19.8, respectively, compared to -22.2 ± 21.2, -11.7 ± 21.6, and -9.5 ± 15.7 for translation-uncorrected scenario. Again, a significant improvement is observed. This

improvement in mean $\Delta V_{95\%} / V_{95\%\_ori}$ verifies the effectiveness of the translation correction method. However, the relative large absolute values of $\Delta V_{95\%} / V_{95\%\_ori}$ and SDs for PTV, CTV and GTV show that the daily changes of patient geometry relative to the original plan still have kind of influence on patient total dose distribution even if translation correction method has been adopted.

Figure 28 plots $\Delta D_{95\%}/D_{95\%\_ori}$ and $\Delta V_{95\%}/V_{95\%\_ori}$ of PTV, CTV and GTV for 32 patients as a function of treatment plan number. The largest $\Delta D_{95\%}/D_{95\%\_ori}$ is about -8% for PTV, -4 % for CTV, and 6% for GTV while the largest $\Delta V_{95\%}/V_{95\%\_ori}$ for PTV, CTV and GTV are -28%, -13%, and -15%, respectively. Compared to those counterparts from scenario 2 (-45%, - 40%, and -22% of $\Delta D_{95\%}/D_{95\%\_ori}$, and -61%, -75% and -51% of $\Delta V_{95\%}/V_{95\%\_ori}$ for PTV, CTV, and GTV, respectively), the improvement is obvious.

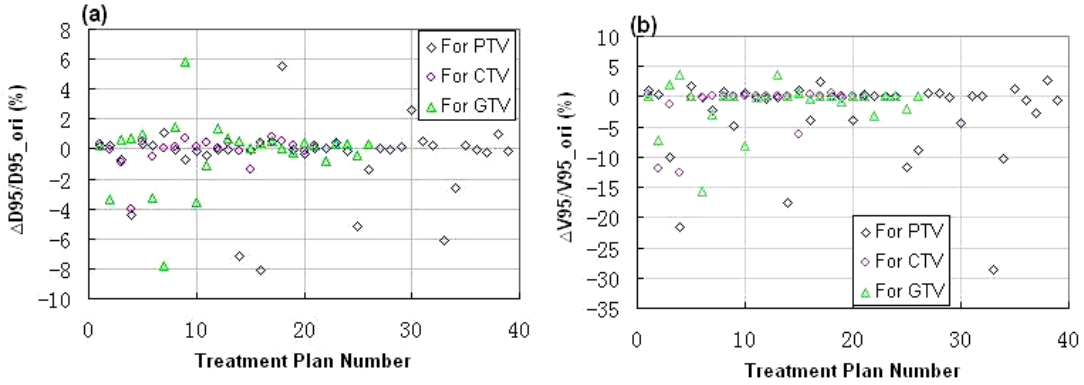

Figure 28: Diagrams plotting (a) $\Delta D_{95\%}/D_{95\%\_ori}$ and (b) $\Delta V_{95\%}/V_{95\%\_ori}$ for PTV, CTV and GTV between scenario 3 and scenario 1 vs. plan numbers for 32 patients

Table 14 displays the mean and SD of percent variation of D_{mean}, $D_{50\%}$ and $V_{50\%}$ for bladder and rectum for 32 patients. Mean $\Delta D_{50\%}/D_{50\%\_ori}$ and $\Delta V_{50\%}/V_{50\%\_ori}$ have been observed to be close to zero with small SDs. This trend is also clearly observed in Figure 29 which plots $\Delta D_{50\%}/D_{50\%\_ori}$ and $\Delta V_{50\%}/V_{50\%\_ori}$ for bladder and rectum as a function of treatment plan numbers. Although an increase in mean $\Delta D_{mean}/D_{mean\_ori}$ (3.7%) has been found for bladder, a decrease (-9.7%) has been found for rectum at the same time, these small changes in mean $\Delta D_{mean}/D_{mean\_ori}$ might not produce significant negative outcomes for bladder and rectum in clinic.

	Bladder	Rectum
	Mean ± SD	Mean ± SD
$\Delta D_{mean}/D_{mean\_ori}$ (%)	3.7 ± 17.5	-9.7 ± 19.3
$\Delta D_{50\%}/D_{50\%\_ori}$ (%)	-0.2 ± 6.3	-0.0 ± 3.6
$\Delta V_{50\%}/V_{50\%\_ori}$ (%)	-1.0 ± 5.0	0.4 ± 1.8

Table 14: Statistical results of percent variations of DVH indices for bladder and rectum between scenario 3 and scenario 1 for 32 patients

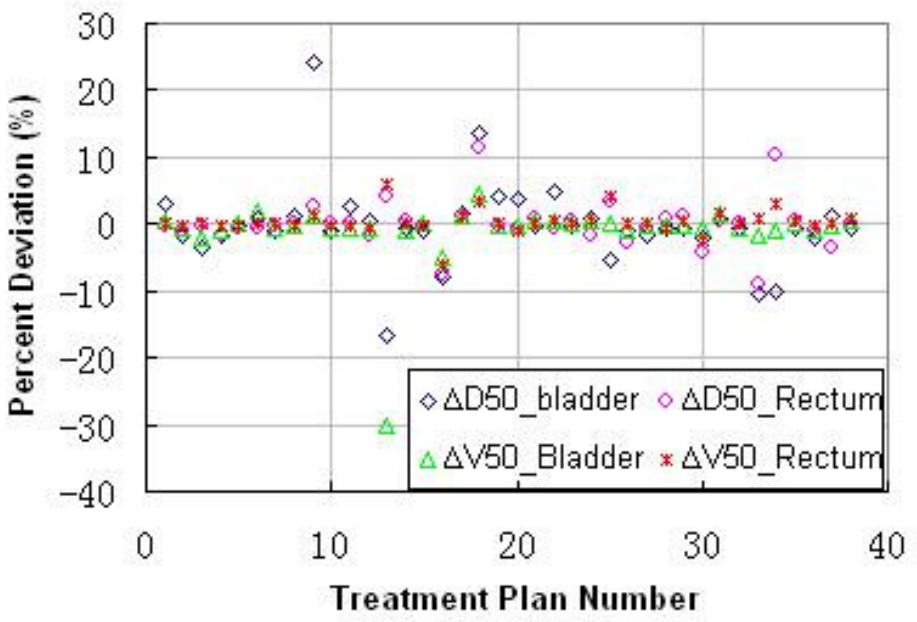

Figure 29: Diagrams plotting $\Delta D_{50\%}/D_{50\%\_ori}$ and $\Delta V_{50\%}/V_{50\%\_ori}$ for bladder and rectum between scenario 3 and scenario 1 vs. plan numbers for 32 patients

5.4 Dosimetric comparison: scenario 4 vs. scenario 1

5.4.1 Comparison of Isodose curves for patient No. 1

Scenario 4 considers the case in which daily prostate translation and rotation would co-occur while assuming OARs (bladder and rectum) would translate along with prostate. Three patient total doses have been calculated with an in-house MATLAB program and normalized to their XVMC-calculated isocenter doses from scenario 1.

Figure 30 displays the comparison of isodose curves between scenario 4 (daily translation plus rotation without correction) and scenario 1 at the isocentric axial plane for patient No. 1. Compared with Figure 22, larger differences are observed for 90% and

95% isodose curves in Figure 30. This shows that daily prostate rotation further deteriorates the patient total dose distribution.

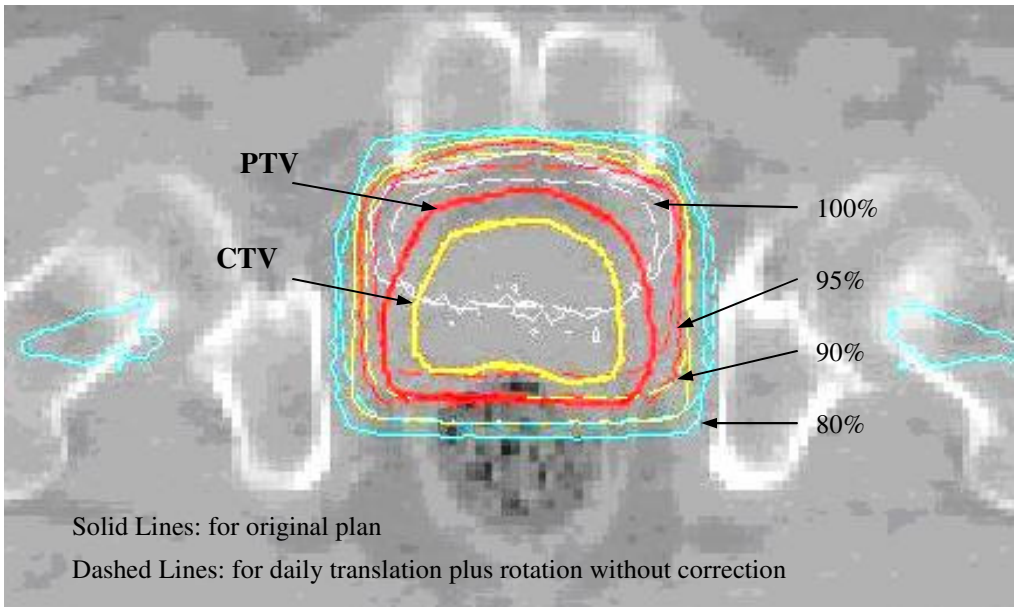

Figure 30: Comparison of isodose curves between scenario 4 (daily translation plus rotation without correction) and scenario 1 at the isocentric axial plane for patient No. 1.

5.4.2 Comparison of DVH curves with scenario 1

Figure 31 plots the comparison of DVH curves for PTV, CTV, bladder and rectum between scenario 4 (daily translation plus rotation without correction) and scenario 1 for patient No. 1. In the figure, "UnCrtTR" is the abbreviation of uncorrected translation and rotation, representing scenario 4. In the regions around 90% and 95% lines, an obvious large discrepancy in DVH curves have been observed for PTV and CTV. $\Delta D_{95\%}/D_{95\%\_ori}$ for PTV and CTV are -6.5% and -2.6%, respectively, compared to -3.5% and -0.95% from scenario 2 which has only daily prostate translation. DVH curves for bladder and rectum are the same as in Figure 27 since we assume they would only translate with prostate.

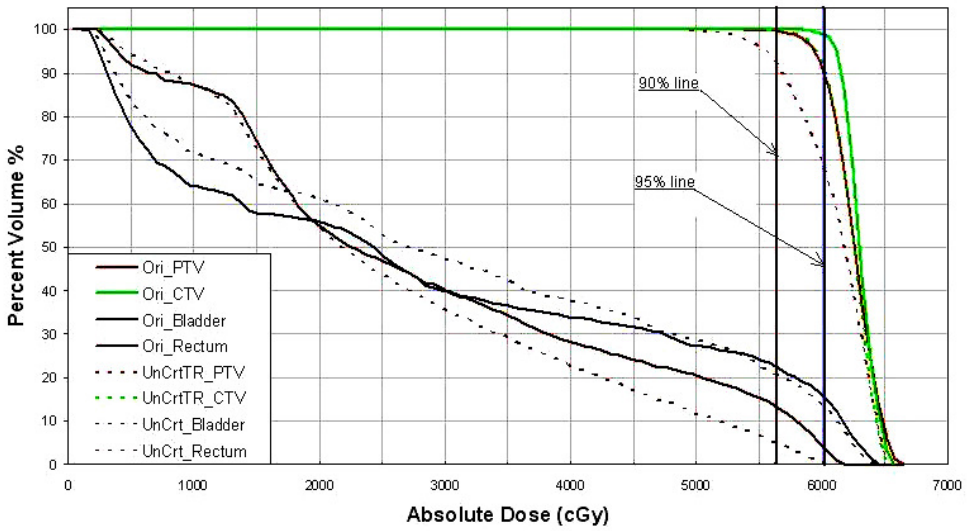

Figure 31: Comparison of DVH curves for PTV, CTV, bladder and rectum between scenario 4 (daily translation plus rotation without correction) and scenario 1 for patient No. 1

5.4.3 Statistics on DVH variations

As mentioned before, there are only three patients who are available for the study on translation-plus-rotation impact among 32 patients. Among them, patient No. 1 has no contours for GTV. Table 15 shows their $D_{95\%}/D_{95\%\_ori}$ and $\Delta V_{95\%}/V_{95\%\_ori}$ for PTV, CTV and GTV, compared with scenario 1. Means and SDs might have no statistical meaning since the sample number is only 3. Up to -28.6% of $\Delta D_{95\%}/D_{95\%\_ori}$ and up to -52.6% of $\Delta V_{95\%}/V_{95\%\_ori}$ have been found for the patient No. 3 who has non-spherical shapes of PTV, CTV and GTV. When there was only daily translation, the corresponding largest percent variations are -14% for $\Delta D_{95\%}/D_{95\%\_ori}$ and 23.1% for $\Delta V_{95\%}/V_{95\%\_ori}$. This shows that daily prostate rotation further deteriorate the dose distribution patient actually received.

		Patient 1	Patient 2	Patient 3	Mean ± SD
$\Delta D_{95\%}/D_{95\%\_ori}$ (%)	PTV	-6.5	-3.1	-28.6	-12.7 ± 13.8
	CTV	-2.6	-0.5	-13.8	-5.6 ± 7.2
	GTV		-0.1	-14.6	-7.4 ± 10.2
$\Delta V_{95\%}/V_{95\%\_ori}$ (%)	PTV	-23.7	-8.1	-52.6	-28.1 ± 22.6
	CTV	-6.6	-1.4	-40.9	-16.3 ± 21.4
	GTV		0.0	-38.7	-19.3 ± 27.3

Table 15: $\Delta D_{95\%}/D_{95\%\_ori}$ and $\Delta V_{95\%}/V_{95\%\_ori}$ for PTV, CTV and GTV between scenario 4 and scenario 1 for 3 patients

5.5 Dosimetric comparison: scenario 5 vs. scenario 1

5.5.1 Comparison of Isodose curves for patient No. 1

In clinical practice at the MGH, only prostate translation has been corrected even if prostate rotation may happen during the treatment. Scenario 5 is designed to simulate this situation. Patient fraction doses are calculated with the BEAMnrc/XVMC method and summed by taking daily translation and rotation into account to calculate patient total dose.

Figure 32 plots both isodose curves for scenario 5 (daily translation-plus-rotation with translation correction) and scenario 1 at the isocentric axial plane for patient No. 1. Although a great improvement has been observed, the discrepancy is still clearly identified. It implies that translation correction can improve the total dose the patient received, but can not thoroughly eliminate the influence of prostate rotation.

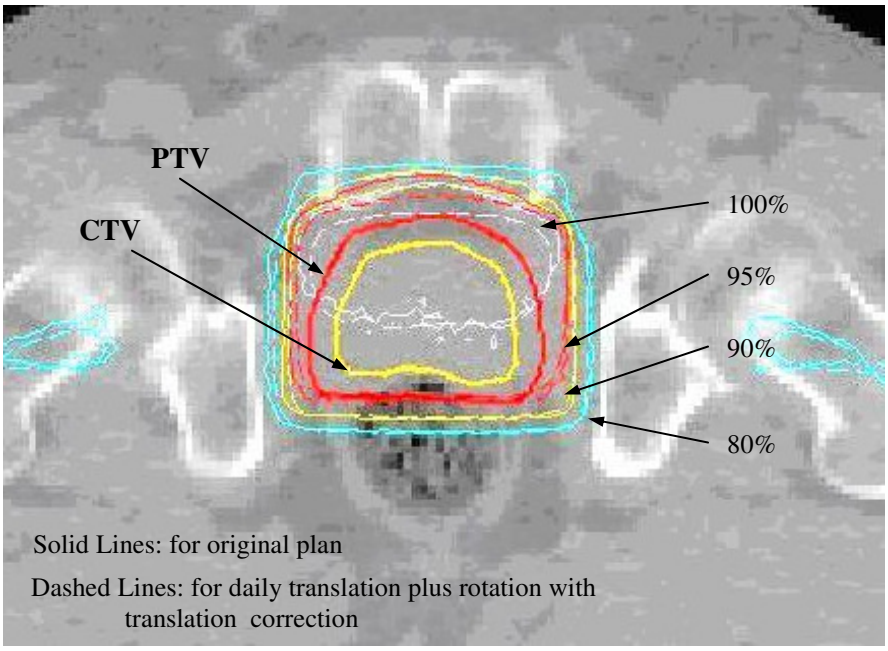

Figure 32: Comparison of isodose curves between scenario 5 (daily translation-plus-rotation with translation correction) and scenario 1 (original plan) at the isocentric axial plane for patient No. 1.

5.5.2 Comparison of DVH curves

Figure 33 plots DVH curves for PTV, CTV, bladder and rectum between scenario 5 and scenario 1 for patient No. 1. In the figure, CrtT_NonR is the abbreviation of corrected translation and non-corrected rotation, representing scenario 5. In the region around 90% and 95% lines, DVH curves for PTV and CTV have been improved significantly, compared to those in Figure 31. $\Delta D_{95\%}/D_{95\%\_ori}$ for PTV and CTV are -4.2% and -1.8%, respectively, compared to -6.5% and -2.6% from scenario 4 in which no correction is done for both translation and rotation. DVH curves for bladder and rectum are almost completely corrected by the translation correction method under the assumption of no rotation for them.

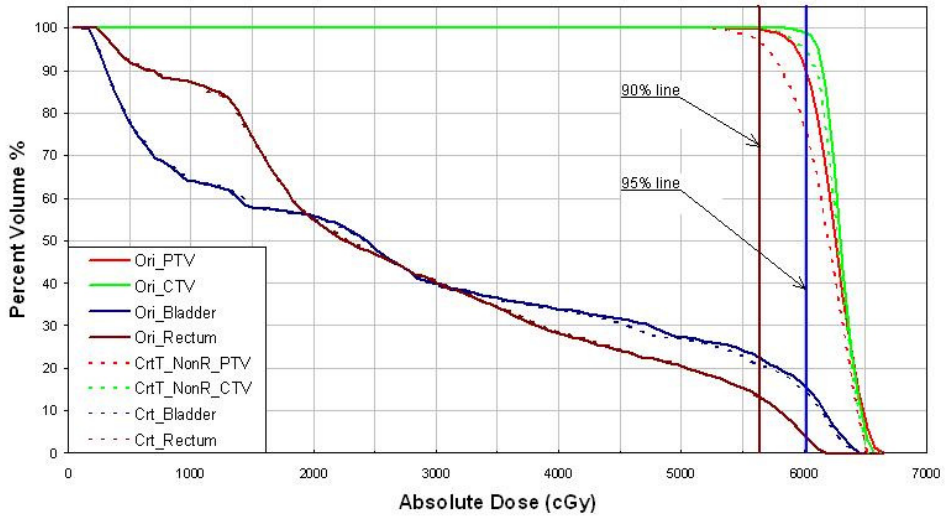

Figure 33: Comparison of DVH curves for PTV, CTV, bladder and rectum between scenario 5 (daily translation plus rotation with translation correction and no rotation correction) and scenario 1 for patient No. 1.

5.5.3 Statistics on DVH variations

Table 16 shows $D_{95\%}/_{D95\%\_ori}$ and $\Delta V_{95\%}/_{V95\%\_ori}$ for PTV, CTV and GTV from scenario 5 by compared them to scenario 1 for 3 patients. For patient No. 2, $\Delta D_{95\%}/D_{95\%\_ori}$ and $\Delta V_{95\%}/V_{95\%\_ori}$ are close to zero, meaning the patient total dose actually-delivered is almost the same as planned in the original plan when the translation correction method has been adopted. For patient No. 1 and patient No. 3, especially for patient No. 3, it still has a relative large $\Delta D_{95\%}/D_{95\%\_ori}$ and $\Delta V_{95\%}/V_{95\%\_ori}$, although $\Delta D_{95\%}/D_{95\%\_ori}$ for PTV is improved from -28.6% to -15.3%, and $\Delta V_{95\%}/V_{95\%\_ori}$ for PTV almost keeps the same

(about -53%). These results disclose a fact that only having translation correction may not be enough to eliminate the dosimetric impact of prostate rotation for some patients, especially when large daily prostate rotations had happened.

		Patient 1	Patient 2	Patient 3	Mean ± SD
$\Delta D_{95\%}/D_{95\%\_ori}$ (%)	PTV	-4.2	0.2	-15.3	-6.4 ± 8.0
	CTV	-1.8	0.6	-7.6	-2.9 ± 4.2
	GTV	-	-0.5	-4.2	-1.9 ± 3.3
$\Delta V_{95\%}/V_{95\%\_ori}$ (%)	PTV	-15.1	1.8	-52.8	-22.0 ± 27.9
	CTV	-3.9	0.5	-29.1	-10.8 ± 16.0
	GTV	-	0.0	-23.3	-11.6 ± 16.4

Table 16: $\Delta D_{95}/D_{95\_ori}$ and $\Delta V_{95}/V_{95\_ori}$ for PTV, CTV and GTV compared scenario 5 to scenario 1 for 3 patients

5.6 Discussion

It has become common clinical practice to overcome daily prostate motion by repositioning the patient according to localization with US, EPID or other imaging techniques. Since patient dose is not daily recalculated and optimized after the patient has been repositioned, a thorough understanding of the dosimetric impacts of translation, rotation, and geometrical changes is crucial.

Orton *et al* (2004) [83] studied the dosimetric effects of the translational isocenter correction with a rectal balloon for an IMRT treatment of the prostate with seven beams. Three scenarios: (1) the initial preplan; (2) a postplan with daily actual shifts; and (3) a postplan with daily actual shifts and correction had been simulated using the ADAC Pinnacle™ TPS in the study. Their results show that when daily shifts are done, doses to the target, rectal wall, and bladder wall are nearly identical to those in the preplan; however, when no shifts were made, the dose distributions are degraded, and the computed target EUD and TCP are lower for all involved five patients.

Wertz *et al* (2007) [44] analyzed the dosimetric consequences (with and without correction) for seven prostate cancer patients with empty and distended rectums in their conformal IMRT treatment. Dosimetric comparison for a single treatment fraction between two extreme situations had been made. Their studies revealed that organ motion decreased the $V_{95\%}$ for target by up to –24% and increased the mean rectum dose by up to

41% while linear translational correction increased $V_{95\%}$ of the prostate by up to 17%, and reduced the mean rectum dose by up to –23% compared to the uncorrected setup.

However, their studies did not cover a whole treatment course of daily prostate motion. For a whole treatment which may have more than thirty fractions, the random daily translation of prostate may compensate each other to reduce their dosimetric impacts in the total dose. Therefore, the dosimetric impacts of prostate motion may not be as significant as shown in the single fraction dose.

To investigate in detail the dosimetric impact of prostate motion, we make a statistical analysis on five hypothesized scenarios for conformal EBRT of the prostate in terms of isodose curves, DVH curves, and DVH indices, based on patient total dose calculated by the BEAMnrc/XVMC method. 39 treatment plans from 32 prostate patients have been recalculated for those scenarios covering cases with or without daily translation correction. All patient total dose distributions are computed by summing each fraction dose with taking daily prostate motion (translation and rotation) into account and normalized to their XVMC-calculated isocenter dose from their original plans.

Dosimetric comparison in section 5.2 shows that DVH indices for PTV, CTV and GTV can decrease significantly when daily translation is present and no correction is performed. In Figure 22 and Figure 23, a degradation of total dose distribution and a degradation of DVH curves for PTV and CTV have been observed clearly. Statistical results on 32 patients shown in Table 11 also indicate DVH indices for PTV, CTV and GTV are degraded significantly. Figure 24 shows the differences in DVH indices like $D_{95\%}$, $V_{95\%}$ and $V_{50\%}$ are considerably high for individual cases, showing a high patient dependence. For OARs, the rectum $D_{50\%}$ reduces by up to 15.7% on average while the bladder $D_{50\%}$ increases by up to 9.0%. Our findings agree with the findings from Wertz (2007) [44], Schaly (2005) [84] and Orton (2004) [83] in the same order of magnitude.

For scenario 4 where both translation and rotation are present and no correction method is performed, the degradation of dose distribution is more serious than for scenario 2 which has only translation as shown in Figures 30 and 31. For the typical patient, up to -28.6% of $\Delta D_{95\%}/D_{95\%\_ori}$ and up to -52.6% of $\Delta V_{95\%}/V_{95\%\_ori}$ have been observed for PTV, as shown in Table 15. Though only 3 patients are available for the rotation study, it still clearly indicates that daily prostate rotation further deteriorates the

patient dose distribution. The dosimetric effects of rotation on the bladder and rectum are not investigated here since we assume bladder and rectum were not to rotate with prostate.

Our analysis between scenario 3 and scenario 5 shows that translation correction method effectively improves the delivered patient dose. If only translation is present and the translation correction method is adopted (scenario 3), the isodose curves and DVH curves for PTV, CTV, GTV as well as bladder and rectum are nearly identical to those from the original plan (scenario 1), as shown in Figures 27 and 28. Statistical analysis shown in Table 13 also proves that translation correction method could almost completely eliminate the dosimetric impact of prostate motion if only daily translation is present. These findings agree with the results provided by Wertz *et al* (2007) [44] and Orton *et al* (2004) [83].

If both translation and rotation are daily present and only translation correction method is performed (scenario 5), our simulation shows that the isodose curves and DVH curves for PTV, CTV, and GTV are improved dramatically compared to those from the scenario 4 in which no correction adopted, as shown in Figures 33 and 34. Nonetheless, compared to the original plan, the percent variation of $D_{95\%}$ and $V_{95\%}$ for PTV are relatively high for some patients, e.g. -15.3% and -52.8% for patient No. 3 in Table 16. These large discrepancies show that the translation correction method alone may not be enough to eliminate the dosimetric impacts of translation and rotation, largely depending on individual patient anatomy and the shape of clinical targets. Large margins for PTV or rotation correction method may be necessary for those treatments. This claim may need further consolidation by future study.

In our study, we considered interfraction motion (translation and rotation) of the prostate as a rigid body. The actual motion may include intrafraction motion, deformation, and volume change due to prostate shrinking and extending (radiation effect or hormone therapy). These kinds of motion would also influence the actual dose delivered to the clinical target. Besides, the 3D US localization system has a potential to provide the daily volume information. The daily volume of PTV, which is derived from daily GTV of prostate cancer, is of clinical significance since different PTV volume may lead to different results of DVH analysis.

Chapter 6 Results and Discussion (3)
Dosimetric Impacts of Metal Prostheses on Prostate EBRT

Chapter 6 summarizes a preliminary study on the dosimetric impact of prostate PTVs derived from artefact-degraded CT images with or without 3D US aiding. These metal streaking artefacts are come from metal hip prostheses in prostate cancer patients. The artefact influences 1) the accuracy of target and OAR delineation, and 2) the accuracy of dose calculations due to an incorrect Hounsfield number to density conversion.

6.1 Introduction

The impact of metal objects in patients on MC dose calculations has been investigated by many authors, most recently by Bazalova *et al* [85]. She reported that the dose bias in 6 MV photon dose calculations with the DOSXYZnrc code decreased from 25% for CT images with artifacts to less than 2% for CT artifact-corrected images, compared to the dose calculated based on the actual phantom geometry. Besides, these CT images with artifact correction allow identifying and delineating organ structures that are initially invisible in the original images containing artifacts.

In this chapter, we apply Bazalova's artifact-correction algorithm on three prostate patients with metal hip prosthesis. Patients A and B have metal prostheses in both hips, and patient C has a metal prosthesis in only his right hip. Besides, patient A has two sub-plans in his original treatment planning, and patient C only has four beams planned for his treatment.

6.2 Comparison of PTVs from artifact-degraded, artifact-corrected and US-aided CT images

Figure 34 displays an axial CT image from patient C. Figure 34a, 34b and 34c show the same axial slice image from artifact-degraded, artifact-corrected, and US-aided CT images, respectively.

Figure 34a shows that, even for patient C with a metal prosthesis, the metal streaking artifact is severe enough to cause ambiguity in identifying the prostate behind the metal prosthesis. As shown in Fig. 34b, the correction algorithm employed by Bazalova *et al.* (85) removed most of the streaking artifacts but the improved CT image is still not good enough to clearly identify the prostate target. Figure 34c shows that the prostate on US-

aided CT images (Fig.34d) can be clearly identified and delineated, demonstrating that US, which can image a select portion of the pelvic region and be unaffected by objects outside the transducer range, may help in organ delineation on images that suffer from metal artifacts.

Figure 35 shows the PTV contours delineated from artifact-degraded, artifact-corrected and US-aided CT images for patient C. Artifact-degraded PTV contours (original PTV) were drawn by a clinical oncologist and was used as the clinical treatment target. The artifact-corrected and US-aided PTVs were drawn by the author (Chen Y) with help from an experienced dosimetrist. Figure 35 shows that the PTV contours from artifact-degraded, artifact-corrected and US-aided images tend to be similar, but have small differences in the regions which are close to patient metal prostheses. Among them, in order of increasing PTV size is the US-aided, artifact-corrected, and artifact-degraded images.

(a)

(b)

(c)

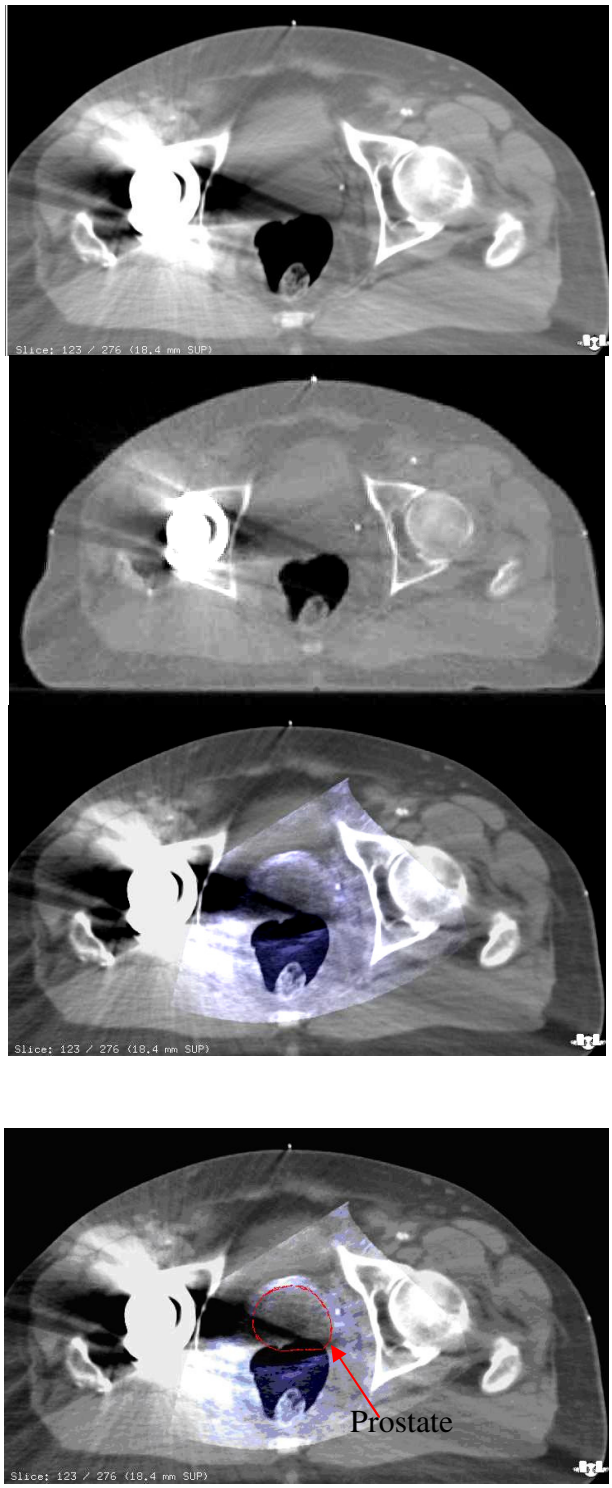

(d)

Figure 34: Axial CT images of a patient © with one hip prosthesis: a) original CT image with metal streaking artifacts; b) artifact-corrected CT image; c) original CT image fused with US image; d) prostate contoured on US-aided CT images.

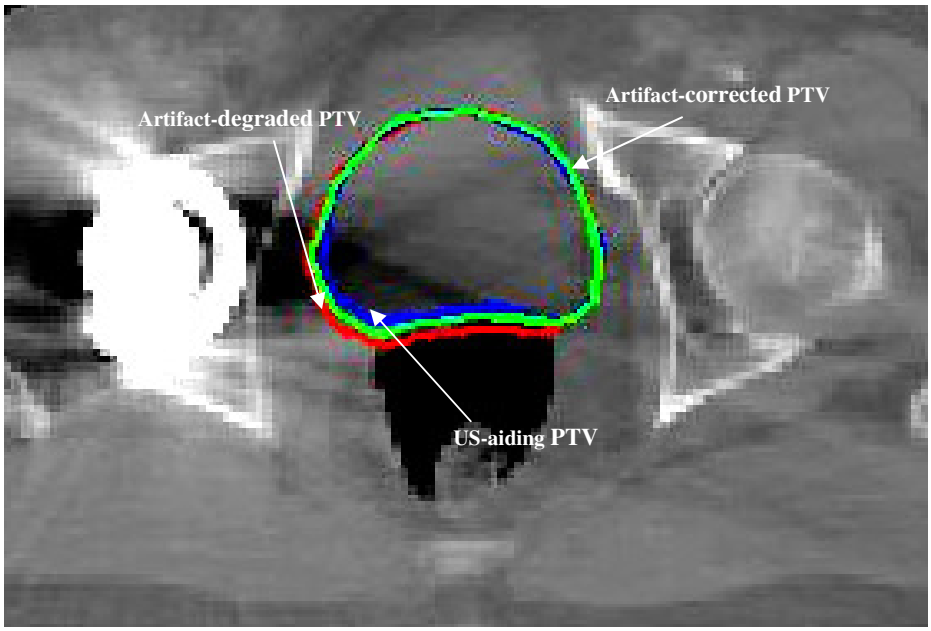

Figure 35: PTV contours from artifact-degraded, artifact-corrected and US-aided CT images for patient C at isocenter axial slice.

Table 17 shows the PTV volume and the volume change relative to $PTV_{Artifact\text{-}degraded}$ for three patients. On average, the US-aided PTV volume is about 5.2 % smaller than the artifact-degraded PTV volume.

		$PTV_{Artifact\text{-}degraded}$	$PTV_{Artifact\text{-}corrected}$	$PTV_{US\text{-}aided}$
Patient A	Volume cm^3	159.7	158.7	150.6
	Volume change %	-	-0.6	-5.7
Patient B	Volume cm^3	147.4	145.8	141.2
	Volume change %	-	-1.5	-4.2
Patient C	Volume cm^3	176.7	173.6	166.8
	Volume change %	-	-1.7	-5.6
Average Volume change %		-	-1.3	-5.2

Table 17: Volume and percent volume change of PTV relative to artifact-degraded PTV for three patients.

6.3 DVH comparison: artifact-degraded vs. artifact-corrected scenarios

Dose distributions based on artifact-corrected and artifact-degraded CT images were calculated with XVMC for all three metal hip prosthesis patients. A DVH analysis in

terms of $D_{95\%}$, $D_{90\%}$, $V_{95\%}$, and $V_{90\%}$ for PTV and $D_{50\%}$, $V_{50\%}$ for bladder and rectum is made based on those calculated dose distributions.

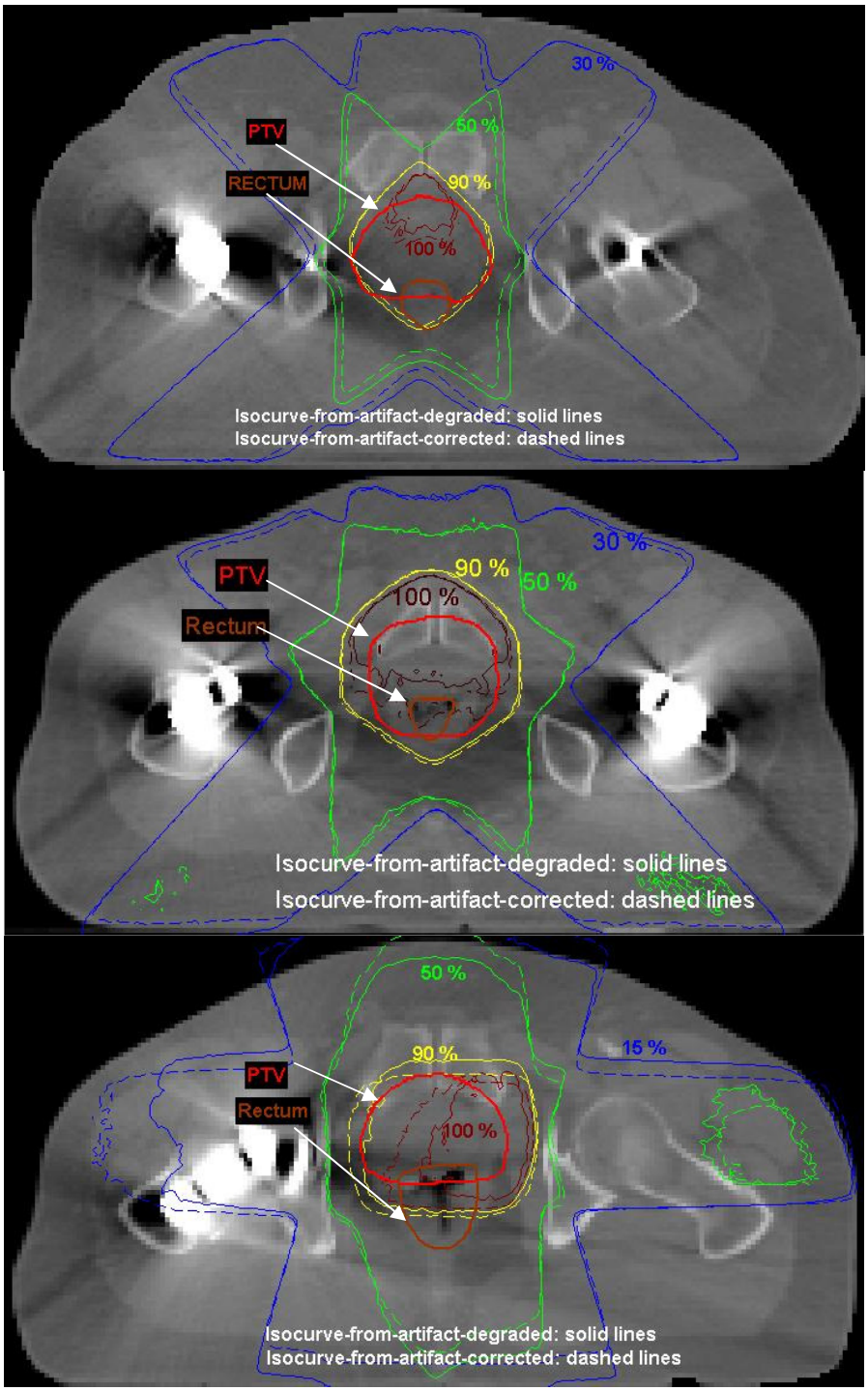

Figure 36: Isodose curve comparison at isocenter axial slice for (a) patient A, (b) patient B, and (c) patient C: artifact-degraded vs. artifact-corrected scenarios.

Figure 36 displays isodose curves derived from dose distributions calculated based on artifact-degraded and artifact-corrected CT images for patients A, B and C, respectively. All dose distributions are normalized to the isocenter. Figure 36 shows the isodose curves of 50% and 90% for three patients have a good agreement. A large discrepancy is observed on the 90% and 100% isodose curves.

Patient B's DVH curves for PTV, bladder and rectum are displayed in Figure 37. With artifact correction, the DVH curves for PTV, bladder and rectum obviously move to the right. This shows that the dose calculated based on artifact-corrected CT images is higher than the original planned dose calculated based on artifact-degraded CT images for the target, bladder and rectum. It implies that the dose delivered to the target and OAR may be under-estimated if the dose derived from artifact-degraded CT images was used for treatment planning.

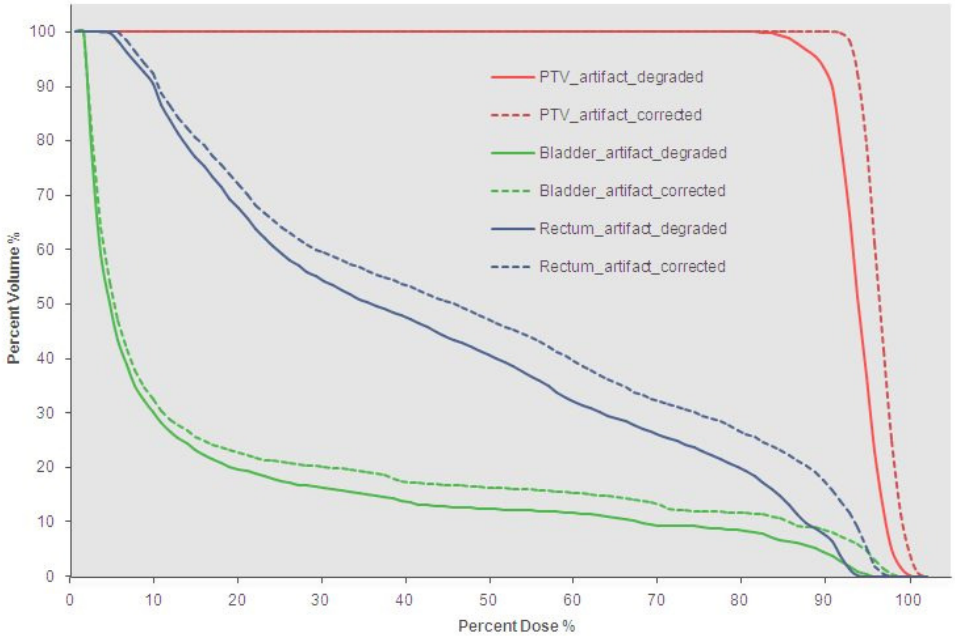

Figure 37: DVH curves for PTV, bladder, and rectum derived from artifact-degraded and artifact-corrected scenarios for patient B.

Table 18 shows the percent changes of DVH indices on PTV for three metal prosthesis patients in terms of $\Delta D_{90\%}$, $\Delta D_{95\%}$, $\Delta V_{90\%}$, and $\Delta V_{90\%}$ which are calculated with equations 3.13 and 3.14. Compared to the artifact-degraded scenario, artifact correction increases these DVH indices for patient B and C while decreases DVH indices for patient

A. The similar trends are observed in the comparison of DVH indices ($\Delta D_{50\%}$ and $\Delta V_{50\%}$) for bladder and rectum as shown in Table 19.

	Patient A	Patient B	Patient C
$\Delta D_{90\%}$ (%)	-11.7	3.9	5.2
$\Delta D_{95\%}$ (%)	-19.9	5.2	10.3
$\Delta V_{90\%}$ (%)	-8.0	1.0	6.9
$\Delta V_{95\%}$ (%)	-2.8	7.2	14.6

Table 18: Percent change of DVH indices on PTV between artifact-degraded and artifact-corrected scenarios for three patients

OAR	Bladder			Rectum		
	Patient A	Patient B	Patient C	Patient A	Patient B	Patient C
ΔD_{50} (%)	-41.5	12.9	41.6	-28.6	27.9	1.6
ΔV_{50} (%)	-10.3	4.0	35.0	-12.1	6.5	3.7

Table 19: Percent change of DVH indices on bladder and rectum between artifact-degraded and artifact-corrected scenarios for three patients

6.4 DVH comparison: artifact-degraded PTV vs. US-aided PTV

Based on the artifact-degraded and US-aided CT images, two PTVs have been contoured for each of metal prosthesis patients. The US-aided PTV is smaller than corresponding artifact-degraded PTV as shown in Table 17. The change of PTV volume and position result in the change of DVH analysis results for treatment planning as shown in Table 20.

Table 20 displays the percent changes of DVH indices for artifact-corrected PTV relative to artifact-degraded PTV for three patients. These DVH indices are computed with equations 3.13 and 3.14 for four scenarios: artifact-degraded, artifact-degraded with daily prostate displacements, artifact-degraded with daily displacement correction, and artifact-corrected. Table 20 shows that adopting US-aided PTV increases $\Delta D_{90\%}$, $\Delta D_{95\%}$, $\Delta V_{90\%}$, and $\Delta V_{90\%}$ by 1% - 4% on an average for three patients for four above-mentioned scenarios.

Scenario	Artifact-degraded				Artifact-degraded with displacements			
	Patient A	Patient B	Patient C	Ave.	Patient A	Patient B	Patient C	Ave.
$\Delta D_{90\%}$ (%)	1.4	0.5	0.8	0.9	2.1	1.3	3.2	2.2
$\Delta D_{95\%}$ (%)	1.1	1.3	2.7	1.7	2.7	1.7	6.7	3.7
$\Delta V_{90\%}$ (%)	2.5	0.8	1.3	1.5	2.9	2.2	2.9	2.7
$\Delta V_{90\%}$ (%)	3.9	2.9	2.4	3.1	2.4	4.4	5.3	4.0
Scenario	Artifact-degraded with displacement correction				Artifact-corrected			
	Patient A	Patient B	Patient C	Ave.	Patient A	Patient B	Patient C	Ave.
$\Delta D_{90\%}$ (%)	0.7	0.5	1.1	0.8	3.7	0.2	0.7	1.6
$\Delta D_{95\%}$ (%)	0.7	1.0	3.4	1.7	3.0	0.3	1.0	1.4
$\Delta V_{90\%}$ (%)	1.5	0.5	1.6	1.2	2.0	0.0	0.5	0.8
$\Delta V_{90\%}$ (%)	2.8	1.5	2.8	2.4	2.5	0.0	2.6	1.7

Table 20: Percent changes of DVH indices for US-aided PTV relative to artifact-corrected PTV under four scenarios: artifact-degraded, artifact-degraded with displacements, artifact-degraded with displacement correction, and artifact-corrected scenarios.

6.5 Discussion

In this study, an investigation on dosimetric impact of metal streaking artifacts in patient CT images has been carried out by comparing DVH results derived from patient CT images with and without artifact correction. This study shows that the streaking artifacts due to metal hip prostheses affect prostate delineation and dose calculations.

Table 17 shows that with US images smaller PTV (CTV from US-aided images plus 7mm margin) volumes could be obtained. This means with US images the prostate target may be reduced in size thus sparing more normal tissue and the OARs.

Metal prosthesis produces streaking artifacts in patient CT images. These metal artifacts cause the CT Hounsfield number to be mis-assigned. Since MC dose calculation methods (VMC and DOSXYZnrc) are based on heterogeneous information, converted from CT numbers, the accuracy of the dose calculation will be affected. Then the artifact-corrected images will provide a different dose distribution than the artifact-degraded images.

For patients B and C, adopting artifact-corrected CT images can improve the DVH curves of PTV, especially increase the $D_{95\%}$ and $V_{95\%}$ for PTV by more than 5% as shown in Table 18. $D_{50\%}$ and $V_{50\%}$ for rectum and bladder are also raised up to 41.6% as shown in Table 19. This implies that the dose calculation based on the artifact-degraded

CT images may under-estimate the dose in the region of target and the OARs in the vicinity, thus potentially raising the risk of giving higher dose to these organs. For patient A, however, adopting artifact-corrected CT images decreases the $D_{95\%}$ and $V_{95\%}$ for PTV up to 19.9%, $D_{50\%}$ and $V_{50\%}$ for rectum and bladder up to 41.5%. These conflicting results may come from beam angles in their treatment plans. In fact, three studied patient cases are not sufficient to make any solid conclusions.

Table 20 shows the DVH change for PTVs delineated with artifact-degraded and US-aided CT images. Although the US-aided PTV tends to 5% smaller than the artifact-degraded PTV, the changes of DVH indices for them are quite small, less than 4% for four studied scenarios. This may imply that, although using US image to aid delineating PTV contours may be helpful for oncologists to more clearly identify the prostate, it may not bring significant clinical benefits for patient treatment planning in terms of DVH analysis.

Chapter 7 Conclusion

7.1 Summary of Retrospective analysis on daily displacements

A retrospective statistical analysis is made on the database of daily displacements from 32 prostate patients, amounting to 890 pretreatment localizations. Those patients were treated with prostate localization with Restitu™ at the MGH between July of 2006 and March of 2008.

Our retrospective statistical analysis shows the measured displacements in the AP, SI, and RL directions are -3.3 ± 7.9 mm, -1.1 ± 6.4 mm, -0.2 ±5.6 mm, respectively. The largest rotation of prostate occurs about the lateral axis with a mean ± SD of -0.9° ± 4.6°, ranging between -6.7° and 8.0°. The population systematic and random uncertainties suggest a non-uniform PTV margin across the major axes (16.8 mm AP, 12.8 mm SI, and 12.1 mm RL) when US localization is not accessible.

7.2 Summary of Dosimetric impact of prostate motion

All prostate patient dose were planned and optimized in CADPlan and delivered with an 18 MV photon beam using a CL2300 Varian linac at the MGH. Daily prostate translation deteriorates the patient total dose distribution. Our statistics shows that up to -11.9% mean variation of $D_{95\%}$ is observed for the PTV, -5.1% for the CTV, and -4.2% for the GTV while $V_{95\%}$ of the PTV is reduced by a factor of -22.2% when daily prostate displacement is present and no correction method is performed. Similarly, the bladder and rectum also display dosimetric variations of $\Delta V_{50\%}/V_{50\%\_ori}$ to be 9.0% and -15.8%, respectively.

Rotation further deteriorates the patient total dose distribution, especially when the shape of the target (PTV, CTV, or GTV) is not spherical and non-uniform dose distribution exists in the target region. Up to -28.6% of $\Delta D_{95\%}/D_{95\%\_ori}$ and up to -52.6% of $\Delta V_{95\%}/V_{95\%\_ori}$ have been observed for patient No. 3 who has non-spherical shapes of PTV, CTV and GTV. Though our study is only based on 3 patients, it still clearly indicates that rotation with a mean angle of 0°, ranging from -6.7° to 8° during treatment course, may produce a non-negligible dosimetric impact.

The translation correction method dramatically improves the actual dose delivered to the patient target, even if rotation and translation are present at the same time. For the

case with only daily prostate translation, the correction method which repositions the patient according to 3D US localization has shown an effective correction in MC-calculated dose distributions. With correction, the MC-recalculated dose distributions for scenario 3 have almost the same dose distributions as the baseline (scenario 1), giving almost identical isodose curves, similarly for $D_{95\%}$, $V_{95\%}$ for PTV, CTV, and GTV, as well as similar $D_{50\%}$ and $V_{50\%}$ for bladder and rectum. For the case with rotation and translation, translation correction method could reduce $\Delta D_{95\%}/D_{95\%\_ori}$ for PTV from -6.5% to -4.2% and for CTV from -2.6% to -1.8% for one patient. For another patient, the effect of translation correction method showed a less pronounced improvement. For instance, $\Delta D_{95\%}/D_{95\%\_ori}$ for PTV is improved from -28.6% to -15.3% while $\Delta V_{95\%}/V_{95\%\_ori}$ for PTV remains the same (about -53%).

In summary, our study shows that prostate motion (translation and rotation) will deteriorate the total dose delivered to the patient target and OARs. With the translation correction method, the degraded patient dose could be recovered nearly completely for the case in which only translation is present. For the case with both translation and rotation, translation correction method could dramatically improve the degraded patient dose, but could not completely eliminate the dosimetric impact of rotation.

7.3 Summary of Dosimetric impact of metal prosthesis

Metal prosthesis produce streaking artifacts in patient CT images which affect prostate delineation and dose calculations. Sometimes the artifacts surrounding metal hips are too severe for oncologists to makes accurately contouring. At this situation, expanding the PTV contours based on oncologist's experience to make a conservative guess is clinically practical. The study on three prostate patients shows that artifact-degraded PTV is the largest, about 1.3 % larger than artifact-corrected PTV and 5.2% larger than US-aided PTV. This implies artifact-correction and US images may be helpful for accurately delineating prostate target and sparing more normal tissues.

MC calculation based on artifact-corrected and artifact-degraded images provides different dose distributions for the studied patients with metal hip prosthesis. DVH analysis is made based on those dose distributions. For patients B and C, adopting artifact-corrected CT images can improve the DVH curves of PTV and increase the $D_{95\%}$ and $V_{95\%}$ for PTV by more than 5% while $D_{50\%}$ and $V_{50\%}$ for rectum and bladder are

raised by up to 41.6%. For patient A, however, adopting artifact-corrected patient CT images decreases the $D_{95\%}$ and $V_{95\%}$ for PTV by around 19.9%, $D_{50\%}$ and $V_{50\%}$ for rectum and bladder by about 41.5%. The beam angles in their treatment plans may contribute to the conflicting results among patients A, B and C.

DVH analysis on artifact-degraded PTV and US-aided PTV shows a small difference in the changes of their DVH indices, less than 4% for four studied scenarios. However, a small study group consisting of only three patients is not sufficient to draw any solid conclusions. Further investigation on the dosimetric impacts of metal hip prosthesis based on a larger population needs to be done in the future.

Bibliography

[1] Prostate cancer statistics, Canadian Cancer Society website: http://www.cancer.ca/ccs/internet/standard/0,3182,3172_14471_langld-en,00.html, accessed July 5, 2008

[2] "Treatment Options at a Glance", Canadian Cancer Society website: http://info.cancer.ca/E/CCE/cceexplorer.asp?tocid=41, accessed July 5, 2008

[3] DeVita VTJ, Hellman S, and Rosenberg SA, "Cancer: Principles and Practice of Oncology", 6th ed, Philadelphia: Lippincott, Williams & Wilkins, 2001

[4] Clarisse Mark, "Image-guided radiotherapy using 2D and 3D ultrasounds combined with Monte Carlo dose calculations in prostate treatments", ETD Theses of Master degree, Medical Physics Unit, McGill University, 2005

[5] Frazier A, Du M, Wong J, Vicini F, Taylor R, Yu C, Matter R, Martime A, and Yan D, "Dosimetric evaluation of the conformation of the multileaf collimator to irregularly shaped fields", Int. J. Radiat. Oncol. Biol. Phys., 33(5): 1229-1238 (1995)

[6] Low DA, Mutic S, Dempsey JF, Gerber RL, Bosch WR, Perez CA and Purdy JA, "Quantitative dosimetric verification of an IMRT planning and delivery system", Radiotherapy & Oncology, 49(3): 305-316 (1998)

[7] Mackie TR, Balog J, Ruchala K, Shepard D, Aldridge S, Fitchard E, Reckwerdt P, Olivera G, McNutt T and Mehta M, "Tomotherapy", Seminars in Radiation Oncology, 9(1): 108-117 (1999)

[8] Pickles T, "What's a man to do?", Canadian Family Physician (50): 65-72 (2004)

[9] Eng TY, Thomas CR, and Herman TS, "Primary radiation therapy for localized prostate cancer", Urologic Oncology (7): 239–257 (2002)

[10] Malone S, Crook JM, Kendal WS, and Szanto J, "Respiratory-induced prostate motion: Quantification and characterization", Int. J. Radiat. Oncol. Biol. Phys. (48): 551-557 (2000)

[11] Van den Heuvel F, Tanya P, Edward S, Peter L, Mubashra K, Yue W, and Jeffrey DF, "Independent verification of ultrasound based image-guided radiation treatment, using electronic portal imaging and implanted gold markers", Med. Phys. (30): 2878-2887 (2003)

[12] Cury FL, Shenouda G, Souhami L, Duclos M, Faria SL, David M, Verhaegen F, Corns R, Falco T, "Ultrasound-Based Image Guided Radiotherapy for Prostate Cancer - Comparison of Cross-Modality and Intra-Modality Methods for Daily Localization during External Beam Radiotherapy", Int. J. Radiat. Oncol. Biol. Phys. (66): 1562-1567 (2006)

[13] Mellab E, Mageras GS, Fuks Z, Leibel SA, Niehaus A, lorant H, Zelefsky M, Baldwin B and Kutcher GJ, "Variations in prostate position quantification and implications for three-dimensional conformal treatment planning", Int. J. Radiat. Oncol. Biol. Phys. (38): 73-78 (1997)

[14] Djemil T, Mahadevan A, Kupelian P, Willoughby T, Enke C, Solberg T, Weinstein G, Flores SJN, Liu D, “Prostate Rotation Measured by Electromagnetic Tracking System: A Multi-Center Analysis”, Int. J. Radiat. Oncol. Biol. Phys., 66(3) supplement: S340 (2006)

[15] Aubrey JF, Beaulieu L, Girouard LM, Aubin S, Tremblay D, laverdiere J, and Vigneault E, “Measurements of intrafraction motion and interfraction rotation of prostate by three-dimensional analysis of daily portal imaging with radiopaque markers”, Int. J. Radiat. Oncol. Biol. Phys. (60): P30-39 (2004)

[16] Kuppersmith RB, Greco SC, Donovan DT, Grant W, Chiu JK, Cain RB, and Butler EB, “Intensity-modulated radiotherapy: first results with this new technology on neoplasm of the head and neck”, Ear, Nose & Throat. Journal, 78(4): 241-246 (1999)

[17] Pugachev A, Li JG, Boyer AL, Le Q, Hancock S, Donalson S, and Xing L, “Role of beam orientation optimization in intensity-modulated radiation therapy”, Int. J. Radiat. Oncol. Biol. Phys., 50(2): 551-60 (2001)

[18] Loef J, Lind BK, and Brahme A, “An adaptive control algorithm for optimization of intensity modulated radiotherapy considering uncertainties in beam profiles, patient setup and internal organ motion”, Phys. Med. Biol. (43): 1605-1628 (1996)

[19] Lockman DM, Yan D, and Wong J, “Estimating the dose variation in a volume of interest with explicit consideration of patient geometric variation”, Med. Phys., 27(9): 2100-2108 (2000)

[20] Lehnert SM, “Radiation Biology, Course Manual: part 2”, Medical Physics Unit, McGill University, P151-153 (2007)

[21] Di Y and David L, “Organ/patient geometric variation in external beam radiotherapy and its effects”, Med. Phys., 28(4): 593-602 (2001)

[22] Balter JM, Lam KL, and Sandler HM, “Automated localization of prostate at the time of treatment using implanted radiopaque markers: Technical feasibility”, Int. J. Radiat. Oncol. Biol. Phys., 33: 1281-1286 (1995)

[23] Nederveen A, Lagendijk J, and Hofman P, “Detection of fiducial gold markers for automatic on-time megavoltage position verification using a marker extraction kernel (MEK)”, Int. J. Radiat. Oncol. Biol. Phys., 47: 1435-1442 (2000)

[24] Jaffray D, Drake DG, Moreau M, Maritienz AA, and Wong JW, “A radiographyic and tomographic imaging system integrated into a medical linear accelerator for localization of bone and soft-tissue targets”, Int. J. Radiat. Oncol. Biol. Phys., 43: 773-789 (1999)

[25] Jaffray D, Siewerdsen JH, Edmundson JW, Wong JW, and Martinez AA, “Cone-beam CT: application in image-guided external beam radiotherapy and brachytherapy”, the 22nd annual EMBS international conference, IEEE, Chicago, IL. (2000)

[26] Spitters-Post I, Van DVLP, Van LENJT, and Visser AG, “The use of fiducial (gold) markers for monitoring prostate movements during radiation therapy”, Radiother. Oncol. (64) (Suppl. 1): S44 (2002)

[27] Nederveen AJ, van der Heide UA, Dehnad H, Jeroen R, Van MA, Hofman P, and Lagendijk JJW, "Measurements and clinical consequences of prostate motion during a radiotherapy fraction", Int. J. Radiat. Oncol. Biol. Phys. (53): 206-214 (2002)

[28] Lattanzi J, McNeeley S, Pinover W, Horwitz E, Das I, Schultheiss TE, and Hanks GE, "A comparison of daily CT localization to a daily ultrasound-based system in prostate cancer", Int. J. Radiat. Oncol. Biol. Phys. (43): 719 – 725 (1999)

[29] Arno J and Mundt MD, "IMRT and IGRT: Current Status", Department of Radiation Oncology, University of California San Diego, Website: http://radonc.ucsd.edu/whatsnew/presentations/Japan2007IMRT_IGRTstatusMundt.pdf

[30] Scarbrough TJ, Golden NM, Fuller CD, Kupelian PA, Ting JY, Wong A, and Thomas CR, "Ultrasound Versus Seed Marker Prostate Localization", Int. J. Radiat. Oncol. Biol. Phys., 63(2) Supplement: 1086 (2005)

[31] Nigel PO and Hazim AJ, "Clinical assessment of three-dimensional ultrasound prostate localization for external beam radiotherapy", Medical Physics, 33(12): 4710-4717 (2006)

[32] Weyers B, Wu C, Goddu S, and Michalski J , "Image Guided Radiotherapy in Prostate Localization: A Comparison of Ultrasound Modalities to Implanted Seed Markers and Assessment of Intrafraction Prostate Motion", Medical Physics, 34(6): 2375 (2007)

[33] Cury FL, Shenouda G, Souhami L, Duclos M, Faria S, David M, Corns R, and Falco T, "Comparison of BAT system and a new 3D trans-abdominal ultrasound-based image-guided system for prostate daily localization during external beam radiotherapy", 46th ASTRO Annual Meeting, 2003

[34] Hilts M, Bull T, Patterson K, Small V, Drever L, and Berthelet E, "Reproducibility of prostate misalignments computed by automatic segmentation of abdominal ultrasound images used for image guided radiation therapy", World Congress on Medical Physics and Biomedical Engineering (14): 1827-1830 (2006)

[35] Szpala S, Morton G, Tirona R, and O'Brien P, "Evaluation of Ultrasound-Based 3D Positioning System (Restitu by Resonant Medical) for Localizing and Delineating Prostate Targets for Image-Guided Radiation Treatment: Phantom Study and Estimates of Distortions in US Images of a Patient", Medical Physics, 33(7): 2675 (2006)

[36] Chan GH, "Investigation of Uncertainties and Interuser Variability in RESTITU™-a 3D Ultrasound System for Image Guided Radiation Therapy: A Phantom Study", Int. J. Radiat. Oncol. Biol. Phys., 69(3): S702 - S702 (2007)

[37] Brandner E, Specht R, Bahri S, Poltinnikov I, Huq M, and Heron D, "Evaluation of Ultrasound Localization Versus MV Portal Images of Fiducial Markers in Prostates", Medical Physics, 34(6): 2332 (2007)

[38] Li X, Ding C, Yang Y, Smith R, Deustch M, Beriwal S, Heron D, Huq M, "Ultrasound-Guided Prostate IMRT Planning: An Ultrasound-CT Application", Medical Physics, 34(6): 2638 (2007)

[39] Ding C, Li X, Yang Y, Heron D, Huq M, “Evaluating the Impact of Probe Depression On Prostate Displacement in Ultrasound-Guided Prostate IMRT Treatment”, Medical Physics, 34(6): 2564 (2007)
[40] Holly A Johnston, “Benchmarking a new three-dimensional ultrasound system for prostate image guided radiation therapy”, ETD Theses of Master degree (Dept. of Physics and Astronomy), University of Victoria, 2008
[41] S Webb, “Motion effects in (intensity modulated) radiation therapy: a review”, Phys. Med. Biol. (51): R403-R417 (2006)
[42] Wells PNT, “Ultrasound Imaging”, Phys. Med. Biol. (51): R83-R98 (2006)
[43] Liang LH, “Statistical analysis and biological effects of prostate motion in ultrasound image-guided external beam radiotherapy”, ETD Theses of Master degree, Medical Physics Unit, McGill University, 2004
[44] Wertz H, Lohr F, Dobler B, Mai S, Welzel G, Boda-Heggemann J, and Wenz F, “Dosimetric consequences of a translational isocenter correction based on image guidance for intensity modulated radiotherapy (IMRT) of the prostate”, Phys. Med. Biol. (52): 5655–5665 (2007)
[45] Fraser D, Mark C, Cury FL, Chang A and Verhaegen F, “Comparison of conventional and Monte Carlo dose calculations for prostate treatments”, J. Phys.: Conf. Ser. 102 012010 (7pp) doi: 10.1088/1742-6596/102/1/012010 (2008)
[46] Photon treatment planning collaborative working group, “Role of inhomogeneity corrections in three-dimensional photon treatment planning”, Int. J. Radiat. Oncol. Biol. Phys. (21): 59-69 (2001)
[47] Sterpin E, Tomsej M, De SmedtB, Reynaert N, and Vynckier S, “Monte Carlo evaluation of the AAA treatment planning algorithm in a heterogeneous multilayer phantom and IMRT clinical treatments for an Elekta SL25 linear accelerator”, Med. Phys., 34(5): 1665-1677 (2007)
[48] Yang J, Li J, Chen L, Price R, McNeeley S, Qin L, Wang L, Xiong W and Ma CM, “Dosimetric verification of IMRT treatment planning using Monte Carlo simulations”, Phys. Med. Biol. (50): 869-878 (2004)
[49] Jone WW and James AP, “On methods of inhomogeneity corrections for photon transport”, Med. Phys. (17): 807-817 (1990)
[50] Fippel M, “Fast Monte Carlo dose calculation for photon beams based on the VMC electron algorithm”, Med. Phys., 26(8): 1466-1475 (1999)
[51] Bland JM and Altman DG, “Measuring agreement in method comparison studies”, Stat Methods Med. Res. (8): 135–160 (1999)
[52] Van den Heuvel F , Fugazzib J, Seppi E, and Jeffrey D, “Clinical application of a repositioning scheme, using gold markers and electronic portal imaging”, Radiotherapy and Oncology, 79(1): 94-100 (2006)
[53] Stroom JC, Peter CMK, Gert AK, Marjolein VO, Marjolein J , Hans CJDB, Peter CL, and Ben JMH, “Internal organ motion in prostate cancer patients treated in prone and supine treatment position”, Radiother. Oncol. (51): 237–248 (1999)

[54] Stroom JC, de Boer HC, Huizenga H and Visser AG, “Inclusion of geometrical uncertainties in radiotherapy treatment planning by means of coverage probability”, Int. J. Radiat. Oncol. Biol. Phys, (43): 905-919 (1999)

[55] Van Herk M, Remeijer P, Lebesque JV, “Inclusion of geometric uncertainties in treatment planning”, Intl. J. Radiat. Oncol. Biol. Phys. (52): 1407－1422 (2002).

[56] Poon E, Le Y, Williamson JF, and Verhaegen F, “BrachyGUI: an adjunct to an accelerated Monte Carlo photon transport code for patient-specific brachytherapy dose calculations and analysis”, Journal of Physics: Conference Series 102, 012018 (2008)

[57] Studholme C, Hill DLG, and Hawkes DJ, “An overlap invariant entropy measure of 3D medical image alignment”, Pattern recognition (32): 71-86 (1999)

[58] Lattanzi J, McNeeley S, Donnelly S, Palacio E, Hanlon A, Schultheiss TE and Hanks GE, “Ultrasound based stereotactic guidance in prostate cancer-quantification of organ motion and setup errors in external beam radiotherapy”, Compu. Aided Surg (5): 289-295 (2000)

[59] Morr J, DiPietrillo T, Tsai JS, Engler M and Wazer DE, “Initial experience with ultrasound localization for positioning prostate cancer patients for external beam radiotherapy”, Int. J. Radiat. Oncol.Biol. Phys. (53): 1124-1129 (2002)

[60] Wertz H, Lohr F, Dobler B, Mai S, Welzel G, Boda-Heggemann J, and Wenz F, “Dosimetric consequences of a translational isocenter correction based on image guidance for intensity modulated radiotherapy (IMRT) of the prostate”, Phys. Med. Biol. (52): 5655–5665 (2007)

[61] Deurloo KE, Steenbakkers TJ, Zijp LJ, de Bois JA, Nowak PJ, Rasch CR, and Van Herk M, “Quantification of shape variation of prostate and seminal vesicles during external beam radiotherapy”, Int. J. Radiat. Oncol. Biol.Phys. (61): 228-238 (2005)

[62] Kupelian PA, Willoughby TR, Meeks SL, Forbes A, Wagner T, Maach M, and Langen KM, “Intraprostatic fiducials for localization of the prostate gland: monitoring intermarker distances during radiation therapy to test for marker stability”, Int. J. Radiat. Oncol. Biol. Phys. (62): 1291－1296 (2005)

[63] Birkner M, Yan D, Alber M, Liang J, and Nusslin F, “Adapting inverse planning to patient and organ geometrical variation: algorithm and implementation”, Med. Phys. (30): 2822－2831 (2003)

[64] Court LE, Dong L, Lee AK, Cheung R, Bonnen MD, O‘Daniel J, Wang H, Mohan R, and Kuban D, “An automatic CT-guided adaptive radiation therapy technique by online modification of multileaf collimator leaf positions for prostate cancer”, Int. J. Radiat. Oncol. Biol. Phys. (62): 154－163 (2005)

[65] Rehbinder H, Forsgren C, and Lof J, “Adaptive radiation therapy for compensation of errors in patient setup and treatment delivery”, Med. Phys. (31): 3363－3371 (2004)

[66] Verhaegen F and Seuntjens J, “Monte Carlo modelling of external radiotherapy photon beams”, Phys. Med. Biol. (48): R107－R164 (2003)

[67] Rogers DWO, Faddegon BA, Ding GX, Ma CM, We J, and Mackie TR “BEAM: a Monte Carlo code to simulate radiotherapy treatment units”, Med. Phys. (22): 503－524 (1995)
[68] Ma CM, Reckwerdt P, Holmes M, Rogers DWO, Geiser B, and Walters B, “DOSXYZ Users Manual”, NRCC Report No. PIRS-0509B, 1996
[69] Kawrakow I, Fippel M, and Friedrich K, “3D electron dose calculation using a Voxel based Monte Carlo algorithm －VMC”, Med. Phys. (23): 445－457 (1996)
[70] Fippel M, Kawrakow I, and Friedrich K, “Electron beam dose calculations with the VMC algorithm and the verification data of the NCI working group”, Phys. Med. Biol. (42): 501－520 (1997)
[71] Fippel M, “Fast Monte Carlo dose calculation for photon beams based on the VMC electron algorithm”, Med. Phys., 26(8): 1466-1475 (1999)
[72] Emily Heath, “4D Monte Carlo investigation of organ motion in radiotherapy for lung cancer”, PH.D dissertation, Medical Physics Unit, McGill University, Montréal, Quebec, 2008
[73] Jeffrey VS, Paul JK, Jong OK and Radhe M, “A method for photon beam Monte Carlo multileaf collimator particle transport”, Phys. Med. Biol. (47): 3225－3249 (2002)
[74] Wamied Abdel-Rahman, “A study of the build-up region of megavoltage radiation beams”, PH.D dissertation, Medical Physics Unit, McGill University, Montréal, Quebec, 2004
[75] van der Zee W and Welleweerd J, “A Monte Carlo study on internal wedges using BEAM”, Med. Phys. (29): 876－885 (2002)
[76] Andrew Alexander, “MMCTP: A radiotherapy research environment for patient-treatment planning”, M.Sc. Thesis, Medical Physics Unit, McGill University, Montréal, Quebec, 2006
[77] Jinxian Dai, “Validation of Monte Carlo techniques for 3D-CRT of lung cancer patients and comparative evaluation of treatment plans”, M.Sc. Thesis, Medical Physics Unit, McGill University, Montréal, Quebec, 2004
[78] Herve A and Paul V, “Lilliefors/Van Soest’s test of normality”, website: http://www.utdallas.edu/~herve/Abdi-Lillie2007-pretty.pdf, accessed at July 2, 2008
[79] Poli MER, Parker W, Patrocinio H, Souhami L, Shenouda G, Campos LL, Podgorsak EB, “An assessment of PTV margin definitions for patients for patients undergoing conformal 3D external beam radiation therapy for prostate cancer based on an analysis of 10,327 pre-treatment daily ultrasound localizations”, Int. J. Radiation Oncology Biol. Phys., 67(5): 1430－1437 (2007)
[80] Smith WL, Lewis C, Bauman G, Rodrigues G, Souza D, Ash R, Ho D, Venkatesan V, Downey D, and Fenster A, “3DUS, MRI and CT Prostate Volume Definition: 3D Evaluation of Intra- and Inter-Modality and Observer Variability”, Medical Physics, 32(6): 2083 (2005)

[81] Padhani AR, Khoo VS, and Suckling J, "Evaluating the effect of rectal distension and rectal movement on the prostate gland position using cine MRI", Int. J. Radiat. Oncol. Biol. Phys. (44): 525-533 (1999)

[82] Little DJ, Dong L, and Levy LB, "Use of portal images and BAT Ultrasonography to measure setup error and organ motion for prostate IMRT: Implications for treatment margins", Int. J. Radiat. Oncol. Biol. Phys. (56): 1218–1224 (2003)

[83] Orton NP and Tome WA, "The impact of daily shifts on prostate IMRT dose distributions", Med. Phys. (31): 2845–2848 (2004)

[84] Schaly B, Bauman GS, Song W, Battista JJ, and Van DJ, "Dosimetric impact of image-guided 3D conformal radiation therapy of prostate cancer", Phys. Med. Biol. (50): 3083–3101 (2005)

[85] Bazalova M, Beaulieu L, Palefsky S, and Verhaegen F, "Correction of CT artifacts and its influence on Monte Carlo dose calculations", Med. Phys., 34(6): 2119–2132 (2007)

[86] A. Gottschalk, S. Hossain, C. Chuang, M. Descovich, L. Ma, Intrafraction Prostate Motion during CyberKnife Radiosurgery: Implications on Planning Margins, Int. J. Radiat. Oncol. Biol. Phys. 72 (1): S569-S569 (2008)

[87] T. Willoughby, P. Kupelian, J. Pouliot, K. Shinohara, M. Aubin, M. Roach III, L. Skrumeda, J. Balter, D. Litzenberg, S. Hadley, Target localization and real-time tracking using the Calypso 4D localization system in patients with localized prostate cancer, Int. J. Radiat. Oncol. Biol. Phys. 65(2): 528-534 (2006)